Investigation of ZnO and TiO_2 Nanocrystalline Thin Films for Resistive Random Access Memory and Solar Cell Applications

Ph. D. Thesis

Submitted by

Praveen Kumar Jain
(College ID: - 2013REC9024)

Under Supervision of

Dr. Mohammad Salim
Associate Professor
Department of ECE, MNIT Jaipur

DEPARTMENT OF ELECTRONICS AND COMMUNICATION ENGINEERING
MALAVIYA NATIONAL INSTITUTE OF TECHNOLOGY JAIPUR
(DECEMBER, 2017)

Certificate

It is certified that:

- The thesis has not been submitted in part or full to any other University or Institute for the award of any degree.
- I have fulfilled all the requirements for submission of the thesis.

(Praveen Kumar Jain)
College ID: 2013REC9024

This is to certify that the thesis entitled "**Investigation of ZnO and TiO_2 Nanocrystalline Thin Films for Resistive Random Access Memory and Solar Cell Applications**", being submitted by Mr. Praveen Kumar Jain to the Department of Electronics and Communication Engineering, Malaviya National Institute of Technology, Jaipur, for the award of the degree of Doctor of Philosophy, is a bonafide research work carried out by him under my supervision and guidance. The results obtained in this thesis have not been submitted to any other university or institute for the award of any other degree.

(Dr. Mohammad Salim)
Associate Professor, Department of ECE
Malaviya National Institute of Technology, Jaipur
Jaipur-302017, Rajasthan (India).

The thesis was examined and approved for the award of the degree of Doctor of Philosophy.

_____

_____

_____

External Examiner

Declaration of Authorship

I, Praveen Kumar Jain, declare that this thesis titled, **"Investigation of ZnO and TiO_2 Nanocrystalline Thin Films for Resistive Random Access Memory and Solar Cell Applications"** and the work presented in it are my own. I confirm that:

- This work was done wholly or mainly while in candidature for a Ph.D. degree at MNIT.
- Where any part of this thesis has previously been submitted for a degree or any other qualification at MNIT, Jaipur or any other institution, this has been clearly stated.
- Where I have consulted the published work of others, this is always clearly attributed.
- Where I have quoted from the work of others, the source is always given. With the exception of such quotations, this thesis is entirely my own work.
- I have acknowledged all main sources of help.
- Where the thesis is based on work done by myself jointly with others, I have made clear exactly what was done by others and what I have contributed myself.

Signed:

Date:

Acknowledgements

The satisfaction and euphoria that accompany the successful completion of any work will be incomplete unless a profound thanks are conveyed to all those whose kind encouragement and valuable guidance made this work a grand success.

I express my sincere gratitude to *Dr. Mohammad Salim, Associate Professor, Department of Electronics & Communication Engineering, Malaviya National Institute of Technology, Jaipur* for his valuable supervision, support and inspiration during my study at MNIT, Jaipur. His constantly energetic attitude, optimism, and result oriented outlook have been helpful to me during the work and in the writing of the thesis. Without his continuous and strong support, my Ph.D. would not have started and finished smoothly.

I am very grateful to *Prof. K. K. Sharma, Head, Dept. of ECE,* my respected DREC committee members *Dr. Vijay Janyani, Dr. D. Boolchandani* and *Dr. C. Periasamy* for their valuable suggestions during my research work and presentations at the end of each semester. I also express my gratitude towards all the faculty members and office staff of ECE department for their support and encouragement.

I extend my sincere thanks to the *Swami Keshvanand Institute of Technology, Management and Gramothan, Jaipur* for allowing me to pursue part time PhD. I am thankful to *Mr. Jaipal Meel (Director), Prof. (Dr.) S. L. Surana (Director-Academics)* and *Prof. (Dr.) S. K. Bhatnagar (HOD-ECE)* to motivating me for quality research work.

I would like to thank *Prof. Davinder Kaur, Functional Nanomaterials Research Laboratory, Department of Physics, Indian Institute of Technoogy Roorkee* for extending their support and facilities to carry out the experimental work in her lab. I have no words to express appreciation to *Dr. Umesh Chand, Department of*

Electronics Engineering and Institute of Electronics, National Chiao Tung University, Taiwan, for providing the help in the experimental work at his place. With their help, I am able to complete my research work very precisely and efficiently. I extend my sincere thanks to faculty and staff members of *Materials Research Centre (MRC), MNIT* for the help and co-operation during the work done at this center.

I am highly obliged and express my sincere thanks to my friends *Dr. Neha Sharma, Dr. Rukhsar Zafar, Mr. Ankit Agarwal, Ms. Monika Mathur, Mr. Vinay Kanungo and Ms. Shubhi Jain* for helping and motivating during this work. I would like to express my deepest love and gratitude towards my Papa (*Sh. Padam Chand Jain*) and Mummy (*Mrs. Kanta Jain*), who have provided me the best education that they could offered and supported my endeavors. Without their support, persistence, initial motivation and love I would not be where I am today.

Above all, I am thankful to the Almighty, whose divine graciously gave me the required courage, strength and perseverance to overcome various obstacles that stood in my way.

(PRAVEEN KUMAR JAIN)

Abstract

Functional oxides are wide class of materials which exhibit a broad range of novel functionalities based on the tuning of their electrical, optical, magnetic and chemical properties. Among these oxides, wide band gap semiconductors have attracted much attention recently due to their potential for improving performance and extended capabilities of products in a number of industrial sectors, including the electronics, bio-medical, aerospace, automotive and optoelectronics. The research efforts include the design and fabrication of engineered heterostructures, multilayer, nanostructures, and composites- that exhibit either enhanced properties and/or multiple functionalities. It is desirable to establish the process for producing high quality thin films (e.g. higher crystallinity, less strain and less stress) of these oxides for their integration into emerging technologies.

ZnO/TiO_2 and TiO_2/ZnO thin films have been deposited on single crystal Si (100) substrate using pulsed laser deposition (PLD) technique in order to improve structural and optical properties of ZnO and TiO_2 thin films. It was observed that the deposition of TiO_2 film prior to ZnO, exhibited higher crystallinity along (002) diffraction peak, small compressive strain and stress and thereby rendering better optical properties as compared to ZnO films deposited directly on Si substrates. On the other hand, TiO_2 thin film deposited on a Si substrate exhibited pure anatase phase while the use of ZnO buffer was found to improve the crystallinity of TiO_2 thin film. The photoluminescence spectra showed that TiO_2 and ZnO buffer layers enhanced ultraviolet emissions of the ZnO and TiO_2 thin films to a larger extent, respectively.

The composite of ZnO and TiO_2, Zinc titanate ($ZnTiO_3$) ceramics were prepared by conventional solid state reaction method using ZnO and TiO_2 in a molar ratio of 1:1 with optimized parameters. It was found that the sample sintered at the 800 ^oC for 12 hour exhibit a single hexagonal phase of $ZnTiO_3$. $ZnTiO_3$ thin films have been deposited on ITO coated glass substrate using pulsed laser deposition (PLD) technique employing a KrF laser source (λ=248 nm). The effect of substrate temperature, which leads to transformation of hexagonal phase to cubic phase, has been studied. The XRD pattern revealed that pure hexagonal phase of $ZnTiO_3$ appear

upto 400 ^{o}C and more increment in substrate temperature leads to transformation of hexagonal phase to cubic phase. We have observed the blue shift in absorption edge at lower temperature. When the substrate temperature increases from 300 to 400 ^{o}C the band gap decreases due to strong hexagonal phase, but more increment in substrate temperature increases the band gap causes by change of phase from hexagonal to cubic. The dielectric constant of $ZnTiO_3$ thin film increases as the substrate temperature increases due to the enhancement in crystallinity and improved morphology.

The uniform and reliable resistive switching characteristics of the ZnO based RRAM device with thin TiO_2 layer was proposed and successfully investigated. In this study, the effect of the thickness of TiO_2 layer on switching characteristics has been investigated. Compared with different thicknesses of thin TiO_2 layers, the remarkable improved resistive switching parameters such as lower forming voltage and the narrower variation of endurance are achieved for TiO_2 layer of thickness 2 nm. The forming voltages are dependent on the TiO_2 thickness, which supports the idea that forming process is governed by dielectric breakdown like phenomenon. The $Ti/TiO_2/ZnO/Pt$ device with the 2 nm TiO_2 layer exhibits good DC endurance up to 10^3 cycles. The non-volatility of data storage is further confirmed by retention test measured at room temperature. It has been observed that both low resistance state (LRS) and high resistance state (HRS) do not exhibit any degradation for more than 10^4 s.

ZnO/CdTe based inorganic thin film solar cell was proposed and successfully fabricated. The efficiency of ITO/ZnO/CdTe/Al and $ITO/TiO_2/ZnO/CdTe/Al$ inorganic solar cell has been investigated. Open circuit voltage, short circuit current, fill factor and power conversion efficiency were calculated using current density-voltage characteristics. The SEM and AFM image indicate the good crystallinity and less roughness of the thin films, overall the quality of thin films is good. The effect of ZnO thickness varying from 50 nm to 150 nm was investigated and maximum efficiency of about 8.39 % was observed for the 100 nm thickness of ZnO layer. However, the efficiency of fabricated solar cells are slightly lower but cost effectively. Initially as we increase the thickness of ZnO layer i.e. thicker the active

layer, the more the excitons induced by light absorption. This increases the efficiency of solar cell. The thickness of ZnO ranging from 75-100 nm also support for perfect antireflection coating which increases the absorption of light. However, a more increment in the ZnO thickness causes the build-in electric field weaker and the pathway becomes longer for transporting the opposite charge carriers derived from exiciton separation to their corresponding electrodes at the same time, which makes the probability of charge collection by respective electrodes lower. For further improvement in the efficiency, thin layer of TiO_2 before ZnO layer was used and efficiency was improved upto 8.76 %. Thin TiO_2 layer improves device performance, excessive thickness degrades the performance of the device because thick TiO_2 reduces mobility and increases series resistance.

Overall, in this present work we have fabricated high quality ZnO, TiO_2 thin films and single phase $ZnTiO_3$ thin films using pulsed laser deposition technique. We have proposed and fabricated ZnO/TiO_2 double layer RRAM devices with improved resistive switching characteristics. ZnO/CdTe based inorganic thin fim solar cells also proposed and fabricated with improved photocurrent efficiency.

Table of Contents

List of Figures

List of Tables

Abbreviations

AFM	:	Atomic Force Microscopy
CVD	:	Chemical Vapor Deposition
DRAM	:	Dynamic Random Access Memory
FeRAM	:	Ferroelectric Random Access Memory
GB	:	Grain Boundaries
HRS	:	High Resistance State
ITO	:	Indium Tin Oxide
LRS	:	Low Resistance State
MIM	:	Metal-Insulator-Metal
MRAM	:	Magnetic Random Access Memory
NVM	:	Non Volatile Memory
PCRAM	:	Phase Change Random Access Memory
PL	:	Photoluminescence
PLD	:	Pulsed Laser Deposition
RRAM	:	Resistive Random Access Memory
PVD	:	Physical Vapor Deposition
SRAM	:	Static Random Access Memory
SEM	:	Scanning Electron Microscopy
TCO	:	Transparent Conducting Oxide
XRD	:	X-ray diffraction
XPS	:	X-Ray Photoluminescence Spectroscopy
ZTO	:	$ZnTiO_3$ (Zinc Titanate)

CHAPTER 1

Introduction

General background of contributed work has been presented in this chapter. The basic structural and physical properties of ZnO and TiO_2 as a semiconductor material have been explained. The different applications of ZnO and TiO_2 thin films in optoelectronic and nano-electronic devices have been presented. The scope of the thesis and organization of the thesis has been elaborated at the end.

1.1 General Background

The world-wide progress of thin film science into a major research area is due to the development of new generation ICs (smaller size with higher speed device). This needs new processing techniques and superior materials which are appropriate for Giga scale integration technology. The costs of thin film materials as a two dimensional system are very less than the bulk material, whereas thin film execute the similar task when it comes to surface processes. As a result, research activities to increase the knowledge and understanding of the chemical and physical properties of the microstructure and the performance analysis of thin films in various applications are continuously required [1-2].

In the last decade, ZnO has drawn a considerable research attention of researchers because of its outstanding properties as a semiconductor material of wide band-gap. The wide and direct band-gap (3.37 eV), good transparency, high electron mobility, large binding energy of exciton (60 meV), high thermal conductivity and easiness of growing different nanostructures (nano-flowers, nano-wires, nano-rods, nano-belts etc.) with different low cost deposition methods make it a potential candidate for several optoelectronic and nano-electronics device applications [3-6]. The radiation hardness of ZnO makes it an appropriate choice for space applications [7]. The high optical transparency of ZnO provides an opportunity to use it in UV detection and solar cell applications [8-9]. ZnO is easily etchable in all alkalis and acids, which can be very useful in the fabrication of nano-dimension devices [10]. An intense near-band-edge excitonic emission of ZnO is due to large exciton binding energy which

ensures its application in lasers [11]. Recent reports also confirm that ZnO is also a promising material for gas sensing, spintronics, flat panel displays, thin film transistor and piezo-electronic nano-generator applications [12-15].

The attractive chemical, electrical and optical properties of Titanium dioxide (TiO_2) make it attractive for research interest. Amongst the transparent metal oxides, TiO_2 possesses a high refractive index (>2.5 for anatase phase, and >2.7 for rutile phase) and about 10 times lesser optical absorption loss as compared to silicon [16-18]. Other characteristic properties of TiO_2 are a small thermal expansion coefficient over a wide range of temperature (room temperature to 1000 ℃) and a high transparency over a wide range of wavelength. In view of these advantages, TiO_2 has been used for different optical application i.e. sensors [19], multilayer optical filter [20], IR detectors [21], photo-catalysts devices [22], antireflective coating [23], integrated optical planar waveguides, [24], solar cell [25] and optical amplifiers [26] etc.

1.2 Functional Oxides

1.2.1 Overview

Functional oxides belong to a wide class of materials which have a wide range of functionalities based on the tuning of their electrical, optical, magnetic and chemical properties. Functional oxides exhibits, anions with deficiencies (vacancies) and cations with mixed valence states. The properties of these oxides can be tuned by varying either or both of these characteristics, giving the opportunity of fabricating smart devices. However, it might happen that the very property that one is trying to use for desired applications, may get modified with a reduction in particle size. This diversity makes these materials interesting for both the fundamental and technological approach. Searching new routes for synthesis and processing of functional oxide thin films and understanding the relationship between the structures and the properties are part of the rapidly growing field of nanotechnology. This interest is fueled by the possibility of miniaturizing electronic devices to much smaller length scales than is currently possible, one would like to grow controlled nano-scale structures with specific tunable properties [27-28].

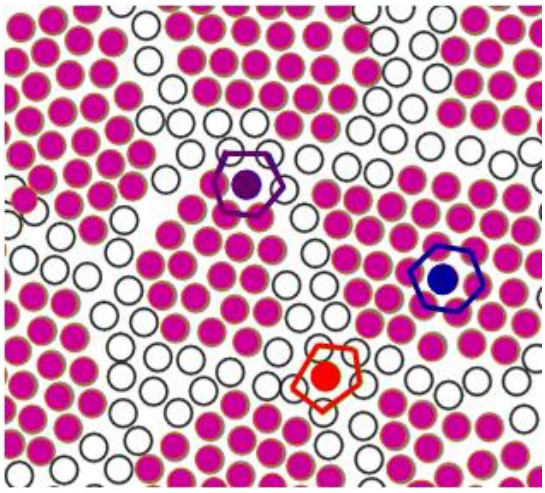

Fig. 1.1: Atomic structure of a two-dimensional nano-structured material. The atoms in the centers and boundary core regions of the "crystals" are indicated in dark and open circles, respectively [29].

Among various functional oxides, wide band gap semiconductors have been paying more attention due to their potential for improving performance in the different field. The research efforts among these include the design and fabrication of nanostructures, multilayer, hetero-structures and composites—that exhibit either improved properties and/or various functionalities. Composite materials with two or more component materials which have inhomogeneity in nanometer scale are called nano-composites which consist of nanometer-sized building blocks mostly crystallites separated by grain boundaries. The composition of grain boundaries and crystallite varies in nano-composite materials. Fig. 1.1 shows the formation of alloys in nano-composite materials with difference in densities of grain boundaries and density of crystallites. A key requirement in preparation of materials is to control the structural and compositional development for attaining excellent properties [29-30].

1.2.2 Zinc Oxide (ZnO)

All the applications of ZnO mentioned in above section originate from its material properties. Hence it is crucial to discuss the various properties of ZnO. This section explains the various properties of ZnO that makes it a popular candidate for variety nano-electronic and optoelectronic device applications. The most desirable features of zinc oxide are listed as follows:

- The direct and large band-gap of ZnO i.e. 3.37 eV with high exciton binding energy (60 meV) makes ZnO a promising material for photonic and optoelectronic applications at room temperature [31].

- A large band-gap of ZnO ensures its usability in ultraviolet application whereas sufficiently higher binding energy of exciton as compared to GaN (~25 meV) permits the efficient excitonic emission even at the room temperature. The large binding energy of exciton is an indication of efficient radiative recombination of photo-generated carriers that make ZnO a potential alternate to GaN in optoelectronic applications [32].
- ZnO thin films behave as transparent layers for the visible wavelength range (400-700 nm) that can be very advantageous in solar cell and transparent electronics applications [33-34].
- ZnO is the II-VI group compound semiconductor whose ionicity lies between ionic and covalent semiconductors [35].
- Furthermore, the heavily n-type doped ZnO acts as a excellent transparent conducting material with resistivity comparable to the indium tin oxide (ITO) [36-37].
- ZnO gets crystallized in either hexagonal wurtzite or cubic zinc blend structure. In wurtzite structure, each anion is surrounded by four cations at the corner of a tetrahedron and vice versa. The nature of this tetrahedral coordination is sp^3 covalent bond. A substantial ionic character also exists in these kind of materials that can increase the band-gap beyond the one expected from covalent bonds. The wurtzite structure consists of hexagonal unit cell with lattice constants varying in the range of 3.2475-3.2501 Å and 5.2042-5.2075 Å for a-parameter and c-parameter respectively. Various point defects such as oxygen vacancies, Zn interstitial and threading dislocations are the probable reasons for the deviation of lattice constants from their ideal values [38-39]. The hexagonal wurtzite structure of ZnO is shown in fig. 1.2.

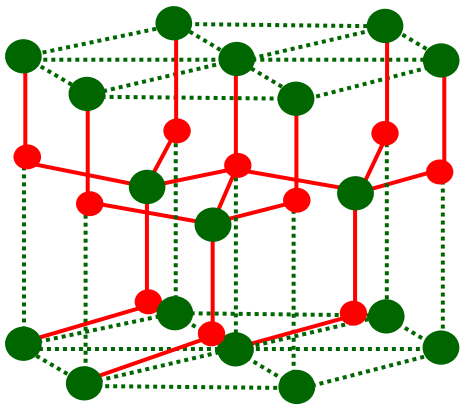

Fig. 1.2: Wurtzite Hexagonal structure of ZnO [38]
(Different parameters are listed in Table 1.1)

Table 1.1: Properties of hexagonal wurtzite structure of ZnO at room temperature

Crystal structures	Wurtzite, Zinc blende, Rock salt
Lattice parameter: *a* (Å) *c* (Å) *c / a* u (bond length parallel to the c-axis)	 3.25 5.20 1.602 0.345
Space group	C^4_{6v} or $P6_3mc$
Density (g/cm^3)	5.606
Melting point (^oC)	1975
Thermal conductivity (Ω^{-1} cm^{-1})	0.6 -1.2
Static dielectric constant	8.656
Linear expansion coefficient ($/^oC$)	a_o: $6.5X10^{-6}$, c_o: $1.0X10^{-6}$
Refractive index	2.008
Energy band gap (eV)	3.37
Intrinsic carrier concentration (cm^{-3})	$< 10^6$
Exciton binding energy (meV)	60
Electron effective mass	$0.24m_o$
Electron Hall mobility for low n-type conductivity ($cm^2/V.s$)	200
Typical defects	Zinc vacancies, Zinc interstitials, Oxygen Vacancies
Relative dielectric constant	8.66
Solubility in water	0.16 mg/100mL
Hole effective mass	$0.59m_o$
Hole hall mobility for low p-type conductivity ($cm^2/V.s$)	5-50

1.2.3 Titanium Dioxide (TiO_2)

TiO_2 is n-type, wide and indirect band gap semiconductor and demonstrates outstanding optical transmittance in the visible and near infrared regions. TiO_2 has applications in electro chromic displays, gas sensors, dye sensitized photovoltaic cells and antireflective coatings. TiO_2 exhibits outstanding photo catalytic property because of its wide band gap and photo-generated holes and electrons have a long lifetime [40-44]. However, there are two main shortcomings during the photo catalytic process: (i) high electron–hole recombination rate (ii) the less use of solar spectrum. The band gap of anatase phase is 3.2 eV and that of rutile phase is 3.0 eV [45]. TiO_2 crystallizes in three different polymorphs: anatase, rutile and brookite. The unit cell structure of three polymorphs of TiO_2 is shown in fig. 1.3. Traditionally, experimentally as well as theoretically, the rutile phase has been widely investigated, due to the comparatively simple crystal structure. But now a day's experimental studies have also been paying attention on the anatase phase, due to its potential efficiency for photo catalytic applications [46]. The various structural and physical properties of three different polymorphs of TiO_2 are shown in Table 1.2.

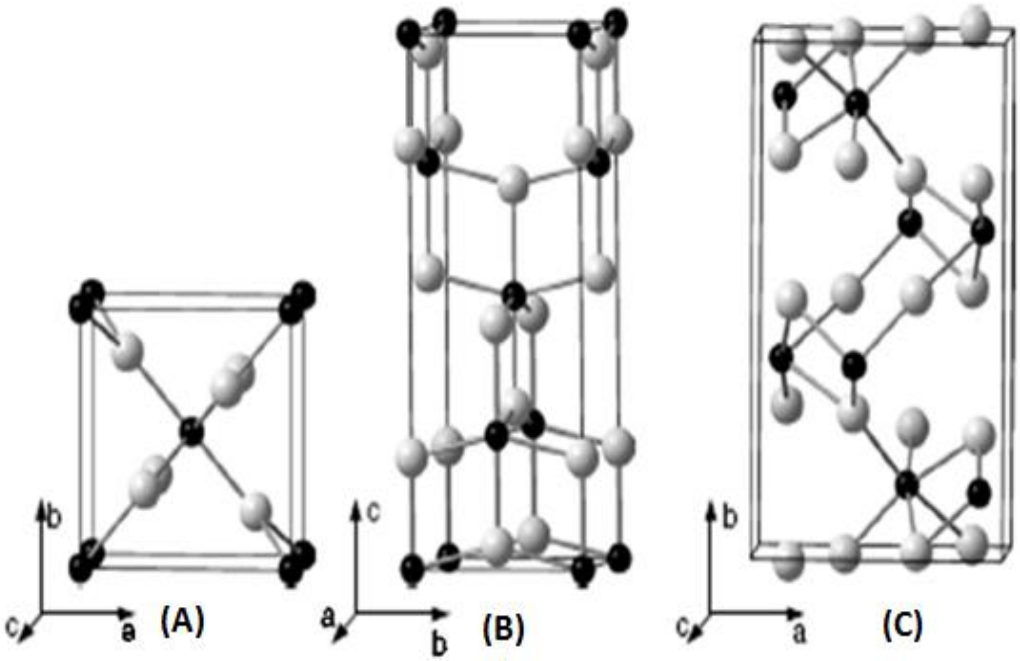

Fig. 1.3: Crystal structure of TiO_2 polymorphs *(A) Rutile, (B) Anatase and (C) Brookite (small black sphere- Ti, large gray sphere- O) [46].*

Table 1.2: Properties of three different polymorphs of TiO_2

Polymorphs	Rutile	Anatase	Brookite
Crystal structure	Tetragonal	Tetragonal	Orthorhombic
Lattice constants (Å)	a = 4.5936 c = 2.9587	a = 3.784 c = 9.515	a = 9.184 b = 5.447 c = 5.145
Ti-O bond length (Å)	1.949 (4) 1.980 (2)	1.937 (4) 1.965 (2)	1.87~2.04
Space group	$P4_2/mnm$	$I4_1/amd$	Pbc*a*
O-Ti-O bond angle	81.2° 90.0°	77.7° 92.6°	77° ~ 105°
Molecular/cell	2	4	8
Volume/molecule ($Å^3$)	31.2160	34.061	32.172
Density (g/cm^3)	4.13	3.79	3.99
Energy band gap (eV)	3.0	3.2	--
Refractive index	2.7	2.5	--
Resistivity (Ω cm)	$3x10^{-3} – 2x10^{1}$	$6x10^{-2} – 8x10^{-2}$	--
Carrier density (cm^{-3})	$10^{18} – 10^{21}$	$7x10^{18} – 2x10^{19}$	--
Mobility ($cm^2V^{-1}s^{-1}$)	0.05 – 0.2	6 – 10	--
Effective mass (m_e^*)	~ 8-20 m_0	~ 1 m_0	--
Dielectric constant	6.33	5.62	--

1.2.4 ZnO-TiO_2 composites

ZnO and TiO_2, because of their versatile properties and vast applications, have gained a lot of interest both as single material [47-48] and as ZnO–TiO_2 composites [49-50]. ZnO–TiO_2 system has three stable phases including $ZnTiO_3$ (with hexagonal and cubic structure), Zn_2TiO_4 (cubic structure), and $Zn_2Ti_3O_8$ (cubic structure). Amongst these phases, $ZnTiO_3$ is unstable and gets decomposed into Zn_2TiO_4 and rutile TiO_2 at about 945 °C [51].

With the current scenario of progressive microwave applications and vast usage of mobile telephones and satellite communication system, the manufacturing and betterment of high-quality microwave dielectrics has been intensified. Recent studies

have proven $ZnTiO_3$ to be an attractive material for applications in microwave dielectrics [52-53]. Because of it's low sintering temperature and suitable dielectric properties, $ZnTiO_3$ has been used for low-temperature cofired ceramics (LTCCs) [54]. Considering its importance in industrial sector, $ZnTiO_3$, due to its good semiconducting and dielectric properties acts as an active catalyst, paint pigment and phosphor. $ZnTiO_3$ works as a good regenerable sorbent for desulphurization of hot coal gases. Some studies have reported enhanced catalytic and luminescent properties using nano-crystalline $ZnTiO_3$ [55-56]. $ZnTiO_3$ belongs to the limonite structure which is a derivative structure of corundum with Zn^{+2} and Ti^{+4} occupying 2/3 octahedral voids, leaving the rest of the 1/3 octahedral voids vacant. The columbic repulsion between the positively charged Zn^{+2} and Ti^{+4} ions causes each to shift slightly towards the adjacent unoccupied octahedral site. The oxygen ions also shift slightly from idealized hexagonal closed packed positions. The phase diagram of ZnO-TiO_2 composite is as shown in fig.1.4.

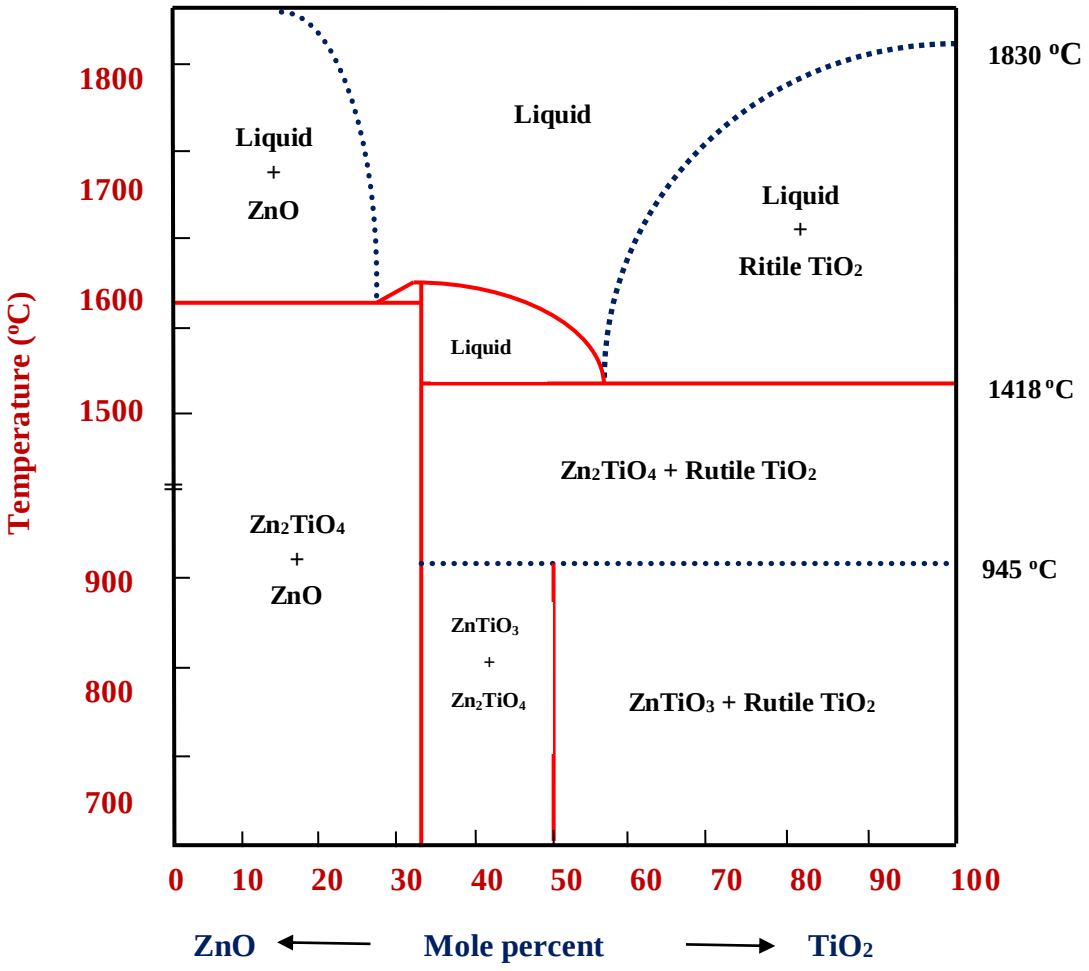

Fig. 1.4: Phase diagram of ZnO-TiO_2 composite [51]

1.3 IC Memories

Semiconductor memory plays a very important role for the development in IC industry during the last few decades. Semiconductor memories are mainly categorized as volatile memories and nonvolatile memories as represented in fig.1.5. In volatile memory the stored data loses immediately as the system power is turned off i.e. to maintain the stored information a constant power is essentially required in volatile memory. In spite of that, the nonvolatile memory can retain the stored data without supplying any power for a long duration [57].

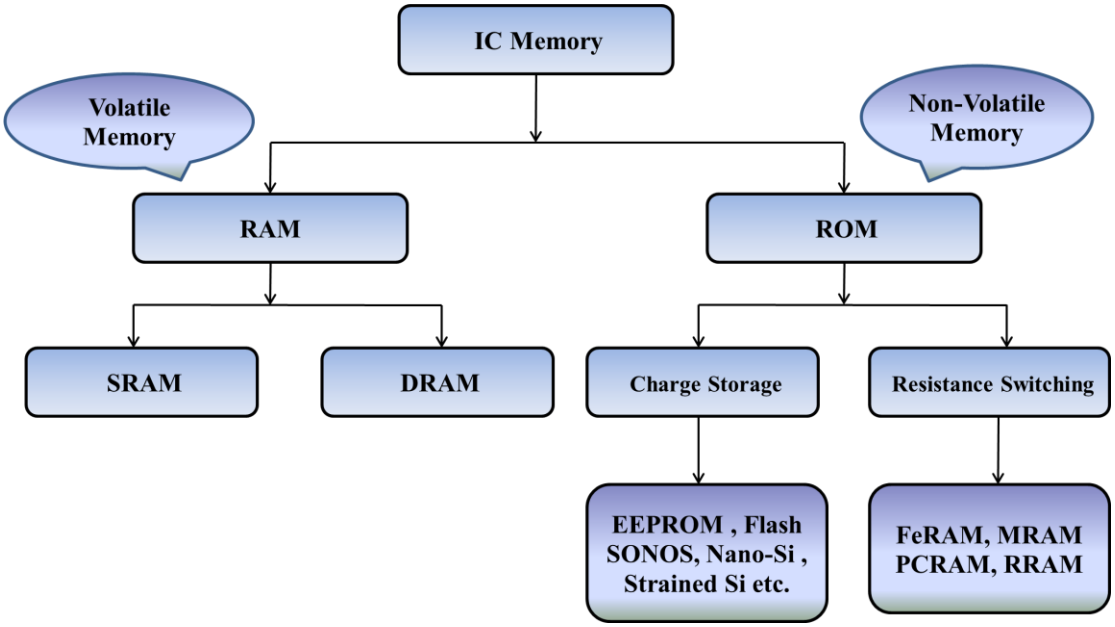

Fig. 1.5: Categories of Semiconductor memories

1.3.1 Volatile Memory

There are two main categories for volatile memory: one is dynamic random access memory (DRAM) which has high capacity and density due to small size (i.e. the size of DRAM cell consisting 1T1C is about 6-12F^2 [58]. But within a few milliseconds the stored data will be lost due to the leakage current. So to retain the stored data, DRAM cell necessarily refreshed regularly. Other one is static random access memory (SRAM). A SRAM cell (size is about 50-80F^2, consists six transistors) is more complicated than DRAM, but has brilliant endurance performance, no requirement of regularly refreshing and the merits of the high operation speed. Consequently, SRAM is generally used as a cache memory.

1.3.2 Nonvolatile Memory

The nonvolatile memory (NVM) has the capability to retain the stored information for a long duration without supplying power. An ideal NVM should have the following properties (i) simple structure (ii) high operation speed (iii) low cost, (iv) nondestructive readout (v) small size (vi) high endurance (vii) low operation voltage (viii) long retention time etc. [58]. Although, perfect NVM to fulfill all the above mentioned properties are not available till now.

The conventional NVM is flash memory, comprise the NAND flash and NOR flash. The NAND flash used for large data storage while the NOR flash has high speed of operation, which is appropriate for the application for mobile phones and computer coding. The main drawbacks of these memories are (i) low operation speed (ii) high operating voltage, (iii) poor retention time, and (iv) coupling interference effect during scaling down [59]. Hence, researchers are utilizing the next-generation NVM with the benefits of DRAM, SRAM, and flash memory. There are different types of next-generation NVMs, including magneto-resistive random access memory (MRAM) [60], ferroelectric random access memory (FeRAM) [61], resistive random access memory (RRAM) [62] and phase change random access memory (PCRAM) [63].

1.3.3 Next-generation Nonvolatile Memory

(a) Ferroelectric Random Access Memory (FeRAM)

Materials having spontaneous electric polarization which can be altered by an external electric field are known as ferroelectric material. The ferroelectric material is typically perovskite type structure. In FeRAM, the signal “0” and “1” can be renowned from the direction of remanent polarization, which can be identified from the polarization hysteresis curve of the ferroelectric material as shown in fig. 1.6. In spite of the fact that FeRAM has the several advantages, i.e. faster programming speed, lower power consumption and compatibility with the semiconductor fabrication process, the size of is too large that it cannot match the semiconductor scaling trend [61, 64].

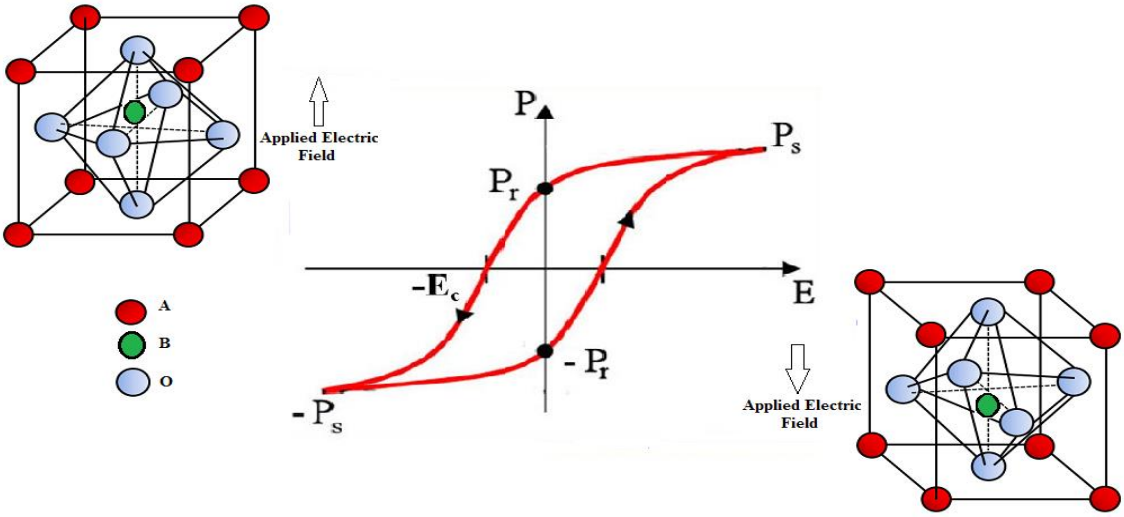

Fig. 1.6: Polarization hysteresis curves of the perovskite materials [64]

(b) Magneto-resistive Random Access Memory (MRAM):

In MRAM cell, a thin tunneling layer is sandwiched between two magnetic layers which form the magnetic tunneling junction as shown in fig. 1.7. The magnetization of one magnetic layer which is also known as reference layer is kept fixed and in a specific direction, while the magnetization of the other magnetic layer (which is called storage layer) can be switched to parallel or anti-parallel with the reference layer by applying a specific magnetic field. The logic "1" and "0" is determined by the resistance of parallel or anti-parallel state. To read data, a small current flowing through the tunneling layer is detected to recognize the resistance states. With the evolution of device shrink, the large operation current, the reliability of the tunneling layer, and the device scaling limitation could be the most important challenges of MRAM [60, 64].

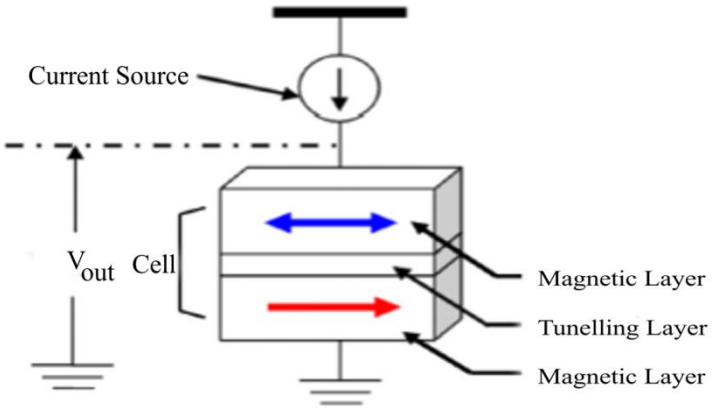

Fig. 1.7 MRAM cell composed of a magnetic tunnel junction [64]

(c) Phase Change Random Access Memory (PCRAM)

The PCRAM is a promising technology to meet the requirements of the ideal NVM. The PCRAM utilizes the important property of chalcogenide alloy i.e. reversible phase change between the amorphous and the polycrystalline state, which is done by proper heating and cooling. In reset process, a high magnitude current pulse with a short trailing edge is applied to the programmable volume of the phase change material. As shown in fig. 1.8, the temperature of the material is more than the melting point, it removes the polycrystalline order in the volume. When the reset pulse is terminated, the device cools to "freeze in" the amorphous structure. In set process, a moderate magnitude current pulse with sufficient duration is applied to maintain the device temperature for crystal growth (fig. 1.8).

The amorphous structural state (low conductive state) or the polycrystalline structural state (high conductive state) is read by applying a low magnitude and long duration current pulse. Due to the small area required to change the film crystallinity, the programming speed is fast (tens of nanoseconds). However, during set and reset process, large Joule heating is applied to the phase change material, and thus, huge power is consumed. Therefore, how to reduce the power consumption during the PCRAM operation is a significant challenge of the PCRAM. The heat interference in the PCRAM is the first obstacle to be overcome when the cell size is scaled down [63].

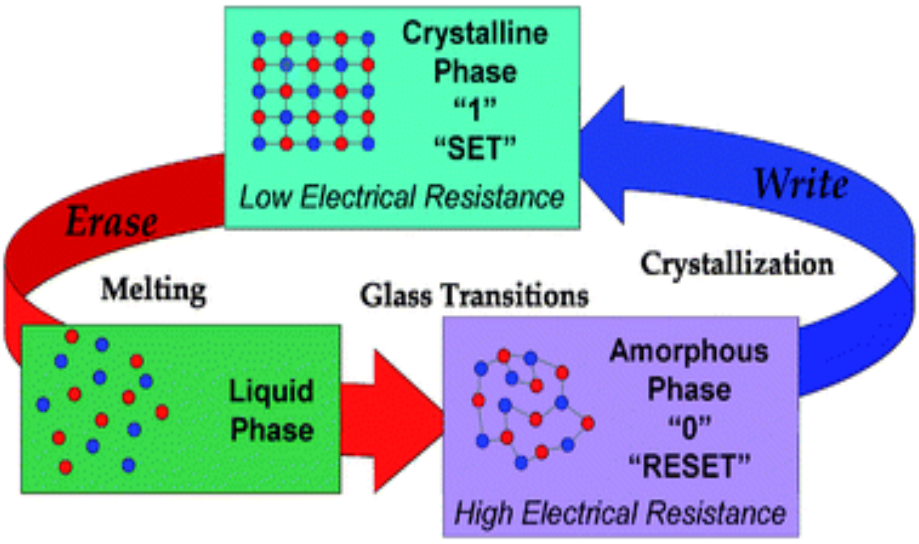

Fig.1.8 Schematic of Phase transitions during PCRAM operation.

(d) Resistive Random Access Memory (RRAM)

RRAM or ReRAM is a non-volatile (NV) random-access memory (RAM). The basic key pont of RRAM is the change in the resistance across a dielectric solid-state material, often referred to as a memristor, with the application of external electric field. This technology have some similarities with conductive-bridging RAM (CBRAM), and phase-change memory (PCM) [62].

CBRAM consists of one electrode which provides ions that get dissolved readily in an electrolyte material, whereas PCM involves producing enough Joule heating effect, phase changes from crystalline to amorphous structure or vice versa. On the contrary, RRAM works by generating defects in a thin oxide layer, acknowledged as oxygen vacancies (generated by removal of oxygen from oxide bond locations), which can consequently charge and drift with the application of an electric field. The movement of vacancies and oxygen ions in the oxide is similar to the movement of holes and electrons in a semiconductor.

The relation between the current (or voltage) polarity and the RS behavior in the memory device needs to be distinguished. In general, the process when the resistance of the device flips from low resistance to high resistance state is called RESET process, while the reverse operation is termed as SET process. The specific resistance state (HRS or LRS) can be retained after the electrical stress is cancelled, which indicate the non-volatile nature of RRAM. Generally the fresh device stays in its original resistance state and switches the resistance state only after the application of a voltage higher than set voltage. This is called the forming process or electroforming [65]. The resistive switching behaviors can be divided into two modes (uni-polar and bipolar) based on the correlation of electrical polarity involving SET and RESET processes. In the uni-polar RRAM, the switching direction depends only on the amplitude and not on the polarity of applied voltage as shown in fig 1.9 (b). The device switching from LRS to HRS take place under the similar voltage polarity as the switching from HRS to LRS. The switching mechanism of the uni-polar RRAM is ascribed that the formation of the conductive filament under voltage stimulus puts the device into LRS and Joule heating caused rupture of the filament switches it back to

HRS. Due to the dependence of Joule heating effect on the amplitude of the applied current, and does not depend on the polarity of the applied current this type of devices shows uni-polar switching behavior. In the bipolar RRAM, polarity of applied voltage play a important role for switching direction as shown in fig 1.9(c).

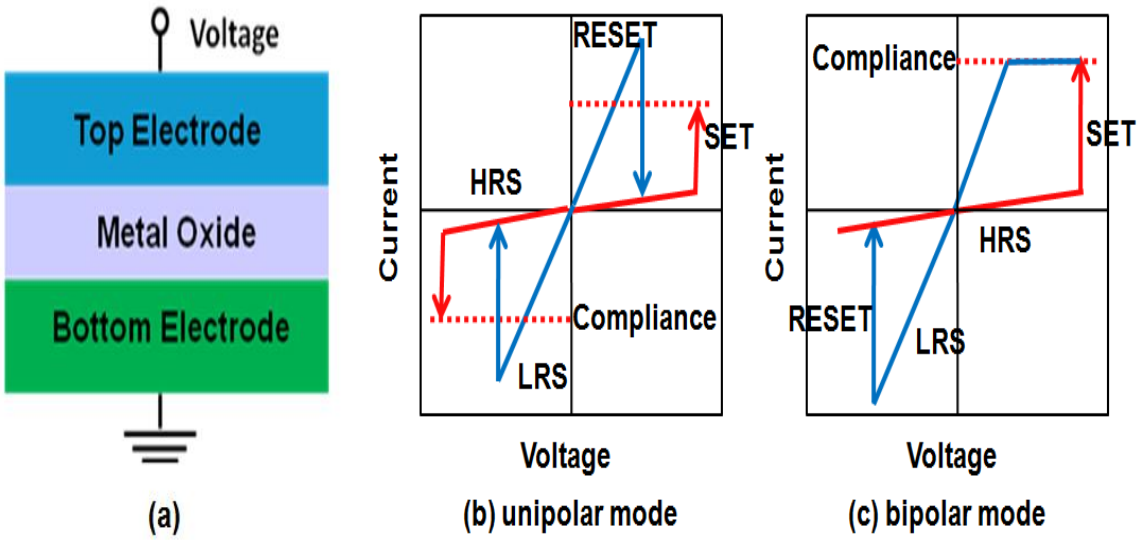

Fig.1.9: (a) Schematic of metal-insulator-metal structure (b) uni-polar I-V characteristic curve of oxide RRAM and (c) bipolar I-V characteristics curve of oxide RRAM [66].

Thus, the process of writing and erasing take place under the different polarity. It is also suggested to make compulsory to set compliance for each switching mode to stay away from the permanent dielectric breakdown in the set process which is usually provided by the memory cell transistor, series resistor or semiconductor parameter analyzer. For reading the data from the memory cell, the state of the cell (low resistance state or high resistance state) is detected by applying a small voltage. This voltage does not affect the memory cell.

1.4 Thin Films Solar Cell

The Photovoltaic solar cell converts sunlight or solar energy, which is the most abundant source of the sustainable and renewable energy on the earth, into electricity. Our earth receives ~1.2×10^{17} W of solar power, which is ~10,000 times larger than the rate of worldwide energy consumption i.e. ~1.3×10^{13} W. Therefore, solar energy alone has the ability to fulfill all the planet's energy requirements for the foreseeable future.

The operations of a photovoltaic solar cell can be explained using following three steps: (i) Light is absorbed by absorbing layer and generates an electron hole pair or excitons. (ii) The charge carriers are separated. (iii) The extraction of separated charge carriers to an external circuit. fig.1.10 demonstrates the operation of this cell.

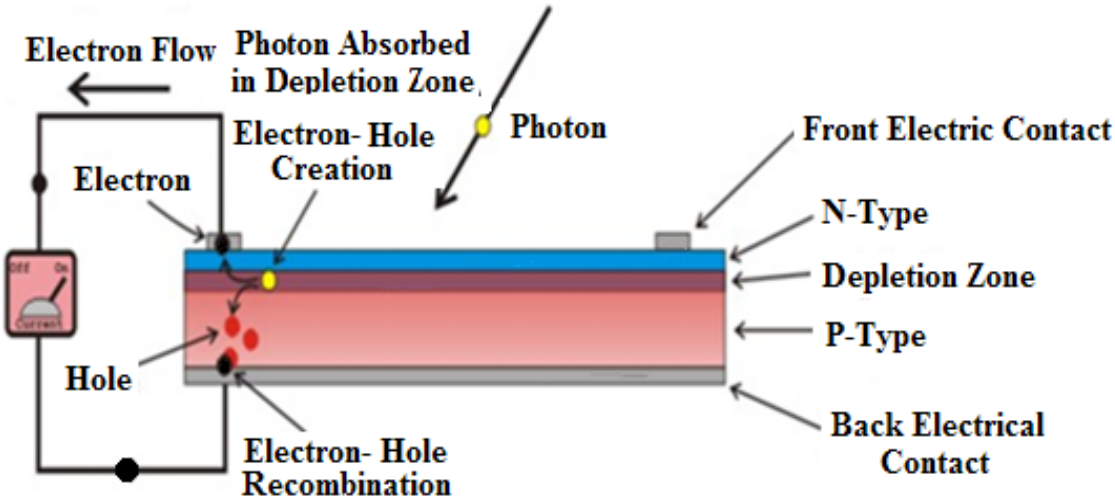

Fig1.10: Schematic of solar cell operation [67]

There are different characteristic factors of a solar cell which tell us how efficiently it can convert the sunlight to electricity [67-68].

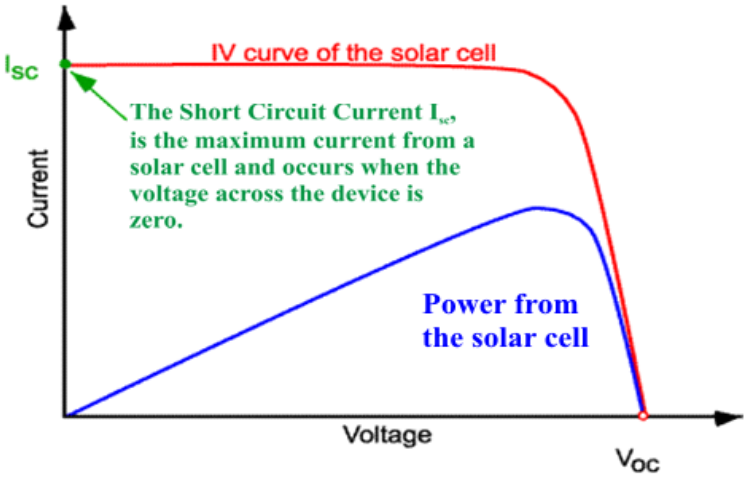

Fig1.11: I-V characteristics curve of solar cell [67, 68]

***Short-circuit Current*:** It is the current measured from the cell by short circuiting the terminals of the cell i.e. the current measured with zero load resistance. In general, the current of the solar cell is represented as current density, J_{sc}:

$$\text{Jsc} = \frac{I_{sc}}{A} \qquad (\text{mA/cm}^2) \tag{1.1}$$

J_{sc} is the short circuit current density, A=effective area of solar cell; I_{sc} = Short circuit current

Open-circuit Voltage: It is the voltage measured from the cell without any load connected to cell. It is the maximum voltage available from a solar cell.

$$V_{OC} = \frac{\eta kT}{q} \ln\left(\frac{I_L}{I_o} + 1\right) \tag{1.2}$$

$$\text{V}_{\text{OC}} = \frac{E_{CB}}{q} + \frac{kT}{q} \ln\left(\frac{n}{N_{CB}}\right) - \frac{E_{redox}}{q} \qquad \text{(Volts)} \tag{1.3}$$

I_0=Dark Saturation Current, I_L=Light generated Current, n = number of electron; N_{CB} = effective density of states; E_{redox} = Nernst potential of the redox mediator.

Series Resistance (R_s): In a solar cell due to the charge transfer resistance and contact resistance, there exists a series resistance.

Shunt Resistance (R_{SH}): For providing an alternate current path to the photo-generated charge carriers causing, there exists shunt resistance.

***Fill Factor (FF)*:** From the I-V characteristics of solar cell, it can be clearly seen that V_{OC} and I_{sc} are the maximum voltage and current respectively, but power from solar cells at both of these operating points is zero. The Fill Factor is defined as the ratio of the maximum power (P_m) from the solar cell to the product of V_{oc} and I_{sc}.

$$\text{FF} = \frac{V_m \, \text{I}_\text{m}}{V_{OC} \times I_{sc}} = \frac{P_m}{V_{OC} \times I_{sc}} \tag{1.4}$$

Efficiency (η): The efficiency of a solar cell is defined as the ratio of maximum electrical power output to the radiation power input from the sun and acts as a measure of the performance of solar cells.

$$\eta = \frac{V_{OC}}{P_{in}} \times I_{sc} \times FF \tag{1.5}$$

***Quantum efficiency (QE)*:** Also referred to as Incident Photon to Charge Carrier Efficiency (IPCE) is a measure of how efficient a solar cell is in producing photo-generated charge at a given frequency.

$$\text{IPCE}\ (\%) \ = \ 1240 \times \frac{I_{SC}}{\lambda} \frac{1}{W_{in}} \text{ x } 100 \tag{1.6}$$

where λ is the wavelength (nm) and W_{in} is the intensity of incident light (W/cm^2).

1.5 Motivation of the Research Work

When annealing is performed after the deposition of ZnO thin films on Si substrates, oxygen atoms from the ZnO thin films gets captured by Si atoms from the substrate thereby deteriorating the quality of ZnO thin films. To overcome this problem, buffer layers need to be deposited between ZnO and Si substrates. TiO_2 has been chosen as a buffer because of following characteristic properties (i) Both TiO_2 and ZnO are wide-band-gap materials. (ii) They possess similarities like high thermal and chemical stability, high refractive indices. (iii) TiO_2 and ZnO thin films have intense absorption in the ultraviolet band and have high transmittance in the visible region, (iv) ZnO and TiO_2 are abundant and low cost, suitable used in actual production.

In recent times, the research has been focused on the preparation of single phase perovskite materials (due to their unique properties and vast applications). So we have made our efforts for the preparation of single phase $ZnTiO_3$ ceramics as well as thin films by using the ZnO and TiO_2.

Non-volatile memory technologies are undergoing vigorous research aiming at replacing the existing technology. Each memory type has its own advantages, they all face their challenges as well. Out of all these memories, RRAM has the best potential to be the next generation NVM device. However, the degradation of its reliability such as endurance and retention is a great challenge that needs to be solved for memory application. The high temperature retention properties in ZrO_2-based RRAM device make it unstable [69]. It is unable to maintain its memory window after few hundred seconds at 200 ^oC. Besides the HfO_2 RRAM devices show the endurance degradation and instability in their reliability properties [70]. The thermal instability of HfO_2 thin film is a critical issue for switching characteristics due to the low crystallization temperature (< 400 °C). ZnO is considered to be n-type high-band gap semiconducting materials. Although the origin of its electron conductivity is not clear, Z_{ni} (zinc interstitial) and V_O (oxygen vacancy) defects are attributed for lower resistance. A large number of these defects may result in insufficient switching properties. So an attempt has been made in the investigation of switching characteristics in TiO_2/ZnO double layer resistive switching memory device. The focus was on the improvement of thermal stability, endurance and retention degradation of high performance in the ZnO based RRAM devices with TiO_2 intermediate layer. Different materials and technologies have been used to fabricate low cost and high efficiency solar cell. CdTe

is one of the most promising candidates for low cost solar cell. Here we have made efforts to improve the efficiency of CdTe solar cell by the use of ZnO and ZnO/TiO_2 buffer layers.

1.6 Organization of the Thesis

The main objective of this thesis is to make a systematic investigation on ZnO and TiO_2 based Solar Cell and Resistive Random Access Memory (RRAM). The thesis consists of eight chapters, organized as follows.

Chapter 1 provides an overview of nano-crystalline oxide thin films and material background of selected semiconductors i.e. ZnO, TiO_2. The chapter includes the discussions on the structural, optical and transport properties of these oxides. An insight of ZnO-TiO_2 has also been presented. The basic working principles of Solar cell and RRAM have also been included in this chapter.

Chapter-2 compiles some important state-of-the-art work in this area. The major work done in this field by various research groups is presented in brief. A detailed review on latest trends in the field of ZnO, TiO_2, ZnO-TiO_2 nano-composite thin films and their applications in solar cell and RRAM have been reviewed in detail. Based on the literature survey, various research gaps in this area have been identified. Finally, the motivation behind this study has been outlined at the end of the chapter.

Chapter 3 presents the details of experimental techniques, which have employed for the preparation and characterization of nano-crystalline thin films and devices. This chapter is divided into three sections which deal with synthesis techniques, basic characterization and measurement of physical properties. Section 3.1- Most of the synthesis of thin films in present thesis has been carried out by PLD technique, which uses pulses of KrF excimer laser energy to remove material from the surface of a target. Amongst various Physical Vapor Deposition (PVD) techniques such as evaporation, sputtering and molecular beam epitaxy; PLD allows stoichiometries transfer of material from the target to substrate being a non-equilibrium process. The other techniques used are RF sputtering and thermal evaporation technique. Section 3.2- The first measurement that is usually carried out after synthesis is to record the X-ray diffraction pattern of the deposited nano-composite material. Analysis of the position and width of the Bragg reflections gives an idea of the crystallographic phase, presence of impurities, particle size etc. Further the surface morphology and

microstructure were studied using Field Emission Electron Microscopy (FESEM) and Atomic Force Microscopy (AFM). Section 3.3- Optical properties of these films were studied by using UV-Vis-NIR spectrophotometer and photoluminescence spectrometer. Current density-voltage characteristics of the devices were measured with a Keithley electrometer with illuminating the devices with solar simulator.

Chapter 4 presents the study of structural and optical properties of ZnO/TiO_2 and TiO_2/ZnO thin films deposited through PLD technique. Deposition of ZnO/TiO_2 and TiO_2/ZnO thin films have been done on single crystal Si (1 0 0) substrate using pulsed laser deposition (PLD) technique in order to improve structural and optical properties of ZnO and TiO_2. The effect of ZnO and TiO_2 buffer layer on structural and optical properties of TiO_2 and ZnO thin film, respectively, have been studied.

Chapter 5 describes the work carried out on investigation of ZnO and TiO_2 nano-composite thin films. Zinc titanate ($ZnTiO_3$) ceramics have been prepared using conventional solid state reaction technique taking ZnO and TiO_2 in a molar ratio of 1:1 with optimized parameters. The sample sintered at the 800 ^oC for 12 hours exhibited formation of single hexagonal phase of $ZnTiO_3$. Deposition of $ZnTiO_3$ thin films has been done on ITO coated glass substrate using pulsed laser deposition (PLD) technique employing a KrF laser source (λ=248 nm). In the present work, the effect of substrate temperature, which leads to transformation of hexagonal phase to cubic phase, on optical and dielectric properties has been studied.

Chapter 6 describes the application of ZnO and TiO_2 thin films in RRAM non volatile memory. The uniform and reliable resistive switching characteristics of the ZnO based RRAM device with thin TiO_2 layer are successfully investigated. In this study, the effect of the thickness of TiO_2 layer on switching characteristics has been investigated.

Chapter 7 presents the application of ZnO and TiO_2 thin films in the Inorganic solar cell. The efficiency of ITO/ZnO/CdTe/Al and ITO/TiO_2/ZnO/CdTe/Al inorganic solar cell has been investigated. The effect of ZnO or TiO_2 thickness has been studied. Open circuit voltage, short circuit current, fill factor and power conversion efficiency were calculated using current density-voltage characteristics.

Chapter 8 presents the summary and conclusions of the entire work presented in the thesis and also propose the future directions in which these studies can be extended.

CHAPTER 2

Thin Films for RRAM and Solar Cell Application: A Literature Review

This chapter presents a review on some important state-of-the-art work reported by various research groups in the area of ZnO and TiO_2 thin film based Solar Cell and RRAM Applications.

2.1 Introduction

Literature survey plays an important role in any kind of research. A thorough understanding of the state of the art work in any research area can only be envisaged by the future trends in that particular research area. Therefore, this chapter is dedicated to presenting some important state of the art work reported by different research groups in the area of ZnO and TiO_2 thin films. This chapter provides a comprehensive review on the recent advancements in the field of Solar cells and RRAM.

2.2 ZnO and TiO_2 Thin Films

Thin films can be defined as the layers whose thickness varies from nanometers to a few micrometers. They exhibit better properties than bulk materials for a variety of applications. Thin film technology has emerged as a very potential candidate for optical coatings and electronic device applications. The nano-structured thin film reduces the material losses, enhances the efficiency of solar cells, improves the sensitivity of gas sensors due to larger surface area to volume ratio and can be very useful in a wide variety of applications. The pivot influence of thin film technology in diverse and challenging frontiers such as optical coatings, metallurgical coatings, micro magnetism, surface science, superconductivity mechanism and microelectronics is now a part of literature survey.

ZnO has attracted much attention due to its potential to grow with large number of nano structures. Recently, different ZnO based nanostructures such as nano wires, nanotubes , nano flowers and nano walls etc. [71-80] have attracted a significant research interest due to their potential applications in next generation sensor and molecular technology. Different techniques such as spin coating [81], thermal evaporation [82], metal organic chemical vapor deposition (MOCVD) [83], pulsed

laser deposition (PLD) [84] and RF sputtering [31] have been employed in the past to grow different ZnO nanostructures. ZnO with metal doping acts as a multifunctional material simultaneously possessing optical, semi-conducting and magnetic properties. A significant research interest in doping ZnO is to improve these properties and put it in various applications. Doping of metal into ZnO allows the creation of sub energy levels in the band gap to make use of it as UV detectors and light emitters. ZnO was doped with Mn [85], Sn [86], Al [83], In [87], Fe [88] etc. for electrical and optical applications. The properties of ZnO thin films also depend on the temperature treatment (Substrate temperature, annealing temperature) as reported earlier [89]. The level of Zn or O atom defects depends on the gas environment within the chamber during the deposition process [82]. The quality of thin films also depends on the used substrate and it can be improved by using a buffer layer which has less mismatching of lattice and thermal expansion coefficient. Y.S. Lim et al [90] reported that insertion of thin CaO buffer layer between ZnO and sapphire substrate increase crystallinity and alleviate the compressive strain.

TiO_2 thin films have also attracted interest of researchers due to its potential applications. TiO_2 have been prepared by different chemical and physical vapor deposition techniques. Several efforts have been made to improve the quality of TiO_2 thin films, so that it can be efficiently utilized in the concern applications.

Several studies have been reported on the characteristics of $ZnTiO_3$ (composite of ZnO and TiO_2) powder synthesized through solid state reaction and sol–gel methods [91-92]. Kim et al. and other researchers [93-94] have reported the suitable dielectric properties by controlling the composition in ZnO–TiO_2 binary system and/or substituting zinc with Ba, Ca, Sr, and Mg. Some unique physical and chemical properties of the perovsktite-type $ZnTiO_3$ have been observed, such as high quality factor (Q=3000), the low band gap (2.88 eV), small temperature coefficient of the resonant frequency (τ_f =55×10^{-6}/°C) and high dielectric constant (ε=19) [95]. The dielectric constant and loss tangent for the pure hexagonal phase of bulk $ZnTiO_3$ was found $\varepsilon_r \approx 19$ and $\tan \delta \approx 0.01$, respectively, which is suitable for application in microwave resonators, filters etc. [96]. Most of the research investigations are based on bulk system. Also, there are minimal studies reporting characteristics of zinc

titanate based thin film. In this work we have made efforts to prepare single phase $ZnTiO_3$ thin films and further investigate the effect of phase transformation on optical and dielectric properties. Some of the previously reported works on ZnO, TiO_2 and ZnO-TiO_2 composites are shown in Table 2.1.

Table 2.1: Some of the studies done on growth of ZnO, TiO_2 and ZnO-TiO_2 composites from previously published work

Structure Type	**Matrix**	**Technique**	**Growth Reagent and Condition**	**Results**	**Ref.**
ZnO nanocrystalline thin films (orientation along the *c*-axis)	*ITO* Substrate	DC magnetron sputtering	Target: Zn metal, Ar and O_2 gas ratio	Higher optical band gap attributed to small particle size.	*[31]*
ZnO nano flowers	-	Hydrothermal synthesis	Zinc acetate, sodium citrate and sodium hydroxide	Observation of photocatalytic activity toward degradation of metamitron.	*[4]*
ZnO nano wires	TCOs	Microwave heating Method	Precursor solution, the growth rate is 58–78 nm/min	Increase in power conversion efficiency with nano wire length	*[5]*
ZnO thin film	CaO buffer layer on sapphire substrate.	sputtering	ZnO target	Attainment of Crystallinity and alleviated compressive strain	*[3]*
Nano crystalline anatase-TiO_2 thin films	Glass substrate	DC magnetron sputtering	TiO_2 Room temperature	Transparency higher than 90% with sharp ultraviolet cut off	*[21]*
Nano crystalline rutile and anatase-TiO_2 thin films	Glass substrate	Pulsed laser deposition	TiO_2, Different substrate temperature	Laser-pulse repetition rate is an important factor for highly efficient photo catalytic TiO_2 thin films	*[22]*
TiO_2–ZnO thin films	Glass substrates	Sol–gel process	Titanium isopropoxide-based and zinc acetate-based precursor solutions	Maximum photo catalytic response by TiO_2 thin films	*[49]*
ZnO/TiO_2 composites	-	Solid–state reaction	ZnO, TiO_2	High/Low values of dc conductivity (10^{-9} – 10^{-5} S/cm) and activation energy (0.13–1.19 eV) were obtained	[50]

2.3 A Brief Review on Resistive Random Access Memory

The first observation that oxide insulator can undergo an abrupt switching event to transit into a conductive state has been reported in 1962 [97]. The device structure is simple capacitor-like metal-insulator-metal (MIM) structure. It indicated that the resistive switching occur in metal-insulator-metal (MIM) structure can be changed by an electrical signal applied on it. In 2004 Samsung has shown NiO memory array integrated with the 0.18 μm silicon CMOS technology [98]. Since then, research activities have been concentrated on binary oxides such as NiOx [99], TiO_x [100], ZrOx [101], ZnO_x [102], HfO_x [103], TaOx [104], AlOx [105] etc., due to the simplicity of the material and good compatibility with silicon CMOS fabrication process. There are two types of resistive switching memory. The first one based on the conductive filaments (CF) of oxygen vacancies (Vo); the other type is based on the CF of metal atoms, which is also called conductive-bridge RAM (CBRAM). The resistance switching behavior attracts broad interest about its memory application from 2004 to present.

Recently, there are many various acronyms to call the memory device which using the resistance switching behavior, such as (1) OxRAM: TMO-based resistive random access memory, (2) ReRAM: Redox-based resistive random access memory, (3) memristor: named by Chua (who predicted the existence of the fourth elementary circuit component with a resistor, capacitor, inductor, and memristor [106] in 1971, and (4) RRAM: resistive (switching) random access memory.

The significant milestone of the improvement of RRAM performance was proposed by Lin et al. in May 2007 [107]. Lin indicated that the resistive switching properties of the RRAM device with binary metal oxide film (the ZrO_2 film was used in his study) can be improved by using an active metal (such as Ti) as top electrode, which can confine the switching reaction region in the interface between top electrode and resistive switching layer. Since that, various high-k dielectric materials or metal oxides with the active Ti as top electrode devices were studied for making high performance RRAM. In 2008, Lee et al. published one paper of using the HfO_2 based RRAM device at the IEDM [108]. As the same concept of the active Ti as top electrode can improve the resistive switching properties, Lee fabricated the HfO2 based RRAM device with 1T1R structure (CMOS compatible) for high performance memory properties. This was another breakthrough in RRAM history, because the HfO2 based

RRAM shows the highly compatible in advanced high-k metal gate (HKMG) CMOS technology. Therefore, RRAM reveals high potential being a main NVM device to replace the currently Flash memory in the future.

This section presents the systematic literature survey for the investigation of resistive switching mechanism, the device structure and the current issues of the resistive random access memory device.

2.3.1 Resistive Switching Mechanisms

A. Charge Transfer

Odagawa et al. reported that the Pt/PCMO/Ag RRAM devices shows its resistive switching is belonging to trapping and de-trapping of carriers (holes), due to the currents of the PCMO-based devices follow the trap-controlled SCLC conduction mechanism [109]. This type of resistive switching mechanism causing by trapping and de-trapping of trap states, and changes in valences, is defined as charge transfer. The resistive switching phenomenon is based on the combined nature in the traps filling and traps de-filling processes caused by strong electron correlation. Moreover, Chen et al. make an effort to explain the resistive switching behavior in the Cu_xO-based system corresponded to carriers trapped and de-trapped in deep level traps [110].

B. Schottky Barrier Modulation

The resistive switching mechanism on metal/perovskite-oxide hetero-interfaces has been modeled on the basis of experiment results. It has been reported that contact resistance resulted from the Schottky barrier formation at the metal/perovskite-oxide interface is altered by bias voltage. The value of the contact resistance is calculated from the Schottky barrier height and the depletion layer width. In addition, the Fermi level lies at the top of the occupied energy level of interface states in a metal electrode while the interface state density is high. Hence, the barrier height and width varies with the net charge in the interface states and an energetic distribution of those in the band gap. At the metal/perovskite-oxide interface, interface states are provided by the existence of oxygen vacancies. According to the viewpoint of the interface-state-induced band bending, application of a high voltage at the metal/perovskite-oxide interface, leads to accumulation (extraction) of a large amount of electrons into (from) the interface states upon reverse (forward) bias. Accordingly, change in the net charge of the interface states will results in a modification of a Schottky-like barrier width and/or height, as the degree of the band bending depends on a net charge in the interface states [111].

C. Oxygen ions migration

Most of resistive switching behaviors are caused by the oxygen ions migration near the interface between the electrode and the resistive switching layer that leads to Schottky barrier [112], and conduction filament [113].

D. Metal ion migration

In solid-state electrolyte, bipolar resistive switching characteristics has been observed when metal electrode is placed in between the range of the electrochemical potential series and formed mobile cations such as Ag^+ and Cu^+. The resistive switching mechanism is explained on the basis of electrochemical redox processes. In the ion-conducting chalcogenide phase, the process of electrochemical formation of metallic filaments is considered as set process, while reset process is activated by dissolution of these metallic filaments. The set process involves the following steps: (1) oxidation of metallic Ag to Ag^+ near the Ag electrode following the reaction $Ag \rightarrow Ag^+ + e^-$, (2) migration of Ag^+ to the Pt electrode because of the potential difference between the Ag and the Pt electrodes, and (3) reduction of Ag^+ to metallic Ag according to the reaction $Ag^+ + e^- \rightarrow Ag$ at the Pt electrode, leading to the formation of a highly conductive filament and the RRAM device switched to LRS. An electrochemical dissolution of the conductive bridges takes place by reversing the polarity of the applied voltage bias, switching the system into the HRS. Therefore, the resistive switching behavior is voltage-polarity dependent [114].

2.3.2 RRAM Device Structures

The architecture of RRAM device is a metal-insulator-metal (M-I-M) structure, in which the insulator often represents the resistive switching thin films. In order to improve the resistive switching properties, several modified RRAM structures have been proposed. According to the present developments, the feasible composed stacks are comprehensively separated into bottom electrode, interface layer-1, resistive switching layer-1, embedded metal, resistive switching layer-2, interface layer-2, and top electrode.

A. Bottom Electrode

The bottom electrode exhibits the effects of the work function, electro negativity, oxygen affinity, the interface reaction, and the inter-diffusion. In addition, the crystallinity and crystal orientation of the resistive switching films are deeply influenced by the bottom electrode which results in the significantly noticeable

resistive switching properties. The bottom electrodes are generally prepared by using novel metals such as Pt, Au, and Ru, which has less reaction and the inter diffusion with the resistive switching films. The activity materials such as TiN, Ti, Al also work as the bottom electrodes and modulate the resistive switching behavior via formation an interface layer near the switching layer, where function as an oxygen reservoir leading to the formation/rupture of the conducting filaments near the interface. However, the activity bottom electrode faces a serious thermal budget issue because that the following high temperature process may lead to the excessive reaction between the bottom electrode and resistive switching thin film [115-116].

B. Top Electrode

Several research reports on the effects of top electrodes on the resistive switching behaviors have been published. The current-voltage (*I-V*) and the capacitor-voltage (*C-V*) curves are used to distinguish between the Ohmic contact and the Schottky contact since the Ohmic contact shows the symmetric *I-V* curve in two voltage bias polarities, but the Schottky contact exhibits the rectifying property causing the difference between the forward and reverse bias currents. The authors determined the I-V curves for Pt/ZnO/Pt device by applying the bias voltage on the top electrode and observed the uni-polar resistive switching behavior. But when the device structure was Ag/ZnO/Pt, then bipolar resistive switching behavior was observed. It may be concluded that switching behavior strongly depends on the electrode materials. The uni-polar and bipolar resistive switching performance are likely bulk-controlled which can be explained by the formation and disruption of the Filamentary [115-117].

C. Resistive Switching Layer

The binary metal oxides such as MgO, ZnO, NiO, TiO_2, ZrO_2, HfO_2 etc., complex metal oxide materials include $Bi_4Ti_3O_{12}$ (BTO), $Ba_{0.7}Sr_{0.3}TiO_3$ (BST), $SrTiO_3$ (STO), $SrZrO_3$ (SZO), $LiNbO_3$ (LNO), $PbTiO_3$ (PTO), and the carrier-doped manganites with the perovskite structure such as $Pr_{1-x}Ca_xMnO_3$ (PCMO), $La_{1-x}Ca_xMnO_3$ (LCMO), $La_{1-x}Sr_xMnO_3$ (LSMO), and $Nd_{0.7}Ca_{0.3}MnO_3$ (NCMO) are used as resistive switching layer. A variety of techniques can be used for the preparation of composite and multilayer resistive switching thin films such as reactive DC sputtering, RF sputtering, sol-gel method, pulsed laser deposition (PLD), atomic layer deposition (ALD), electron cyclotron resonance (ECR) sputtering, metallorganic chemical vapor deposition (MOCVD), plasma-enhanced chemical vapor deposition (PECVD) and

solid-state reaction method. Furnace oxidation and plasma oxidation are proposed to oxidize Zr, Ti, Ni, W, and Cu metallic films into the binary metal oxide films, which are the convenient manners to manufacture the resistive switching films [115-117].

D. Interface Layer

The formation and rupture of the conducting filaments are the most feasible and favored resistive switching mechanism. The conducting filaments are created in the localized high electrical field region and consequently the LRS can be attained and then ruptured due to the reoxidization induced by local Joule heating resulting the device back into the HRS. The formation and rupturing of the conducting filaments within the localized region (3-10 nm thick) near the anode [115-117].

2.3.3 Forming Process

Since the initial resistance of fresh RRAM devices is generally very high, so to trigger the following RS a large voltage is required; this is called the "electroforming" process or "forming" process. The forming process is the common phenomenon in the RS films which is the same as the dielectric breakdown, and then the RRAM device is activated and developed with the RS property. However, the physical meaning of the forming process and the effects of the forming process of the RS mechanism have not been specified yet. There are different forming process for the RS mechanism such as formation of metal islands and the formation of oxygen vacancies [118-119].

2.3.4 Current Issues and scaling ability of RRAM Devices

A. Operation Variation

RRAM can exhibit the outstanding memory reliability such as good memory endurance and long-time data retention. In spite of that, the realization of RRAM is one of the critical issues due to the requirement of minimizing the dispersion of memory switching parameters such as R_{on}, R_{off}, V_{on}, and V_{off}. Here, R_{on} and R_{off} represent the resistance values of the ON- and OFF-states, respectively, and V_{on} and V_{off} are the required voltages for resistive transition from the OFF-state to the ON-state and vice versa. Several methods have been suggested for RRAM to minimize the RS variations. Some of them are (i) reducing active device area by plug-bottom electrode [120] (ii) insertion of IrO_2 buffer layer to stabilize local oxygen migrations [121], (iii) embedding Cr metal layer to reduce the effective RS region [122], (iv) creating locally strong electric field of process control [123].

B. Current Reduction

The crucial drawback of RRAM devices in series with transistor is larger reset current (1-100 mA), which limits the RRAM application combined with CMOS technology, because the allowable channel current of 0.18 μm MOSFET device is too low to switch the memory from the ON-state to the OFF-state. Besides, the larger reset current not only results in unacceptable power consumption, but also leads to serious reliability degradation. In the prior studies, buffer layer is used to reduce the reset current as referred. If the resistive layer and the electrode combinations are well chosen, operation current could be reduced significantly. The operating current is influenced by the material systems deeply [124-125].

C. Device Yield

Device yield is one of the important issues in a forward-moving research of RRAM, deciding whether RRAM application can be realized in future NVM devices. Metal doping into oxides, which might modulate defect distribution and concentration in the RS films, was widely used in the fabrication of RRAM devices for the improvement of device yield. Metal doped binary oxide, such as Al:ZnO, Cu:MoOx, Cu:Al2O3, and epitaxial Al:ZnO, possessed much better device yield than undoped samples [126]. A strong correlation is believed to exist between device yield and defect distribution and concentration in the RS thin films. Therefore, the addition of buffer layer, the surface treatments, and the embedded metal all can enhance the device yield as well.

D. Scaling Ability

Although RRAM shows highly scaling ability, it is interesting to investigate its scaling limit. Several limits have been proposed by Waser [66]. First, scaling limit is imposed by the tunneling distance between neighboring cells together with the leakage current from the word and bit line, again potentially dominated by tunneling. Another limit is due to the lateral extension of the effective switching area, typically the cross-section of the switching filament as mentioned above. These limits are dependent on the class of the RS mechanism. Technologically, the fabrication of effective, dependable and authentic electrode contacts and interconnects is also the scaling limit of the RRAM.

2.3.5 Status of ZnO-Based Resistive Switching Memory Devices

For RRAM applications, ZnO is appearing as a high potential material with its versatile properties and vast applications. A number of investigations have been carried out to study and regulate the switching characteristics of ZnO-based switching memory devices. The effectiveness of ZnO layer with different type of structures, various filament formations, and divergent modes of switching has been reported. The call in question for having ZnO based RRAM is actually of ultra-thin and low power devices. Nonetheless, ZnO not only possess decent memory properties but also has a uniqueness of flexible and transparent nonvolatile memory devices. Table 3.2 demonstrates the switching parameters and performances of ZnO based RRAM device studied earlier.

Table 2.2: Switching parameters and performances of ZnO based RRAM device

Structure	**Switching mode**	**CC (mA)**	**V_f (V)**	**V_R (V)**	**V_S (V)**	**Endurance (Cycle)**	**Retention (sec)**	**Ref.**
Pt/ZnO/Pt	Uni-polar	30	~ 3.3	-1	~-2	100	-	[127]
Ag/ZnO/Cu	Bipolar	-	2.5	~-1.3	~1.3	> 500	-	[128]
Al/ZnO/Al	Uni-polar	1	-	~0.5	~2.5	219	10^3	[129]
Au/Ti:ZnO/ITO	Bipolar	-	FF	~-3	~3	200	$2x10^3$	[130]
Al/IGZO/Al	Bipolar	-	~5	~5	~-5	100	-	[131]
Pt/Co:ZnO/Pt	Bipolar	10	FF	~-1	1.5-3	300	-	[132]
Al/ZTO/Pt	Bipolar	$\sim10^{-5}$	~-2	~1	~-2.5	50	10^4	[133]
Pt/ZnO/ZrO2/Pt	Bipolar	10	~-6.5	-4	~3	100	-	[134]
Pt/ZnLaO/ZnO/Pt	Uni-polar	10	~3.5	~1	~2.3	100	10^4	[135]
Ag/GZO/ZnO/Pt/Ti	Bipolar	10	FF	0.55	0.40	40	$1.1x\ 10^4$	[136]
AZO/ZnO/ITO	Bipolar	10	~3.5	-2	~1.5	10^4	-	[137]
ITO/ZnO/ITO	Uni-polar	15	3.2	1.8	2.6	10^2	10^5	[138]
ITO/IGZO/ITO	Bipolar	10	FF	3.5	~-1	10^2	10^4	[139]

CC= current compliance, V_F= forming voltage, V_S= set voltage, V_R=reset voltage, FF=free forming

2.4 A Brief Review on Solar Cell

A variety of technologies and materials are investigated to fabricate highly efficient solar cell with low cost and high conversion efficiency. The various types of solar cell are shown in fig. Conventional solar cells are generally made from silicon, which includes single/mono-crystalline, and poly/multi crystalline type of structure. At present, solar cells available for residential use are silicon solar cell, which are more efficient and durable than non silicon based cells. But Si based solar cell shows poor efficiency at high temperature. Poly-crystalline silicon solar cells are cheaper to manufacture as compared to mono-crystalline silicon solar cell (efficiency of 18-20 %.) but have less efficiency about 12-15 % [140-141].

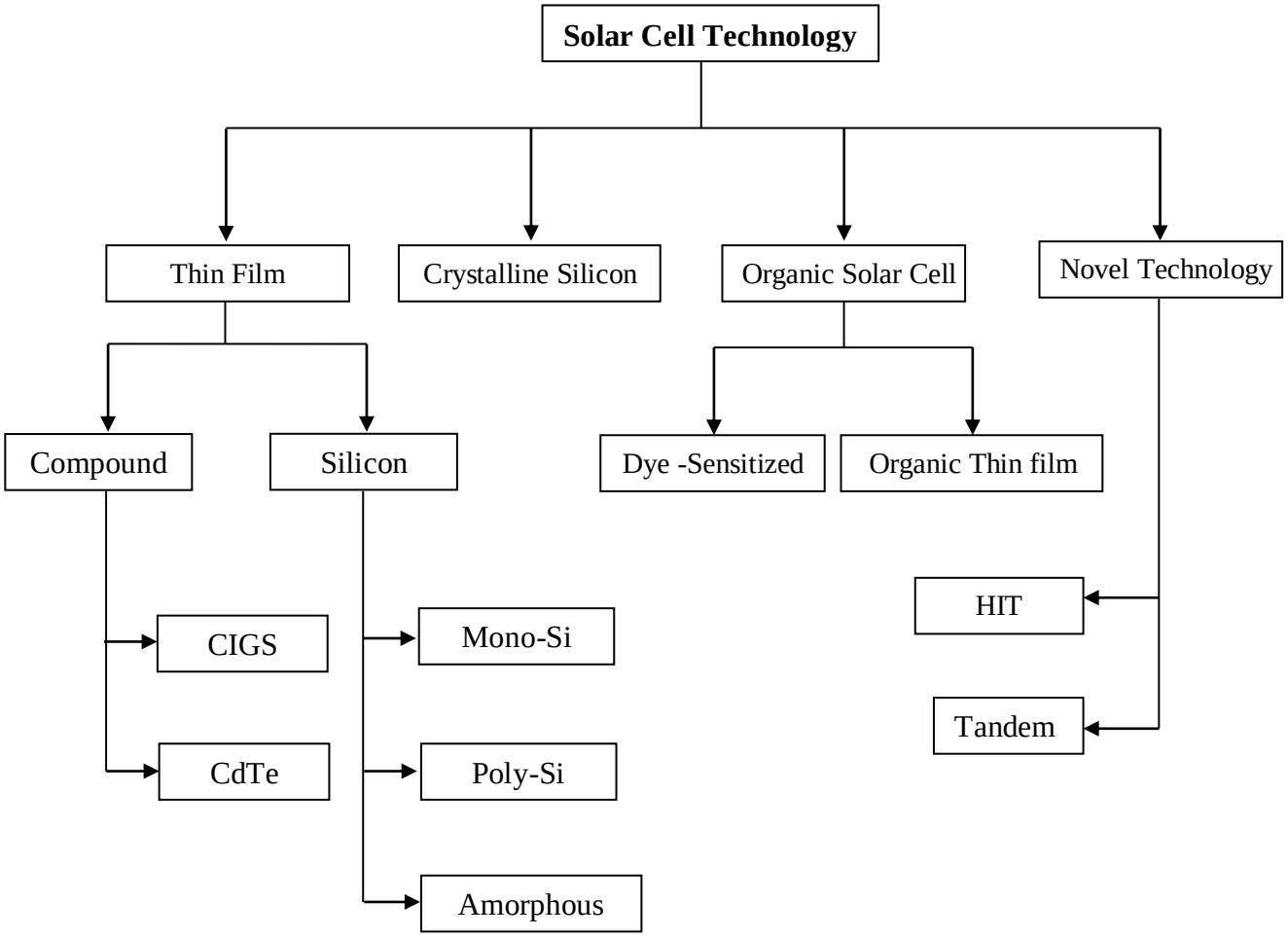

Fig.2.1: Classifications of solar cells

Thin film solar cells, which have multiple layers in each cell which shrinks the losses of current, are proposed for the high conversion efficiency. When the light spectrum endeavor on solar cells, photons get absorbed and converted into electrical energy. Some of the photon doesn't have efficient energy and will be wasted as heat energy [142]. In order to improve the efficiency in next generation solar cell, different buffer layer and absorber layers are used to minimize the energy loss. Most of the thin-film solar cells are fabricated by sandwiching one conducting layer between two glass sheets to make a module. In thin-film technologies, amorphous silicon, cadmium telluride, Copper Indium Gallium Selenide (CIGS) materials are mainly used as an absorbing layer. A literature review of traditional silicon solar cell and thin film solar cells show that CdTe is cost-effective and CIGS are considerably higher efficiency. The maximum output of solar cell is observed for the most favorable energy band gap (E_g) between 1.3-1.6 eV for the absorbing layer. CdTe has band gap near to 1.45eV which is appropriate for optimum output of the solar cell [143-144].

On the basis of this study, we conclude that CdTe solar cells can be used as a future energy resource in the world. The CdTe solar cell is a renewable source of energy and cost efficient. This next generation (hybrid and CdTe) solar cell has many advantages over traditional solar cells. For the fabrication of Tradition (Si solar cell) solar cells very pure silicon is needed. This Si solar cell has a high efficiency compared to next generation solar cells, but the price for fabrication is high because of very pure silicon and due to this price is high compared for unit power output. The objective of this comparative study between traditional solar cell and next generation solar cell is to show that next generation solar cells like CdTe are more cost-effective to be used as a renewable energy resource compared to costly traditional solar cells.

Some of the recent work related to CdTe based solar cell is reviewed and briefly reported as follows:

Hui li et al [145] have studied the effect of temperature treatment on CdS thin film on the performance of n-CdS/p-CdTe solar cell. It has been observed that CdTe film

prepared on CdS thin film with cooling and reheating process had the largest grain size and higher efficiency of a solar cell with a comparison to without treatment of CdS film. *Kai Shen et al* [146] demonstrated that the use of V_2O_5 buffer layer on the Au-back contacts formed the lower Schottky barrier, which improves the solar cell performance. The J-V characteristics, stability with time and band alignment of the reported device is shown in fig.2.2.

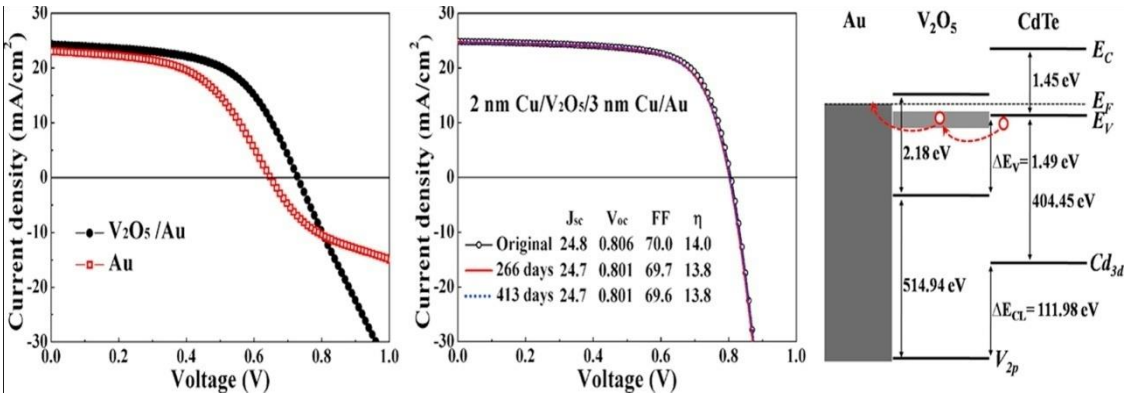

Fig.2.2 : J-V characteristics, stability with time and band alignment of CdTe based solar cell [146]

J. M. Kephart et al [147] have made an effort to improve the performance of the CdTe based solar cell using the SnO_2 and ZnO based high-resistance transparent layer. These HRT layers effectively attached to band alignment of the solar cell. *H. A. Mohamed* [148] theoretically optimized the condition of the CdTe based solar cell. In this study the effect of different layer thickness, i.e. front contact, window layer absorber layer on the solar cell performance has been investigated. *H. A. Mohamed et al.* [149] has also theoretically reported that ZnO and ZnO based alloys is a substitute material of ITO to improve the efficiency of the CdTe based solar cell. The best performance was obtained for Al-ZnO within the studied alloys. *E. Hernandez-Rodriguez et al.* [150] have made an effort to improve the stability of CdTe based solar cells using the TiO_2 buffer layer. TiO_2 buffer layer with 15 nm thickness shows the improved photo response and stability against temperature.

Chen Li et al.[151] have reported a review article on defects in CdTe thin-film solar cells using STEM. The research traces the relations between the structures and electrical activities of individual defects, including intra-grain partial dislocations, grain boundaries and the CdTe/CdS interface as shown in fig.2.3 to fig.2.5.

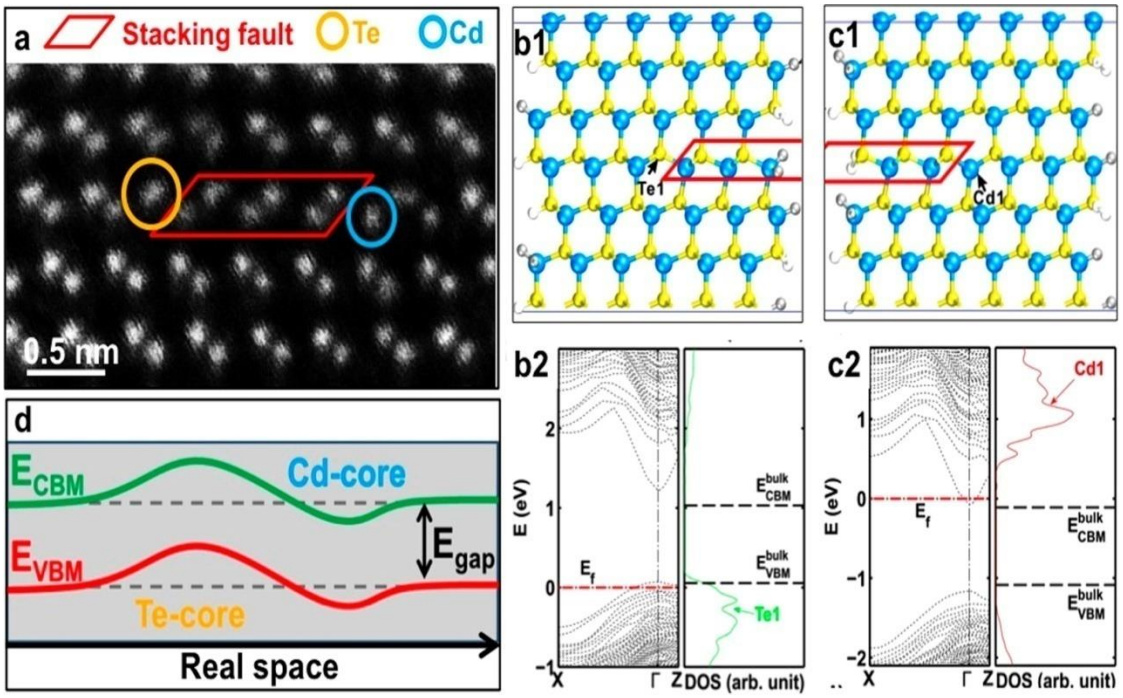

Fig. 2.3. (a) STEM image showing 30° Shockley partial dislocations associated by an intrinsic stacking fault, (b1-b2) Super cells of individual Te core, band structure and DOS,. (c1-c2) super cells of individual Cd core, band structure and DOS [152].

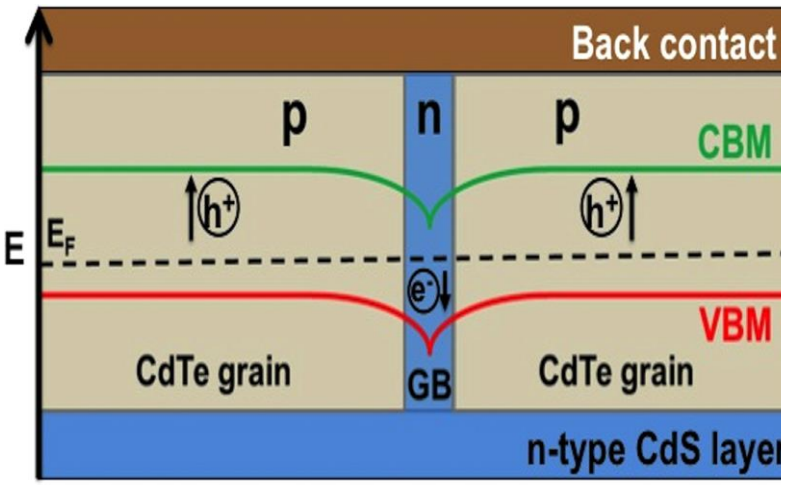

Fig. 2.4: A schamatic p-n-p junction band diagram at the GB [153]

The interpretations of the physical origin underlying the structure-property correlation provide insights that should further the development of future CdTe solar cells.

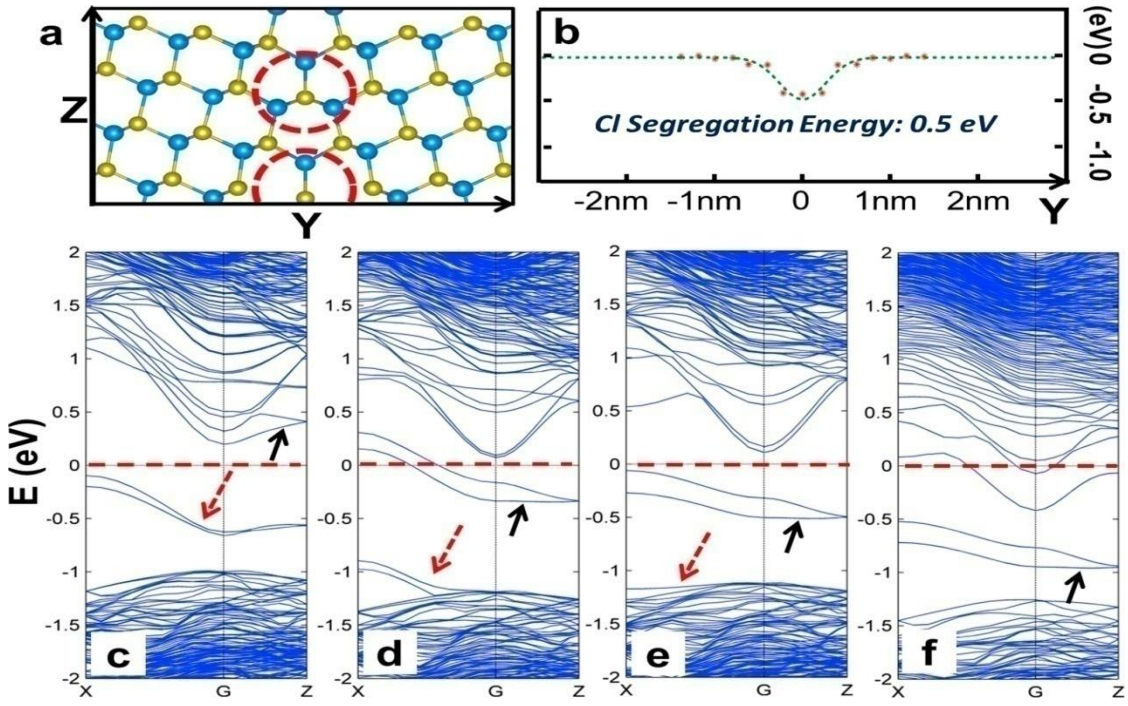

Fig.2.5: (a) Super cell of Cd-core for DFT calculation, which includes two Cd_3Te dislocation cores (red dashed circles). (b) The calculated Cl segregation energy profile. (c-f) The calculated band structures for zero, two, four and five Cl atoms dope in Te sites [153].

Xiaoyan Yang et al. [154] have reported an improved window layer with the use of CdS/Cdse bilayer (thickness of each layer was kept about 70 nm) which was grown using PLD techniques. The best results were observed for the layers which were grown at 400 ^{o}C substrate temperature. *V. V. Brus et al.*[155] studied the CdTe solar cell with graphitic carbon Schottky heterojunction and observed maximum short circuit current density of J_{sc} = 8.47 mA cm^{-2}, an open-circuit voltage of V_{oc} = 0.435 V and fill factor of *FF* = 0.37.

CHAPTER 3

Fabrication and Characterization Techniques

This chapter presents the basic working principle of the deposition techniques that has been used to prepare thin films. It also describes various techniques used for the characterization of thin films, Resistive Random Access Memory and Solar cell.

In order to satisfy the requirements of preparing high quality ZnO thin films, different thin film deposition techniques have been used by researchers in the past. This chapter presents the working principles of Pulsed Laser Deposition (PLD), RF sputtering and thermal evaporation techniques to grow high quality thin films for resistive random access memory and solar cell applications. The basic working mechanisms of various structural, optical, dielectric and electrical characterization techniques such as XRD, AFM, SEM, XPS, I-V and C-V etc. have also been presented.

3.1 Preparation of thin films

Formation/Deposition of thin films consists of three different stages; beginning with nucleation, followed by coalescence and then growth of films; all of which gets changed with varying deposition parameters. The characteristic property of thin films for a particular material varies with the film's real structure which acts as a link between thin films deposition parameters and its properties. Any one of the three growth models for thicker films can occur depending upon interaction energies of substrate and film atoms [156].

A. Layer by layer: In the two-dimensional, adatom-substrate interaction is stronger as compared to interaction between adjacent film atoms, which result in atomically smooth layers, also known as Frank–van der Merwe mode.

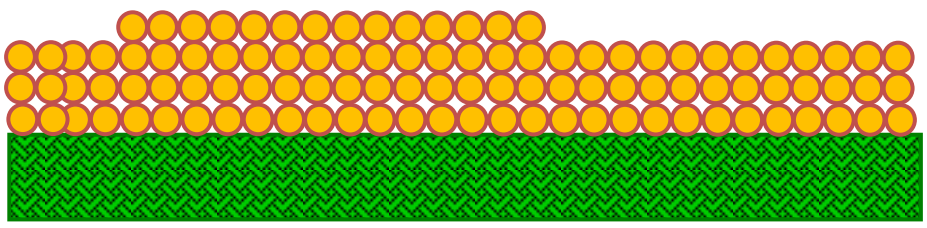

Fig 3.1: Frank-Van der Merwe mode of growth of thin films: Layer by layer growth

B. Islands: In the Volmer–Weber mode, adatom-adatom interaction is stronger than that of adatom-substrate interaction, which results in the generation of three-dimensional adatom clusters or island.

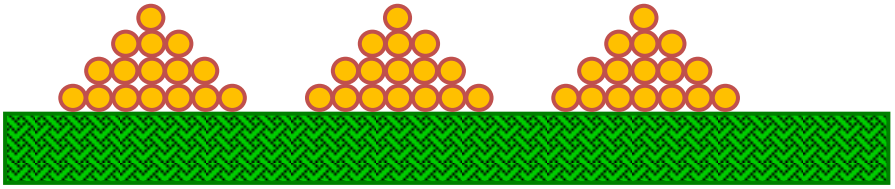

Fig 3.2: Volmer-Weber: Island growth

C. Layer plus islands: Growth is an intermediate process in the Stranski–Krastanov mode, which is further followed by both layer (two-dimensional) and island (three-dimensional) growth. Transition from Frank–van der Merwe mode to Volmer–Weber mode takes place at a critical layer thickness which varies to a large extent with the physical and chemical properties of the film deposited and the substrate used.

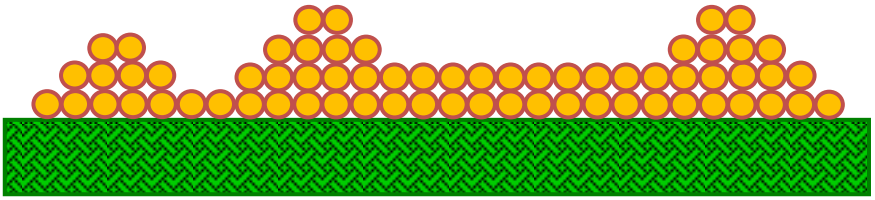

Fig. 3.3 Stranski-Krastanov: layer + island growth

Various chemical vapor deposition (CVD) and physical vapor deposition (PVD) techniques have been applied to fabricate nanocrystalline thin films such as spray pyrolysis [157], sol-gel [39, 81], magnetron sputtering [48], molecular beam epitaxy (MBE) [158], pulse laser deposition (PLD) [84], metal- organic chemical vapor deposition (MOCVD)[83] with each technique having its own specific advantages and disadvantages. The choice of a particular technique generally depends on the requirement of the specific characteristics of thin films or application of interest. If the primary requirement is to get highly uniform composite thin films with a moderate size distribution, then PVD techniques such as laser ablation, magnetron sputtering and evaporation are found to be very efficient whereas for large area deposition, chemical vapor deposition (CVD) techniques such as spin coating and spray pyrolysis technique are found to be more effective. In the present work, Pulsed Laser Deposition

(PLD) and RF sputtering techniques has been employed to deposit functional oxide thin films.

3.1.1 Pulsed Laser Deposition Technique

Pulsed laser deposition (PLD) is used for the growth of high-quality thin films, multilayers and multi-component materials. In 1965, this technique has been for the first time used by Smith and Turner to synthesize dielectric and semiconductors thin films. PLD as a film growth technique has shown a large interest after it has been successfully used to produce superconducting material. Generally, PLD process is comprised of the four steps: (i) laser-target interaction; (ii) dynamics of the target materials removed through vaporization (ablated materials); (iii) deposition of the ablated target materials on the substrate; and (iv) nucleation and growth of thin film onto the substrate surface. Each of the above steps is critical to attain good quality characteristic of the films, i.e. crystallinity, stoichiometry, uniformity, and surface roughness. The most important features of the PLD are as follows:

- The capacity of reproduction of the stoichiometry of the transferred material from the target to substrate, i.e., deposited thin films have the exactly similar chemical composition of the material to be deposited. This happens as a result of the nonequilibrium nature of the ablation process due to high laser energy density absorbed by a small volume of material.
- High deposition rates (~ 100s Å/min) can be attained at a reasonable laser fluence with a good control of film thickness by simply varying the number of laser shots.
- Cost-effectiveness, several vacuum chambers can be arranged around a single laser source and the laser beam can be directed to each chamber just by using different optical assembly.
- Deposition can take place in the presence of both inert and reactive background gases due to the usage of laser as an external energy source.
- Multilayer films can be deposited without breaking vacuum for changing the targets due to use of the carousel.
- It produces a highly forward-directed and confined plume of materials resulting in less contamination during deposition.

Fig. 3.4 shows the different stages involved during interaction of a laser beam with the target material in PLD technique. In the first stage, strong electromagnetic field is generated by laser pulse which removes the electrons from the target material and free electrons starts oscillating within the generated electromagnetic field. A collision between these free electrons and atoms of bulk materials results in the energy transfer from free electrons in the lattice of the target material within the surface region. Heating of the target surface results in vaporization of target material and generation of plasma with a high temperature of about 10^4 K.

In the second stage, because of Coulomb repulsion and recoil from the target surface, the material expands in the form of plasma in a direction parallel to the normal vector of the target surface towards the substrate. The spatial distribution of the plume depends on the background gas inside the PLD chamber. In vacuum the plasma plume is very narrow and forward directed whereas more diffused expansion of the plume can be observed in high background gas pressure. In case of intermediate background pressure, high energy ions get split from the less energetic ones. After the termination of the laser pulse, the plasma expands adiabatically. As, during expansion, conversion of a major part of thermal energy to kinetic energy takes place, no more energy is left for expansion and therefore elongation of plasma in shorter dimensions takes place thereby retaining its profile during the deposition process.

The third stage is important for determination of the quality of the deposited films. The high energetic species ablated from the target bombarding the substrate surface may sputter some of the atoms from the surface and a collision region is established between the incident flow and the sputtered atoms. This collision region serves as a

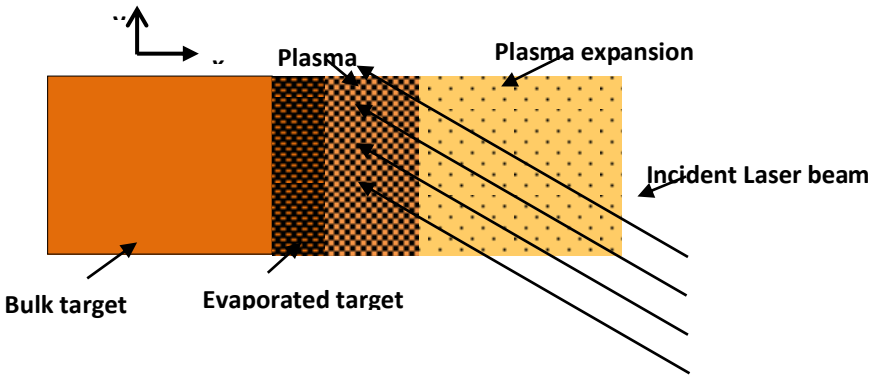

Fig 3.4: Various stages involved during interaction of laser with the target material in PLD technique [159]

source of condensation of particles. At a high enough condensation rate, a thermal equilibrium is attained and the growth of film on the substrate surface takes place at the expense of the direct flow of ablation particles [159].

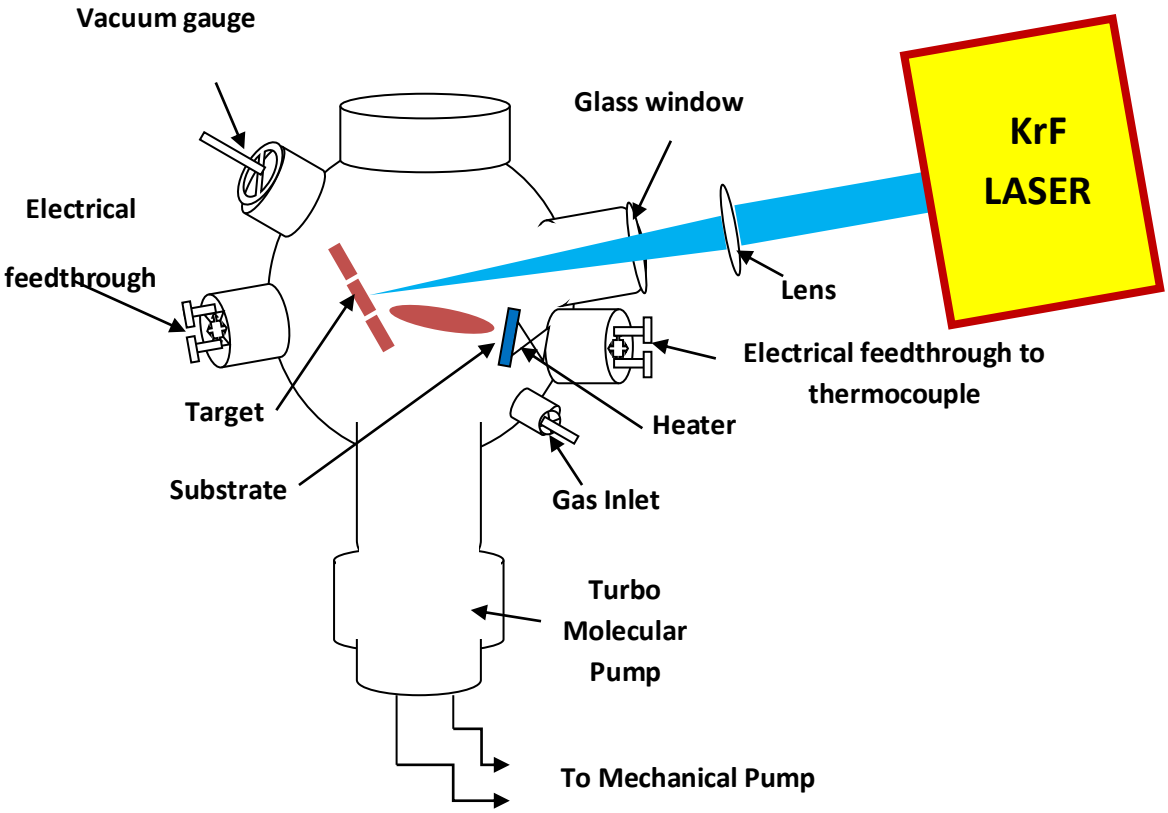

Fig. 3.5: Schematic diagram of the pulsed laser deposition system

Fig. 3.5 shows the schematic diagram of the PLD system. The system assembly mainly consists of an external laser source, a vacuum chamber with inside target, substrate mountings and vacuum pumps for creating low pressure atmosphere and gauges for monitoring the pressure inside the chamber.

The Pulsed Laser System is a COMPex Pro TM manufactured by Lambda Physik Laser Technik using KrF excimer laser source of 248 nm wavelength. The pumps and gauges fitted into the chamber are from Pfeiffer Vacuum. The system chamber is specially designed and developed to overcome the gas leakage and achieve high vacuum in short duration. Target holder is fitted inside the chamber, which can hold six different targets at a time. Circular discs of composite oxides with 15 mm diameter

and 3-5 mm thickness were used as target materials, which were fixed on the target holder. For the fabrication of thin films, the substrates were fixed on a substrate heater (Range: Room temperature - 850 °C) using clips and silver paste. Substrate temperature was maintained using the temperature controller linked with the substrate heater. The target is irradiated by a KrF excimer laser beam. The laser source is operated externally with an automatic laser control machine by fixing the total number of laser pulses required for deposition.

3.1.2 Sputtering

The process of ejecting surface atoms by bombardment of high velocity positive ions (usually inert gas ions), through momentum transfer process between the sputter gas and target atoms is commonly known as sputtering (cathode sputtering). Argon is commonly used as the sputtering gas. The ejected atoms can be made to condense on a substrate at an optimal distance from the target to form a film. Apart of the neutral atoms, charged atoms and electrons are also emitted from the surface. The sputtering yield 'S' (number of atoms ejected from the target surface per incident ion) depends on the target material composition, binding energy, characteristics of the incident ion and the experimental geometry. It also depends on the voltage and current (sputter power) at which sputtering takes place. Schematic of a conventional sputtering process is given in Fig 3.6. The target is connected to a negative voltage supply (cathode) and the substrate holder along with the chamber maintained at a ground potential acts as the anode and faces the target during sputtering. The plasma is maintained between the target and the substrate. The process deals with energy of few tens of eV and hence adhesion of the film on a substrate is better in sputtering.

In sputtering, the entire surface of the target is the source, unlike the evaporation process where a point (where the electron beam hits) on the target is the source. The surface source implies a higher coverage area during deposition as compared to other evaporation techniques. The deposition process in sputtering is not purely ballistic. In sputtering the evaporants bombard the substrate surface, rearrange themselves and then condense on the substrate. The higher kinetic energy of the sputtered particles (~ tens of eV) giving rise to better adhesion to the substrate. Some of the main advantages of sputtering as a thin film deposition technique are due to high kinetic energy of the sputtered atoms, causing their re-distribution on the substrate, leading to (a) high uniformity, density and interface roughness of the deposited film,

(b) deposition over a large surface area. By incorporating target cooling provision in sputtering, higher melting point elements can be deposited. With a better understanding of the sputtering processes, it has become one of the most versatile methods for preparing high quality thin solid films of any material.

The sputtering process is classified as DC or RF depending on the type of power supply used. DC sputtering is generally preferred for conducting materials and RF sputtering can be used for depositing semiconductor and non-conductive materials. In RF magnetron sputtering, the magnets near the target increase the electron travel path which results in many more collisions and hence plasma density increases. In addition to this, magnetic fields near the target traps the electrons in its vicinity and keep the electrons away from the substrate which reduces substrate heating and film damage due to high energy electrons. AC current in RF range prevents the self biasing of the sputtering target which enables the deposition of the insulating films too.

Fig.3.6 Experimental setup of RF sputtering system (Company: Advanced Process Technologies, India).

Sputtering involves many parameters that affect the deposition process such as: base vacuum, sputter gas pressure during deposition (here argon), sputter power, target and substrate temperature, etc. The microstructure of the film or its quality which includes surface roughness, adhesion, impurity, density of the film produced by sputtering process is a result of the interplay of the above parameters. The contribution of such a large number of parameters makes the process complex, but also provides a large degree of control over the film growth process, if optimized properly. Apart from the above parameters the deposition geometry, that is the relative orientation of the target and the substrate, also plays an important role that affects the thin film growth process. Some of the important factors that are important for sputtering are discussed below.

3.1.3 Thermal Evaporation Technique:

Thermal evaporation is one of the popular deposition technique in which electrical energy is used to vaporize the solid material by heating it to a sufficiently high temperature. In thermal evaporation, a high current is passed through the filament/crucible which is generally made-up of metals like tungsten, molybdenum or tantalum so that it can sustain at very high temperature. The selection of the filament/crucible material is dictated by the evaporation temperature and chemical reaction between the material and crucible. Fig.3.7 shows the schematic diagram of the thermal evaporation system. When high electrical current is passed, the material in the crucible gets evaporated and condenses over the substrate in order to form a thin film.
Generally, low deposition pressure in the range of 10^{-5}-10^{-7} mbar is required to avoid the reaction between the vapor and atmosphere. At lower deposition pressure, the mean free path of evaporated material and vacuum chamber has the same order, so that these evaporated particles travel in a straight line from source to substrate. High vacuum is also a necessary condition to obtain contamination free films. Fig. 3.8 shows the experimental setup for thermal vapor evaporation system.

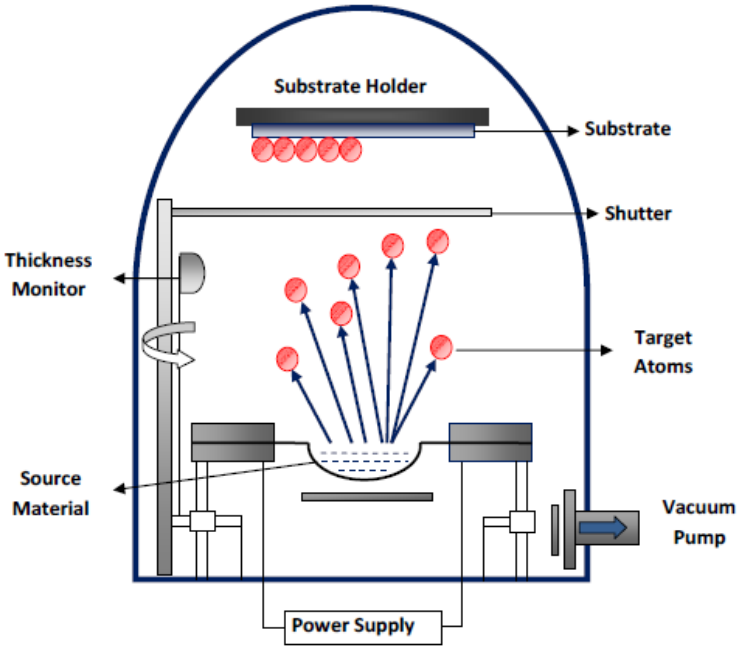

Fig.3.7 Schematic diagram of thermal vapor evaporation technique

Fig.3.8 Experimental setup of thermal vapor evaporation technique (Model: BC-300 HHV).

3.2 Basic structural characterization techniques

3.2.1 X-ray diffraction (XRD)

X-ray diffraction is a non-destructive and most powerful technique for determining the crystal structure, preferred orientation, crystallite size, lattice constants, stress, phase analysis, etc. of solid matter. When X rays, of a fixed wavelength and of the order of interatomic distance of the crystal are incident on a crystalline sample, they get diffracted. In order for constructive diffraction to take place the Bragg's law as given in equation 3.1 must be satisfied

$$2dsin\theta = n\lambda \tag{3.1}$$

Where n is an integer that indicates the order of the reflection, θ is the angle between the incident ray and scattering plane called as Bragg angle, and λ is the wavelength of the X-ray beam.

The structural properties of any crystal can be determined through X-ray diffraction irrespective of it's presence as a pure state or with presence of any other substances as impurities. The XRD data is characterized by intensity of diffracted rays (I) obtained as a function of diffraction angle 2 θ. The peak in the diffraction pattern is obtained depending upon the wavelength of incident radiation and interplanar spacing of the lattice. Quantitative characterization of the sample can be performed through determination of the area under the peaks as the intensity of the diffraction pattern is a function of the concentration of different constituents in the given specimen. Qualitative analysis of any specimen can be performed by identifying the respective diffraction pattern for that specimen. For crystals in the nano range, size is an important parameter, which is obtained using the Scherrer formula

$$t = \frac{0.91\,\lambda}{\beta \cos\theta} \tag{3.2}$$

Where t is the crystallite size in perpendicular direction to reflecting planes, β is FWHM (Full width at half maximum) of the diffraction peak in radians and θ is the Bragg reflection angle. Broadening is XRD peak can also be caused due to strain and other instrumental factors and hence it is important to separate these factors to correctly determine the broadening corresponding to crystallite size [160].

In the present study Bruker D8 Advance X-ray diffractometer (fig. 3.10) used to determine the formation, quality and structure of the samples. The diffractometer uses the monochromatic X-ray (CuK_α = 1.5418 Å) radiation in a wide range of Bragg angle at room temperature. NaI scintillation counters are used as detectors to determine the intensity of the diffracted beam for wavelengths ranging from 0.5 to 3 Å Monochromators, aperture diaphragm was used to improve the quality of diffraction patterns measured as shown in fig. 3.9.

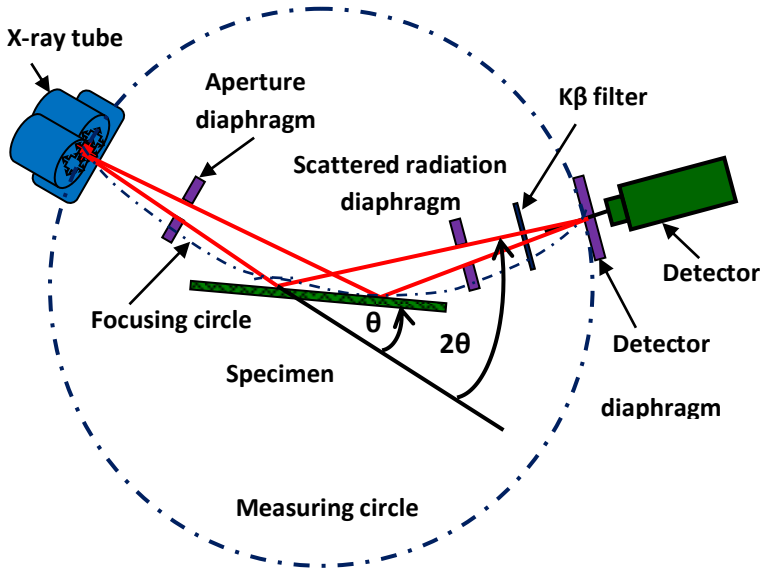

Fig. 3.9: Schematic diagram of beam path in the X-ray diffractometer [160]

Fig. 3.10: Experimental setup of Bruker D8 Advance X-ray diffractometer

3.2.2 Scanning Electron Microscopy (SEM):

When an incident electron beam strikes the specimen composed of a crystalline and amorphous structure, it undergoes a series of complex interactions with the nuclei and electrons of the atoms of the sample (figure 3.11).

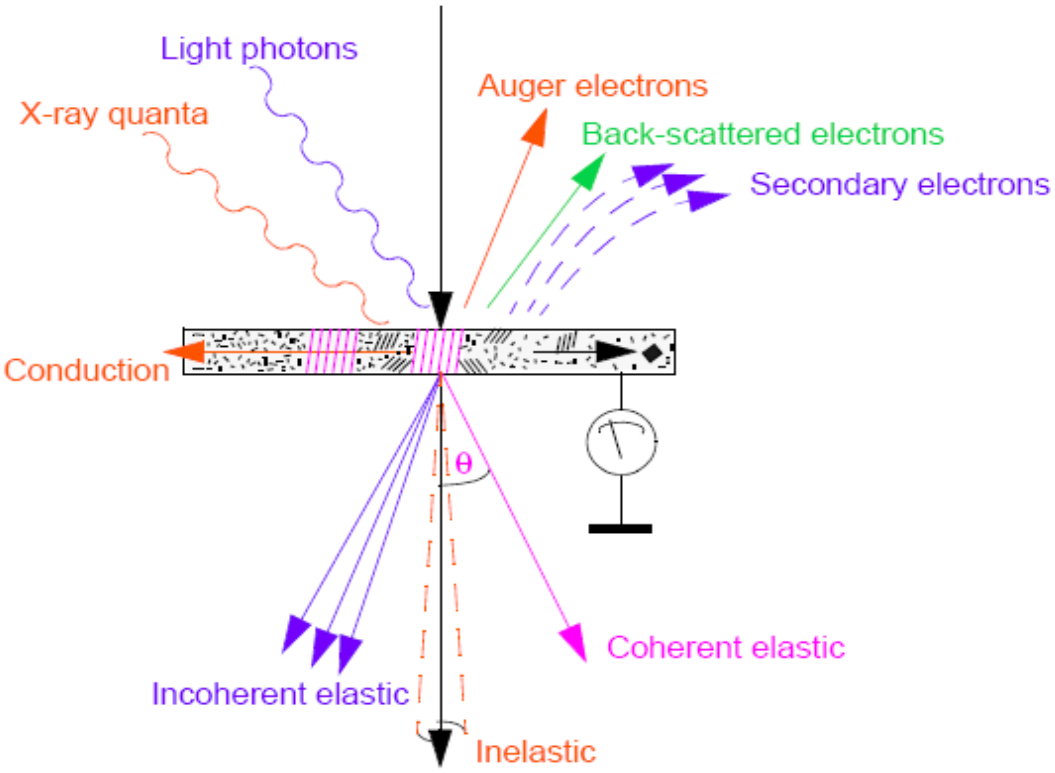

Fig. 3.11: A schematic representation of the various interactions of an electron beam with a solid target [161]

The Scanning Electron Microscope generally produces largely magnified images of deposit films using electrons, so that the surface morphology of the deposited films can be analyzed. Figure 3.12 and figure 3.13 shows the basic working principle and experimental setup of SEM. An electron gun at the top of the microscope is used to produce a high energy electron beam having energy typically in the range of a few hundred eV to 50 keV. The beam travels vertically through the electromagnetic fields and lenses under vacuum to fall over the sample surface. When the focused electron beam strikes the sample surface, X-Rays, secondary electrons and back scattered electrons are ejected from the sample which are collected by detectors and converted into the signals that can be seen at computer screen [161].

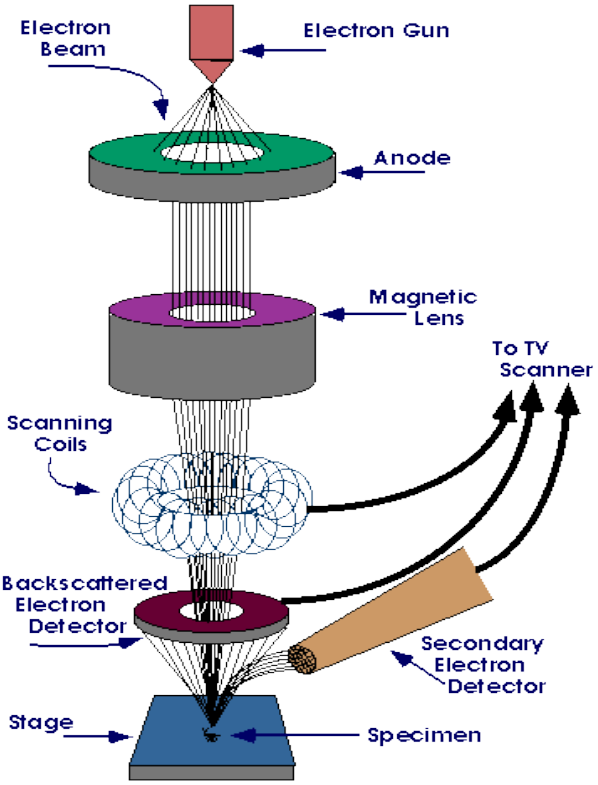

Fig.3.12: Basic working mechanism of scanning electron microscope[161]

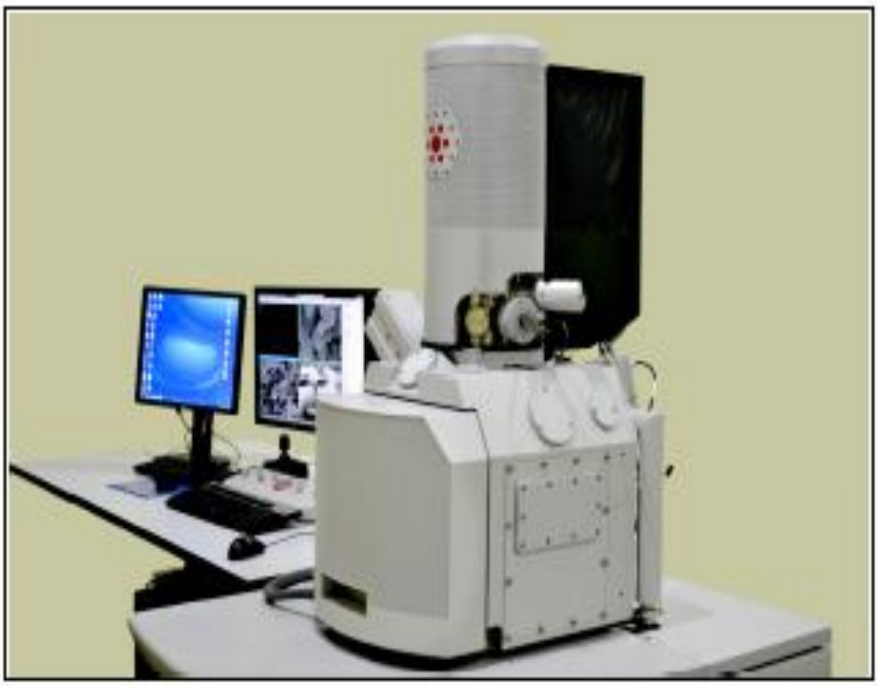

Fig.3.13 Experimental setup of scanning electron microscope (Model: Nova Nano FESEM 450).

3.2.3 Atomic Force Microscopy (AFM)

The Atomic Force Microscope (AFM) is used to obtain surface forces and images at nano and micro level. Fig. 3.14 shows the working principle of AFM. The cantilever spring is attached with standard microscopic tip. The basic working of AFM depends upon the bending of the cantilever spring when some external force is applied. When an adhesive interaction between tip and surface takes place, very sensitive cantilever bending due to surface and tip contact comes into the picture. In order to detect this bending, a laser beam from the laser source is focused on the cantilever that reflects from cantilever and reaches towards the position sensitive detector as shown in fig. 3.14. Depending upon the deflection of the cantilever, the position of reflected laser beam changes. The position sensitive detector senses this deviation and converts this change into electrical signals. The surface imaging of the surfaces in AFM can be done using two measurement methods.

Contact Mode: In contact mode, physical contact between sample and tip takes place. The electronic feedback maintains the resulting deflection at a constant value by changing the Z position and thus the force is measured.

Non-contact mode: In the non contact mode, the tips scans the surface, maintaining a distance of about 50 - 150 Å. The topographic images are constructed by sensing Van der Waals forces between the tip and top surface of the sample.

Tapping Mode: In tapping mode, the cantilever tip is forced to vibrate near the resonant frequency. The vibration amplitude of cantilever decreases with the decreasing distance between tip and top surface of the sample and hence the interaction force between the tip and the surface will shift the resonant frequency. In tapping mode, the surface is scanned in terms of change in oscillation amplitude. The atomic force microscope can achieve a lateral resolution of 0.1-10 nm. Fig. 3.15 shows the experimental setup for atomic force microscope.

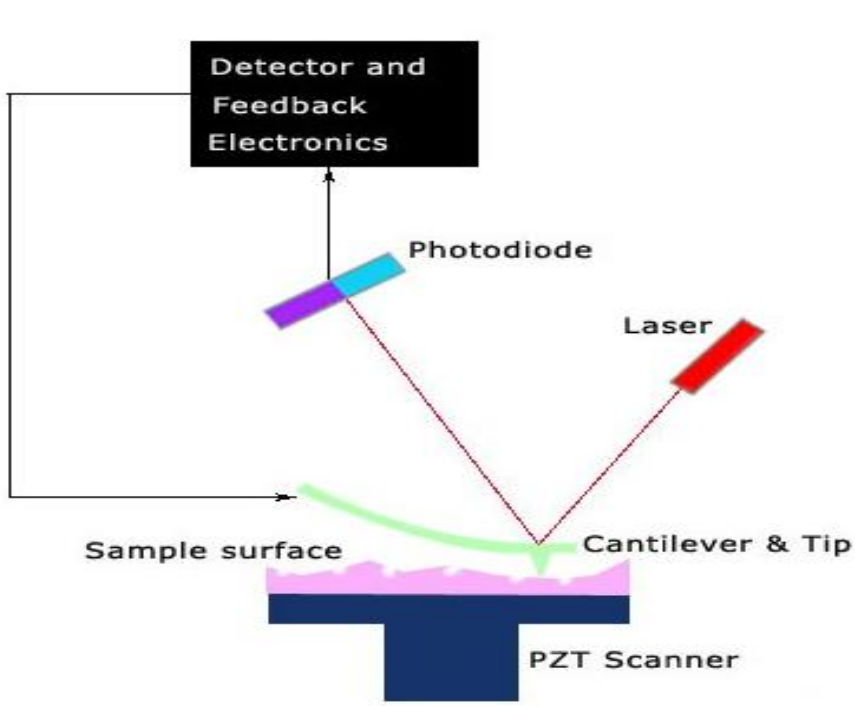

Fig 3.14: Schematic diagram of AFM [161]

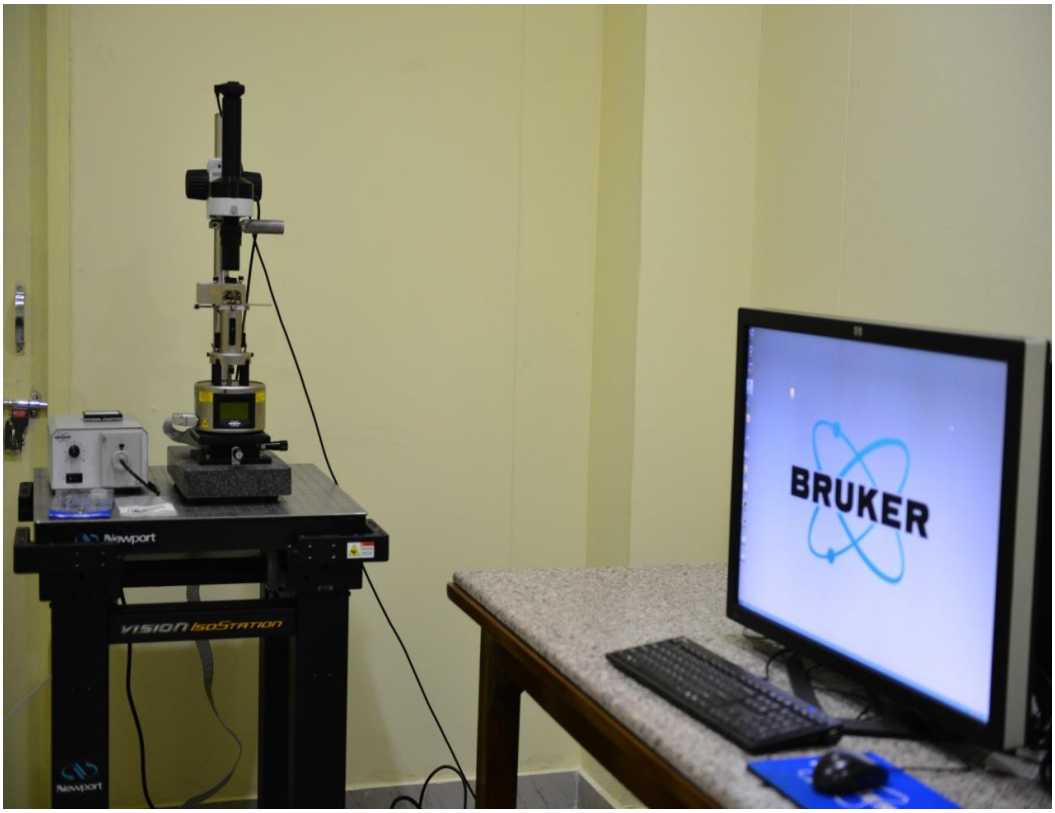

Fig.3.15 Experimental setup of atomic force microscope
(Model: Multimode -8 Scanning Probe Microscope from Bruker).

3.2.4 X-Ray Photoelectron Spectroscopy (XPS)

A primary incident particle (photon) with sufficient energy can knock-out the inner shell electron, and consequently the kinetic energy of the emitted electrons can be measured. According to the following equation, it is possible to determine characteristic electron binding energy from the following relationship:

$$E_{binding} = E_{photon} - (E_{kinetic} + \varphi) \tag{3.3}$$

where $E_{binding}$ is the binding energy of electron, E_{photon} is the energy of incident X-ray photon ($h \cdot \nu$), $E_{kinetic}$ is the energy of measured knock-out electron and ϕ is the work function of spectrometer (not the material). XPS spectrum gives a variation of quantity (number) of detecting electrons with the binding energy of the emitted electrons. Each chemical element produces a specific set of peaks at characteristic binding energy and according to the peaks it is possible to confirm the element's presence in the specimen. These peaks correspond with an electron configuration, for example 1s, 2s, 2p, etc. Based on the physical principles, XPS enables the detection of all elements, but the real X-ray sources are able to analyze the elements from lithium. The measured volume (analyzed depth) is very small, usually around 2-10 nm, depending on the chemical composition and the density of the material. The XPS analysis can also be used for the determination of the chemical and electronic states of the elements that exist within any material. The final spectrum evaluation is not trivial due to the presence of a lot of state effects such as satellite and “ghost” peaks, multiplet slitting, shake-up (and off) satellites, asymmetric (non-) metallic lines, noise, contamination on the top and shifting causes due to the charging or interaction with other electrons (so called chemical shifting).

3.3 Measurement of Optical, Dielectric and Electrical Properties

3.3.1 UV-VIS-NIR Spectroscopy

UV-VIS-NIR spectroscopy provides direct evidence about electron energy jumps between the two distinct energy levels. A large number of phenomena; such as reflection, transmission, diffusion, absorption, refraction, polarization; can take place when a beam of light interacts with a solid. The probability of occurrence of a certain phenomenon depends on the incident beam's angle of incidence with respect to the solid. UV/Vis/NIR spectroscopy makes it possible to estimate the proportion of light reflected, transmitted or absorbed by the specimen within the spectral range between 200 nm and 3300 nm.

In the present study, UV-VIS-NIR spectrometer (Varian Cary 5000 model) has been used for optical characterization of the deposited nanocomposite thin films and multilayers. Figure 3.16 shows the schematic diagram of the optical arrangement of the spectrometer. The spectrometer is equipped with three continuous light sources a mercury lamp for measuring transmission in the NIR range (from 3300 nm to 1100 nm), tungsten lamp for visible range (1100 nm to 320 nm) and a deuterium lamp for the measurement in the ultraviolet range (from 320 nm to 200 nm). The Schwarzschild coupling optics are used which ensures the maximum level of light throughput. They

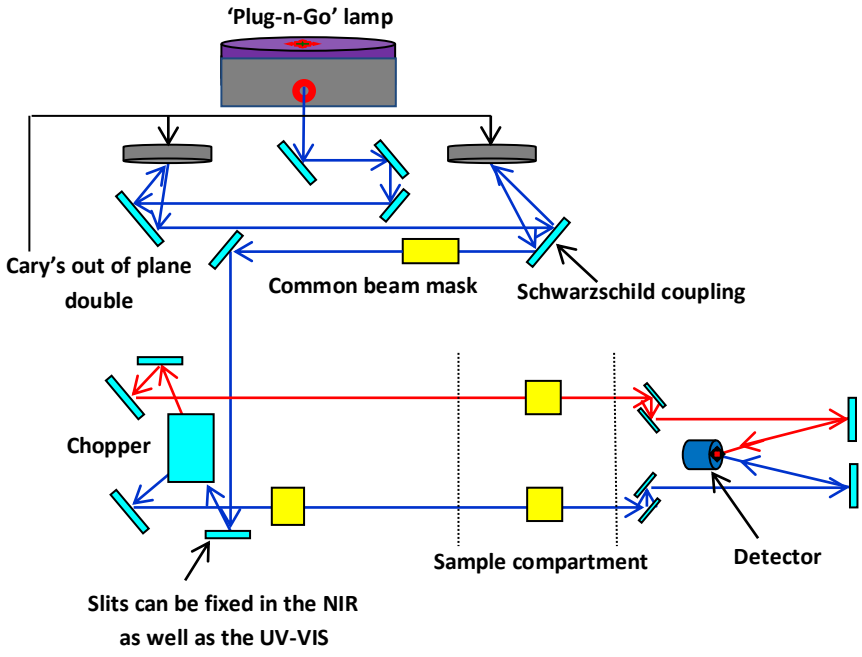

Fig 3.16: Schematic diagram of the optical system arrangement of Varian Cary 5000 UV-VIS-NIR spectrometer

are coated with silica so that they can be cleaned without any damage to the reflective surface. Double holographic grating monochromator are used to minimize the photometric noise and stray light which provide high resolution. The slits can be fixed in the NIR as well as the UV-Visible region. The radiation source and fixing of slit is automatic during monochromator slewing. After passing through the monochromator, the height of the beam is precisely adjusted to match samples of different dimensions by using a common beam mask in the arrangement. The use of chopper provides a switch between the sample and the reference beam. PbS detector is used which provide flexibility in the NIR range. Before loading the sample, we have made zero/baseline correction in the setup. This is done by loading the clean substrate for reference data and black sample to block the beam for baseline data. Then the setup automatically subtracts these data when the film deposited on a substrate is loaded for characterization, thus finally we get the precise data of the thin film. Let I_o defines the intensity of the reference beam with very less or ideally no light absorption and I defines the intensity of sample beam, then for a sample compound which does not absorb given wavelength radiation we have $I = I_o$. For a sample that absorbs given light radiation, we will have $I < I_o$. For such samples Absorption may be presented as $A = \log I_o/I = \log (1/T)$.

3.3.2 Photoluminescence Spectroscopy

Photoluminescence spectroscopy is a contactless, nondestructive method through which electronic structure of the materials can be determined. When a material is irradiated with light of sufficient energy, it absorbs and gains excess energy through a process called photo-excitation. Dissipation of this excess energy can be done with the sample through the emission of light, or luminescence. This luminescence is called photoluminescence. The intensity and spectral content of photoluminescence provide important material information about surface state density and band gap shifting. Two types of spectra can be obtained by PL measurement: (i) photoluminescence-excitation (PLE) spectrum and (ii) photoluminescence spectrum. Measurement of photoluminescence excitation spectrum can be performed by studying the variation of luminescence intensity at fixed wavelength whereas the variation of luminescence intensity as a function of wavelength provides an idea about photoluminescence spectrum.

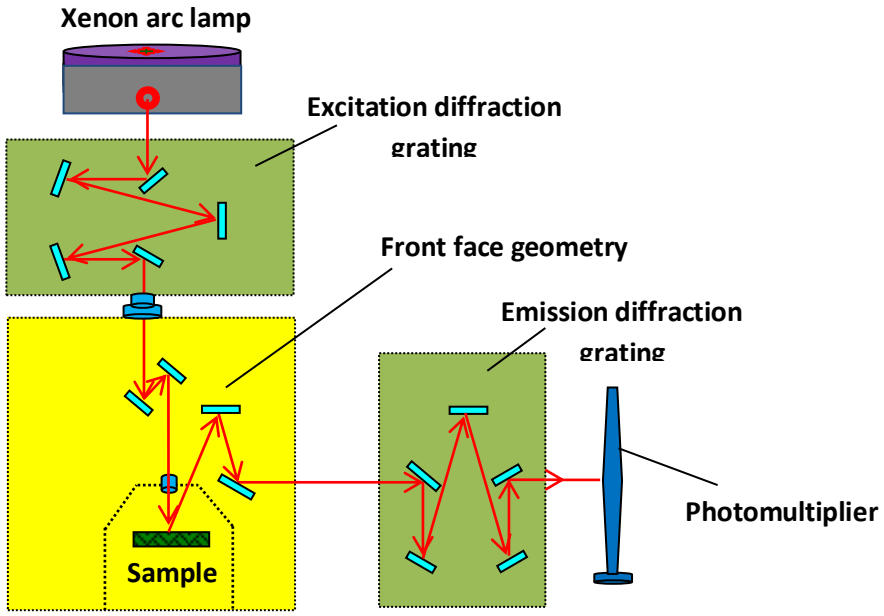

Fig 3.17: Schematic diagram of the PL experimental set-up (Perkin Elmer LS 55 Fluorescence spectrometer)

In the present study, Perkin Elmer LS 55 Fluorescence spectrometer was used to study PL spectra of nanocomposite thin films and multilayers. Figure 3.17 shows the schematic diagram of the PL set-up. Xenon lamp was used as the excitation source in the spectrometer. Excitation diffraction grating was used to select the desired wavelength for the excitation beam. Light from the Xenon arc lamp is monochromatized by the excitation diffraction grating and is incident normally on the sample surface. The emitted PL light is collected to the front face geometry which again monochromatized by the emission side grating and then sent to the photomultiplier and finally recorded by the computer.

3.3.3 Impedance Analyzer

Impedance is an important criteria used for characterization of electronic circuits, components, and the materials used to manufacture components. Impedance (Z) is represented as a complex quantity and defined as the total opposition offered by an electronic component or circuit to the flow of an alternating current (AC) at a given frequency. The quality factor Q, defined as Q = X/R, is a dimensionless quantity. It is defined as the ratio of the energy stored in an electronic component to the energy dissipated by that component and serves as a measure of reactance purity; in other words, how close it is to being a pure reactance with no resistance. Loss tangent, defined as tan δ=R/X, is the reciprocal of Q. The real and the imaginary parts of

impedance can be measured by an impedance analyzer. We have used Agilent 4294A Precision Impedance Analyzer 40 Hz to 110 MHz for the measurement of dielectric properties.

3.3.4 Electrical Analysis of RRAM Device

The RS properties of various combinations of the electrodes and the memory films are characterized by the semiconductor parameter analyzer (Agilent B1500A) and the pulse pattern generator (Agilent 81110A) with a low-leakage switch mainframe (Agilent E5250A) to switch the input and output signals. All the above measurement instruments are controlled by a computer with the assistant of the Agilent VEE software. During the electrical analyses, the voltage source is applied to the top electrode with the bottom electrode common. Fig. 3.18 shows that the measuring schematic diagram of the combination of the Agilent B1500A, E5250A, and VEE software, which is used to measure current-voltage (I-V) curve, data retention time, endurance, and nondestructive readout properties. Fig. 3.18 depicts the combination of the Agilent B1500A, 81110A, E5250A, and VEE software, which is employed to perform the electrical-pulse-induced resistance (EPIR) change phenomenon and the electric pulse endurance measurement.

A. Current-voltage Measurement The current-voltage (I-V) characteristics of various combinations of electrodes and memory films are performed by Agilent B1500A. The RS phenomenon is that the resistive state of the memory device can be altered by applying a specific voltage, which is reproducible. While switching the device from OFF-state to ON-state, a large current pass through the RRAM device and a current compliance is imposed on the memory device to prevent the electrical damage. In addition, the relevant conduction mechanisms in insulator, listed in table 2-1, are studied by analyzing I-V characteristics, which can help to reveal the corresponding physical meanings. The conduction mechanisms in the different memory states are also discussed to elucidate the origin of the RS mechanisms.

B. Data Retention Time Measurement The data retention time is the time of the stored information which can be kept without any power supply. In this dissertation, the retention time of the memory device is measured by Agilent B1500A. First, two identical devices were switched to different memory states, respectively. After a specific period, a small voltage, cannot change the current memory states of the device, is applied to read the current to calculate the resistance value of the memory

states. The data retention time measurement is performed in a dry environment at room temperature or at higher temperature to perform the thermal acceleration test.

C. Nondestructive Readout Measurement The nondestructive readout, measurement of the memory devices is demonstrated by Agilent B1500A. Various memory states of the devices are obtained by sweeping DC voltage bias or applying an electric pulse. Subsequently, a dc voltage bias is applied on the device to read the current of various memory states over 10^4 s at room temperature or at 85 ^oC. Based on the experimental results, the maximum read times and the stability of the memory states can be estimated.

D. Endurance Measurement The endurance is the number that a memory device can be stably operated among various memory states by sweeping voltage bias or applying a voltage pulse, and the endurance cycle with excellent stability is expected to be as large as possible. Endurance measurement by sweeping voltage bias is achieved by Agilent B1500A, and that by applying a voltage pulse is achieved by the VEE program, Agilent B1500A, 81110A, and E5250A.

3.3.5 I-V measurement and Solar Simulator

Solar Simulators are used to provide illumination approximating natural sunlight. It basically provides, under laboratory conditions, a controllable indoor test facility used for the testing of solar cells. A solar simulator generally consists of three main components (i) source(s) of light (ii) associated power supply; (iii) optics and filters for modification of the output beam to match the classification requirements. In our measurements we have used Xenon Lamps as a light source with AM1.5 filter. The xenon lamp allows the design of an optical system that produces an intense, collimated beam as shown in Fig.3.18. Keithley electrometer 6517A is used to measure of I-V characteristics of the solar cell.

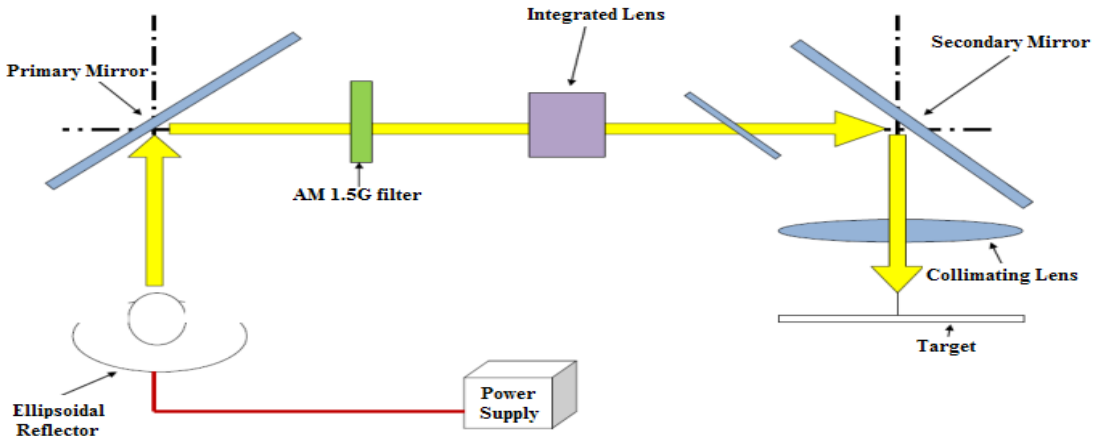

Fig. 3.18: Working principle of a 1 Lamp Solar Simulator, using a Xenon short arc lamp

CHAPTER 4

Structural and Optical Properties of Pulsed Laser Deposited ZnO/TiO_2 and TiO_2/ZnO Thin Films

In this chapter structural and optical properties of pulsed laser deposited ZnO/TiO_2 and TiO_2/ZnO thin films has been reported. An effort has been made to improve the quality of ZnO and TiO_2 thin film using a buffer layer of TiO_2 and ZnO, respectively. The pulsed laser deposition technique was used for the preparation ZnO and TiO_2 thin films on Si (100) substrate at room temperature. Structural and optical properties have been investigated and it has been observed that the crystallinity and photoluminescence spectra of ZnO and TiO_2 considerably improved by using TiO_2 and ZnO buffer layer, respectively.

4.1 Introduction

ZnO is suitable and potential candidate for the fabrication of light emitting devices and the future electronic devices due to its large binding energy of excitons (60 meV) and wide band gap (3.37 eV) [31]. ZnO thin films have an important role in solar cells, solid-state display devices, and exciting acoustic waves at microwave frequencies [162]. Consequently, for the design and analysis of various optical and optoelectronic devices using ZnO, it is desirable to have the precise understanding of the structural and optical properties of ZnO. The structural and optical properties of ZnO thin films depend on the fabrication methods, pre and post deposition temperature treatment, type of substrate material etc. TiO_2 thin films have good photocatalytic behaviour [42], high refractive index [40], and high transparency in visible light [43], due to which TiO_2 thin films have been widely studied. In addition, TiO_2 thin films have good thermal stability and high dielectric constant, which make it appropriate for capacitors in microelectronics, high-density dynamic-memory devices, insulated gate in MIS structures, etc. in Si devices [163]. Furthermore, it has also been reported that when the crystallinity of dielectric film increases, its dielectric constant increases and smooth film surface leads to the decrease in leakage current. Many researchers have studied the ultraviolet and visible region emission properties of TiO_2 thin film. It is reported that the exciton related recombination process is dependent on the structural imperfection and defects. So it is essential to fabricate high quality films for high

efficiency solar cell applications. TiO_2 thin films have been deposited using different techniques like, aerosol pyrolysis, molecular beam epitaxy, sol–gel method, chemical vapour deposition, and electro-deposition technique. The investigation of the influence of various substrates such as Si (100), glass and ITO coated glass has also been studied.

Above all, the choice of substrate is very important for the fabrication of the thin film because the crystal growth behaviour of the film is strongly depends on the matching in lattice parameters between the film and substrate. When metal oxides thin film e.g. ZnO, TiO_2 thin films are prepared on Si substrates at high temperature or it has been treated with high annealing temperature, It has been observed that Si atoms available at surface easily capture oxygen atoms from ZnO thin film [164], which reduces oxygen atoms in the films or increases oxygen vacancies and as a result the quality of the ZnO thin films become poor.

Therefore, it is supposed that the use of single or multi buffer layer between ZnO film and Si substrates may improve the quality of thin films. Some research groups have reported high quality ZnO thin films grown on homo ZnO buffer layer and CaO buffer layer [3]. The choice of buffer layer material depends on the value of lattice parameters, thermal expansion coefficient and physical properties. Here, we have chosen TiO_2 as a buffer layer material for ZnO thin film and vice versa, based on the considerations that both TiO_2 and ZnO are wide-band-gap materials, both have high refractive indices, high chemical and thermal stability, high transmittance in the visible region, intense absorption in the ultraviolet band, abundant and low cost, suitable used in actual production.

4.2 Experimental Details

4.2.1 Thin Film Preparation: The targets of ZnO and TiO_2 were prepared using 99.99% pure ZnO and TiO_2 powder as the starting materials (Loba Chemie, India), respectively. ZnO and TiO_2 powder were grounded for 24 h and then calcined at 400 ^{0}C for 12 h. The calcined powder was reground for 6 h and was then pressed into pellets of 15 mm in diameter and 2 mm thickness under the pressure of 90 MPa. Then, the pallets were sintered at 800 ^{o}C for ZnO and 1000 ^{o}C for TiO_2. The Si (100) substrates were cleaned sequentially with a diluted HF solution, distilled water and acetone. ZnO thin films have been deposited on different substrate using pulsed laser

deposition (PLD) technique employing a KrF laser source (λ=248 nm). The thickness of the grown film is typically ~200 nm and buffer layer thickness is ~50 nm, which is confirmed using a surface profilometer. The pulse repetition rate was 10 Hz with laser fluence of about 2–3 J cm^{-2}. The target to substrate distance, working O_2 pressure and deposition temperature were kept 35 mm, 50 mTorr, and 500 ℃ respectively. The thickness of the grown film is typically ~200 nm which is confirmed using the surface profilometer.

4.2.2 Thin Film Characterization: The phase and orientation of as-grown thin films were characterized by X-ray diffractometeter (XRD, Bruker AXS D-8 Advance Diffarctometer) using CuK_α (λ=1.5407 Å) radiation. The surface topography and microstructure were examined by atomic force microscope (NTMDT: NTEGRA model). Photoluminescence study in the wavelength range 200 nm to 800 nm was done using Perkin Almer LS-55.

The facility of pulsed laser deposition technique and characterization techniques provided by functional nanomaterials research laboratory (FNRL), IIT Roorkee and Materials Research Centre, MNIT Jaipur.

Table 4.1: Parameters used for the thin films preparation using PLD technique

Target used	:	ZnO, TiO_2
Laser source	:	KrF eximer source
Laser wavelength	:	248 nm
Laser fluency	:	2-3 J-cm^{-2}
Laser energy	:	300 mJ
Repetition rate	:	10 Hz
Gas used	:	High purity oxygen (99.7%)
Base pressure	:	2×10^{-6} Torr
Background pressure	:	50 m Torr
Substrate used	:	Si (100)
Target to substrate distance	:	35 mm

4.3 Results and discussion

4.3.1 Effect of Buffer Layer on Structural Properties

XRD pattern shows that ZnO thin film grown on Si (100) substrate was preferentially oriented along the c-axis with a hexagonal wurtzite structure and the use of TiO_2 buffer layer increases crystallinity along (002) diffraction peak as shown in fig.4.1. On the other hand, TiO_2 thin film exhibit pure anatase phase and crystallinity was improved along (200) plane by inserting the ZnO buffer layer between substrate and TiO_2 thin film.

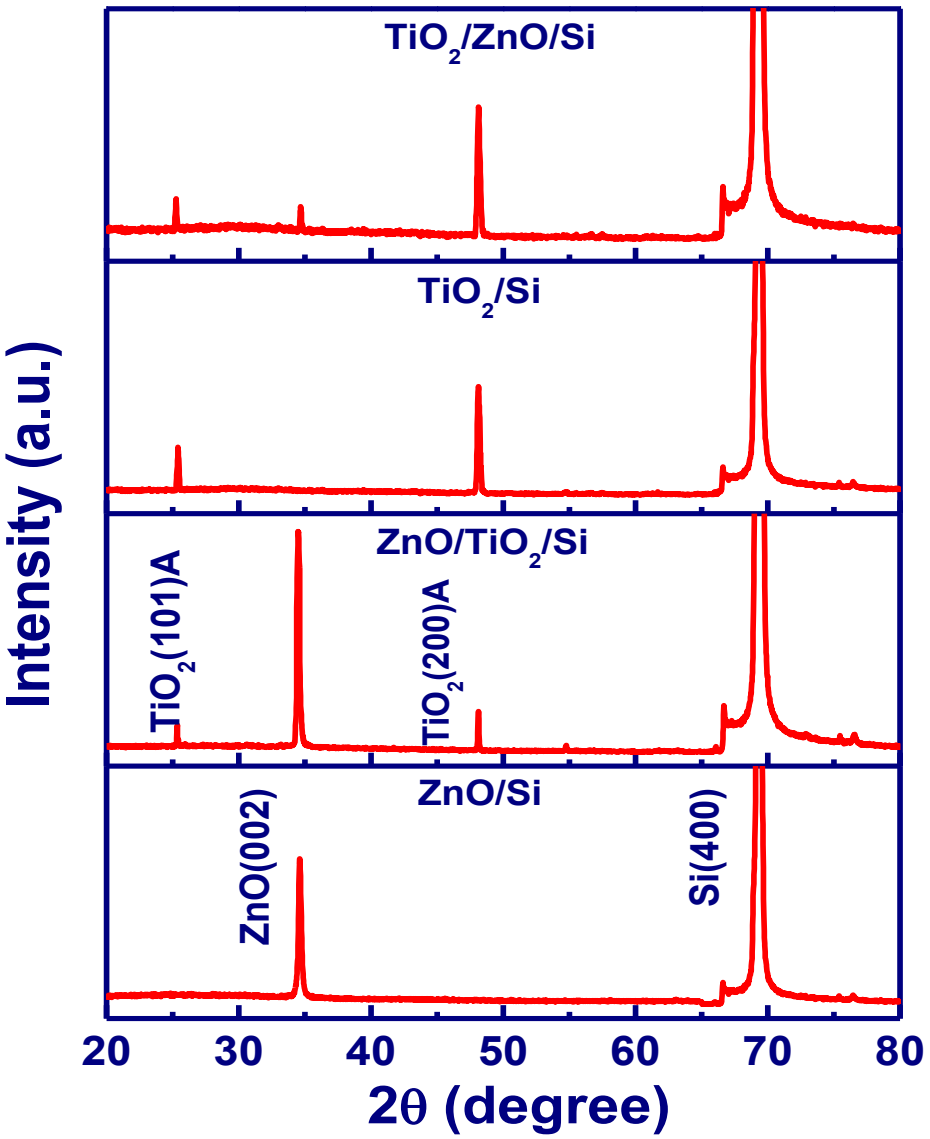

Fig.4.1: XRD pattern of ZnO and TiO_2 thin films

The improved crystallinity of thin film using buffer layer resulted from the mismatch in thermal expansion coefficient between TiO_2 and ZnO, which is smaller than that of between ZnO and Si or TiO_2 and Si. The lattice mismatch between substrate Si (100) and ZnO is 40%, whereas for their counterparts i.e. between anatase-structured TiO_2 and ZnO is 14%. As a result, the decrease of lattice mismatch is an additional reason for the improved crystallinity.

The crystallite size of these samples was calculated using the following Scherrer's expression [165]:

$$t = \frac{0.91\,\lambda}{\beta \cos\theta} \tag{4.1}$$

where λ= wavelength of x-rays (1.5407 Å), β = Full width at half of the maximum peak (FWHM), θ = Angle of maximum intensity. The crystallite size of the samples calculated along the (101) orientation for TiO_2 and along the (002) orientation for ZnO thin films using Scherrer's formula is shown in Table 4.2.

The lattice parameter is calculated using the following formulas:

Hexagonal:
$$\frac{1}{d^2} = \frac{4}{3}\left(\frac{h^2+hk+k^2}{a^2}\right) + \frac{l^2}{c^2} \tag{4.2}$$

Tetragonal:
$$\frac{1}{d^2} = \left(\frac{h^2+k^2}{a^2}\right) + \frac{l^2}{c^2} \tag{4.3}$$

where h, k, l are miller indices of crystal planes and d is the spacing between adjacent planes. For a lattice spacing d value, the h, k, l value can be found by comparing with standard data and then by using above equation a and c can be calculated.

The strain along the *c* axis, ε_{zz} is given by the following equation [166]:

$$\varepsilon_{zz} = \frac{(c-c_0)}{c_0} \times 100\ \% \tag{4.4}$$

where c_0 is the lattice parameter of unstrained ZnO, *c* is the lattice parameter of the strained ZnO films, calculated from X-ray diffraction data . According to the above equation the strain can be negative (compressive) or positive (tensile). ε_{zz} values are calculated using the equation (4.4) and are summarized in Table 4.2.

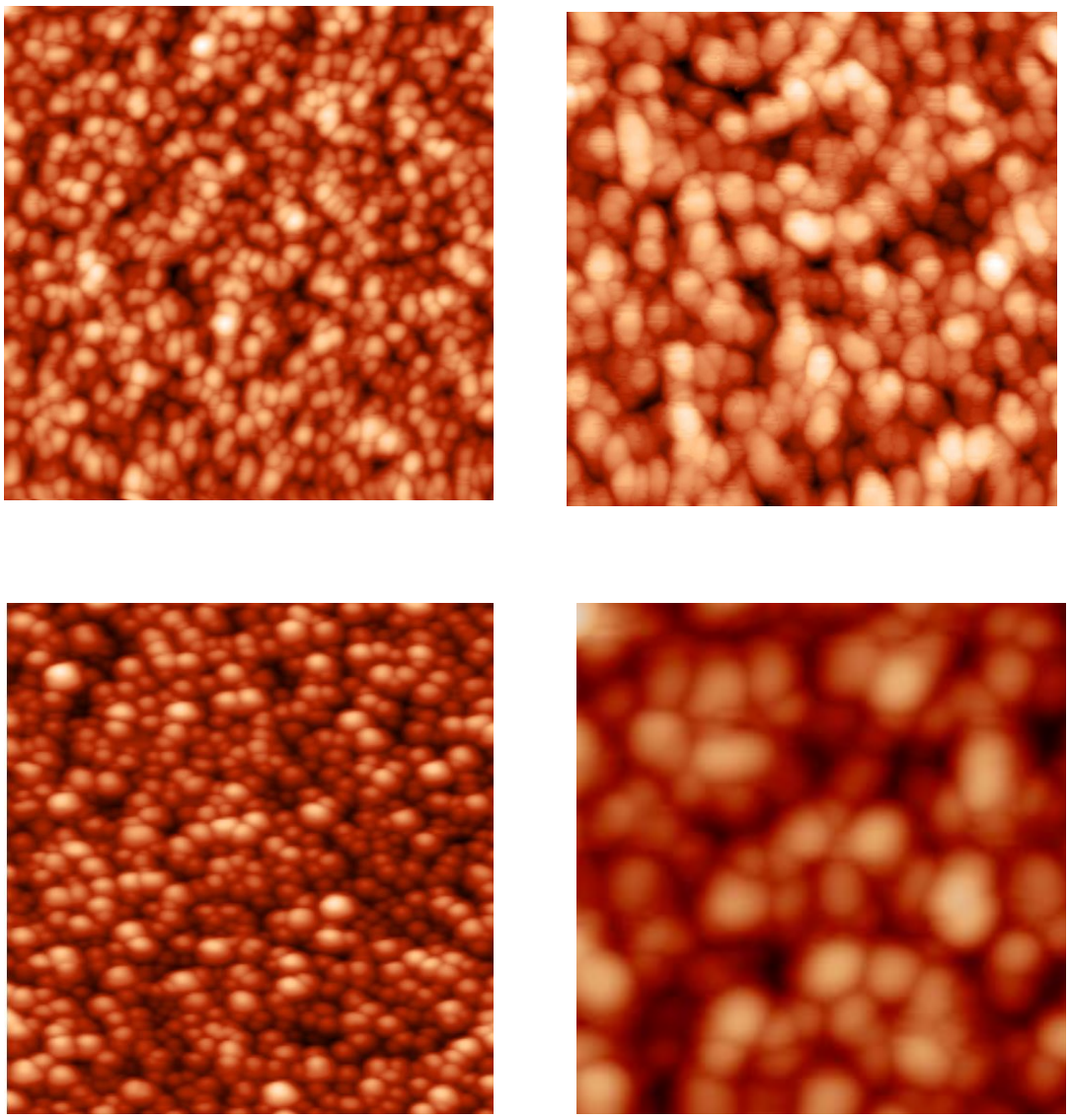

Fig 4.2: AFM images of the ZnO and TiO_2 thin films prepared by PLD

The lattice mismatching between the film and substrates, results in the stress in the thin films which arises during the growth process. The numerical values of stress can be camputed by the following formula:

$$\sigma = \frac{2c_{13}^2 - c_{33}(c_{11}+c_{12})}{2c_{13}} \times \frac{c-c_0}{c_0} \qquad 4.5\ (a)$$

$$\sigma = -453.6 \times 10^9 \times \frac{c-c_0}{c_0} \qquad 4.5\ (b)$$

$$\sigma = -282.76 \times 10^9 \ \frac{c-c_0}{c_0} \qquad 4.5\ (c)$$

where c_{ij} is elastic constant, c_0 is the lattice constant of bulk and c is the lattice constant of thin films.

Table 4.2: Various calculated parameters of ZnO and TiO_2 thin films using XRD and AFM

Sample	FWHM (β) (degrees)	Crystallite size (nm)	Lattice-constant (Å)	Strain (x 10^{-2})	Stress (10^9 N/m^2)	Grain size AFM (nm)	Roughness (nm)
ZnO	0.256	32.02	5.182	0.442	2.00	68	6
ZnO/TiO_2	0.236	35.31	5.198	0.127	0.69	94	8
TiO_2	0.318	25.57	9.427	0.792	2.24	82	5
TiO_2/ZnO	0.287	36.36	9.472	0.319	0.902	162	9

The lattice mismatch between the film and substrates can result in varying degrees of stress during the growth process of thin films. The results show that the compressive strain is present in all fabricated ZnO and TiO_2 films, which is derived from a lattice mismatch between substrates and films owing to increase in crystallite size, and the stress is decreased with the buffer layer. Fig. 4.2 shows the AFM image of the deposited thin films. The grain size and average surface roughness increases when buffer layer is used due to enhancement in crystallinity.

4.3.2 Effect of Buffer Layer on Optical Properties

Fig. 4.3 shows the room temperature PL spectra of ZnO and TiO_2 thin films grown on Si substrate with and without buffer layer. The ZnO film deposited on Si (100) substrate exhibits a strong ultraviolet emission peak along with weak green–yellow emission band. The ultraviolet emission of ZnO films is generally considered to be resulted from recombination of free exciton, whereas the green emission is mainly resulting from oxygen vacancies. The PL spectra of TiO_2 thin film deposited on Si (100) substrate shows a broad emission band from 390 to 450 nm and there are two emission peaks superimposed on the broad emission band. The peak before 350 nm (~3.5 eV) is ascribed to direct electron-hole recombination, which should be equal to or slightly bigger than the TiO_2 band gap. The emission band from 390 to 450 nm

(corresponding to 3.2–2.75 eV) arises from indirect band gap and surface recombination processes. Further observation indicates that there are two small peaks in the wavelength range from 460 to 500 nm. These PL signals are attributed to excitonic PL, which mainly result from surface oxygen vacancies and defects of the films.

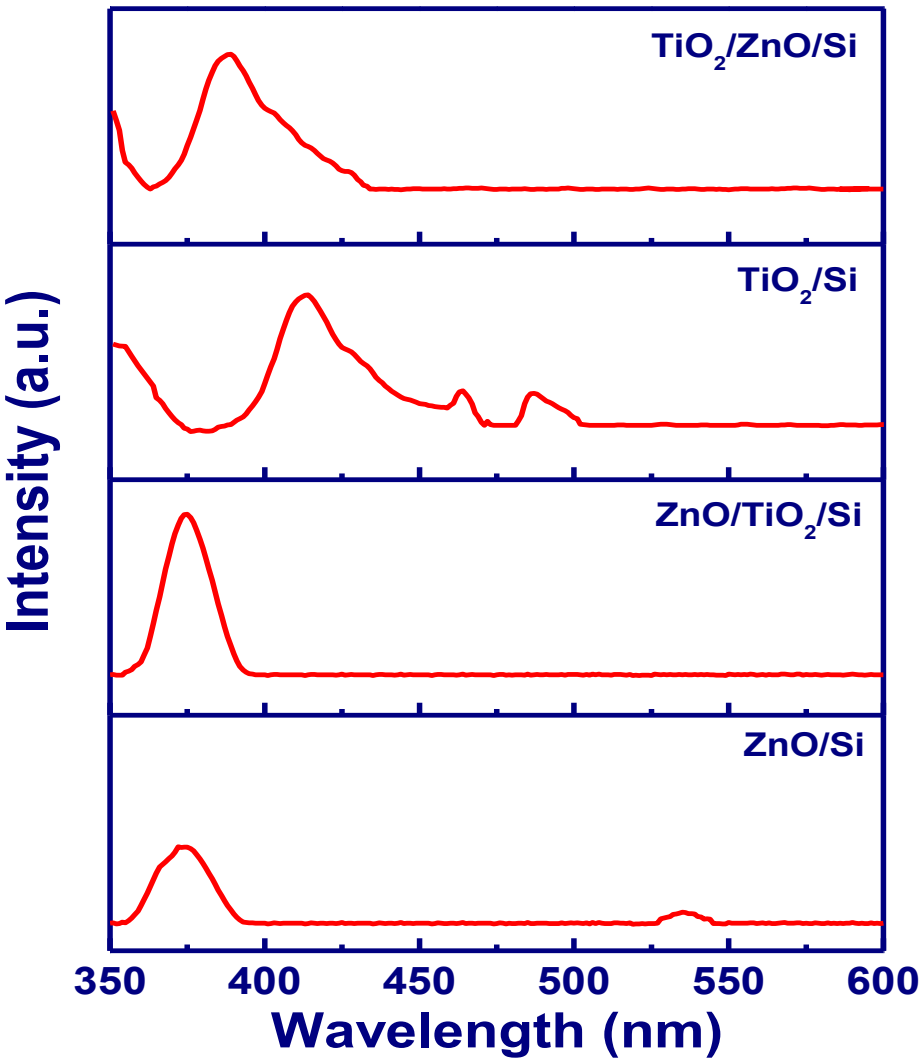

Fig. 4.3: Room temperature photoluminescence of thin films deposited on Si (100) substrate

It is observed that ZnO thin film deposited on the TiO_2 buffer layer shows stronger ultraviolet emission, as compared to ZnO thin film grown without buffer layer, with no visible emission. The absence of visible emission shows the defect free formation of film. Similarly, the use of ZnO buffer layer also removes the oxygen defects emission peak of TiO_2 thin film.

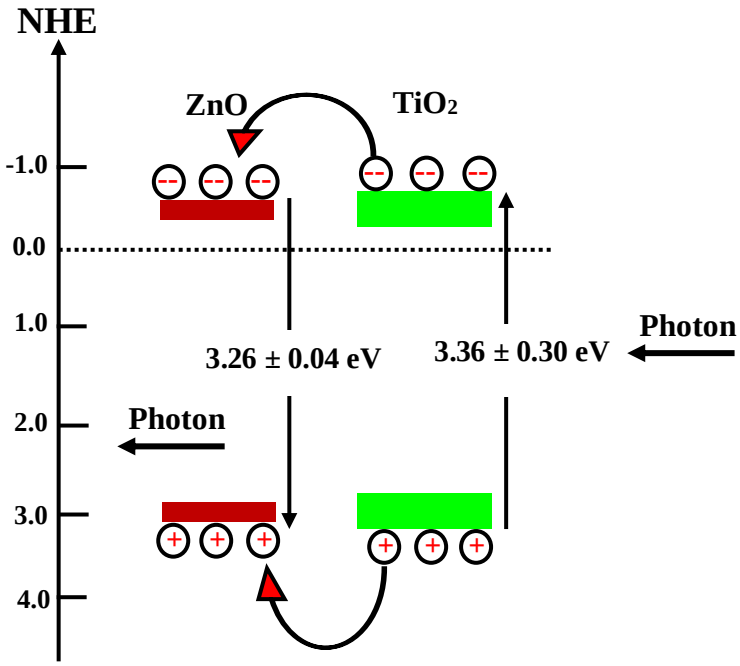

Fig. 4.4: Energy band alignment of ZnO/TiO_2 composite.

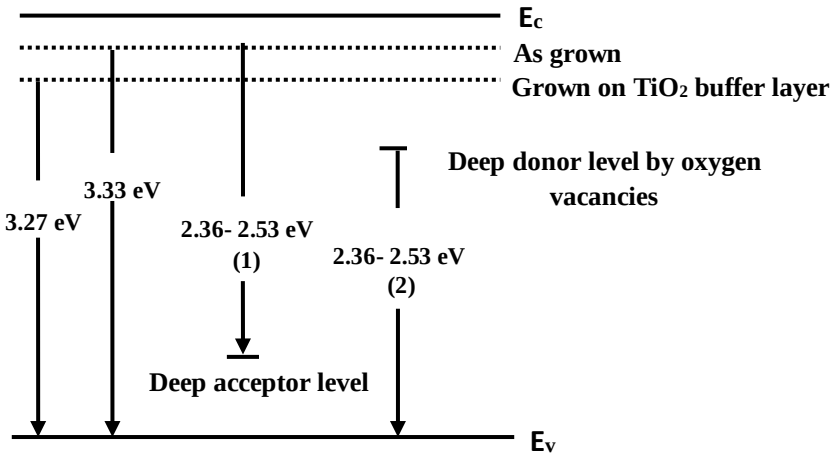

Fig. 4.5: The photoluminescence transitions of PLD deposited ZnO thin film: (1) transition from near conduction band edge to deep acceptor level, (2) transition from deep donor level by oxygen vacancies to valence band.

The enhanced ultraviolet emission from ZnO thin films grown on TiO_2 buffer layer is also probably connected with fluorescence resonance energy transfer (FRET) between ZnO and TiO_2. Fluorescence resonance energy transfer (FRET) is a process to express the transfer of energy between two molecules. The molecule which is in excited state (donor) may transfer its energy to another molecule which is in lower energy state (accepter). This process is based on non dipole-dipole coupling phenomenon. After the excitation of electron–hole pairs in TiO_2 layer, the energy is easily transferred to ZnO films due to resonance effect [167] as a result, the band gap emission of ZnO is enhanced.

The value of the direct band gap was found to be 3.29 and 3.24 eV for ZnO thin films grown on Si substrate without and with TiO_2 buffer layer, respectively. On the other hand, the value of indirect band gap was found to be 3.24 and 3.19 eV for TiO_2 thin films deposited on Si (100) substrate without and with a ZnO buffer layer. The decrease in the optical band gap of the films could be related to the enhancement in crystallite (grain) size leading to a smaller number of grain boundaries. On the other hand the compressed lattice will provide a wider band gap because of the increased repulsion between the oxygen 2*p* and the zinc 4*s* bands [168].

4.4 Conclusion

ZnO, TiO_2, ZnO/TiO_2 and TiO_2/ZnO thin films on Si (100) substrate were prepared by pulsed laser deposition technique. XRD and AFM result demonstrate that the crystallinity of ZnO and TiO_2 thin films are considerably improved by using TiO_2 and ZnO buffer layer, respectively. Compared with PL of ZnO thin film, UV intensity of ZnO grown on TiO_2 buffer layer has increased about two fold. Similarly, the ZnO buffer layer improved the UV emission of TiO_2 thin film. The band gap of ZnO and TiO_2 thin film grown on the buffer layer found to decrease due to improved crystallinity.

CHAPTER 5

Effect of Phase Transformation on Optical and Dielectric Properties of Pulsed Laser Deposited $ZnTiO_3$ Thin Films

In this chapter, the effect of substrate temperature, which leads to transformation of hexagonal phase to cubic phase, has been studied. The structural, optical and dielectric properties have been measured and the effect of phase transformation has been analyzed.

5.1 Introduction

Perovskite-phase metal oxides reveal a variety of attractive physical properties which include dielectric, ferroelectric, piezoelectric and pyroelectric behavior. Particularly, the materials having linear dielectric behavior shows linear polarization as a function of applied field. In ferroelectric ceramics the permanent electric dipole can be oriented with the application of applied electric field. On the other hand Pyroelectric materials exhibit spontaneous polarization and the direction of polarization cannot be reversed by external electric field. Piezoelectrics materials either suffer mechanical deformation as external electric field is applied or exhibits an electrical charge as mechanically stressed are applied. In general, these various properties occurs from the crystal symmetry adopted by these materials [169].

The multifunctional development of high-frequency electronic materials becomes essential due to the requirements of electronic components with the highest reliability. Zinc titanate ($ZnTiO_3$) has been reported to have superior electrical properties that are adequate for applications of microwave dielectrics [52]. $ZnTiO_3$ has also been regarded as a good candidate for low-temperature cofired ceramics (LTCCs) due to its relatively low sintering temperature and good dielectric properties [54]. The ZnO – TiO_2 system has three stable phases, including $ZnTiO_3$ (with hexagonal and cubic structure), Zn_2TiO_4 (cubic structure), and $Zn_2Ti_3O_8$ (cubic structure). Amongst these phases, $ZnTiO_3$ is unstable and gets decomposed into Zn_2TiO_4 and rutile TiO_2 at about 945 °C [51]. To the best of our knowledge, references concerning the characteristics of zinc titanate based thin film are lacking.

In this work, we have reported the effect of phase transformation on optical and dielectric properties of $ZnTiO_3$ thin films prepared by pulsed laser deposition technique using solid state reacted ceramic target. Various parameters are optimized in order to achieve single phase $ZnTiO_3$ thin film.

5.2 Experimental Details

5.2.1 Thin Film Preparation: The conventional solid state reaction method was used for the preparation of $ZnTiO_3$ target material. ZnO and TiO_2 powder (99.99% pure, Loba Chemie, India) was taken in a molar ratio 1:1. The materials were ground for 24 h followed by calcinations at 400 ^oC for 12 h. After that powder was reground for 6 h and pressed into pellets (1.5 cm in diameter and 1.15 mm thickness) under the pressure of 90 MPa. Then, the pallets were sintered at different temperatures ranging from 700 ^oC to 1000 ^oC for 12 h. Thin films were deposited using KrF excimer pulsed laser system. The wavelength of KrF excimer laser source was 248 nm. The laser fluence of about 2–3 Jcm^{-2} was kept with pulse repetition rate 10 Hz. The distance between target and substrate was kept at 35 mm. Before deposition of thin films, the base pressure in the chamber was $2x10^{-6}$ Torr, and after that the pure oxygen was introduced and sustained at a pressure of 50 mTorr. The chamber was filled to 900 mTorr oxygen after the deposition of thin films and the films were cooled down naturally. The film thickness was measured using a surface profilometer and found to about ~200 nm.

5.2.2 Thin Film Characterization: The orientation and phase of as prepared thin films were characterized by X-ray diffractometry (XRD, Bruker AXS D-8 Advance Diffarctometer) using CuK_α (λ=1.5407 Å) radiation. The surface topography and microstructure were examined by atomic force microscope (NTMDT: NTEGRA model). Absorption spectra have been taken using UV-vis-NIR spectrophotometer (Varian Cary 5000) in the wavelength range 200 to 800 nm. Dielectric properties as a function of frequency were studied using an impedance analyzer (Agilent 4294A precision).

The facility of pulsed laser deposition technique and characterization techniques provided by functional nanomaterials research laboratory (FNRL) IIT Roorkee and Materials Research Centre, MNIT Jaipur.

5.3 Results and Discussion

5.3.1 Structural and Surface Morphology Study

The preparation of single phase $ZnTiO_3$ is usually difficult due to the coexistence of both cubic and hexagonal phases at low temperature and the decomposition of $ZnTiO_3$ into Zn_2TiO_4 and TiO_2 (rutile) at high temperature. Consequently, we need to optimize several parameters to prepare the single phase $ZnTiO_3$ in the form of powder and thin film. Fig. 5.1 shows the XRD patterns of the ZnO-TiO_2 composites sintered at different temperatures varying from 700 ^oC to 1000 ^oC for same time period (for 12 h). The ZnO-TiO_2 composite powder sintered at 800 ^oC reveals pure crystalline hexagonal phase of $ZnTiO_3$ without any existence of cubic-phase. This sample is used as a target material for the fabrication of $ZnTiO_3$ thin film using pulsed laser deposition technique. The ITO coated glass substrate was used for the preparation of thin films.

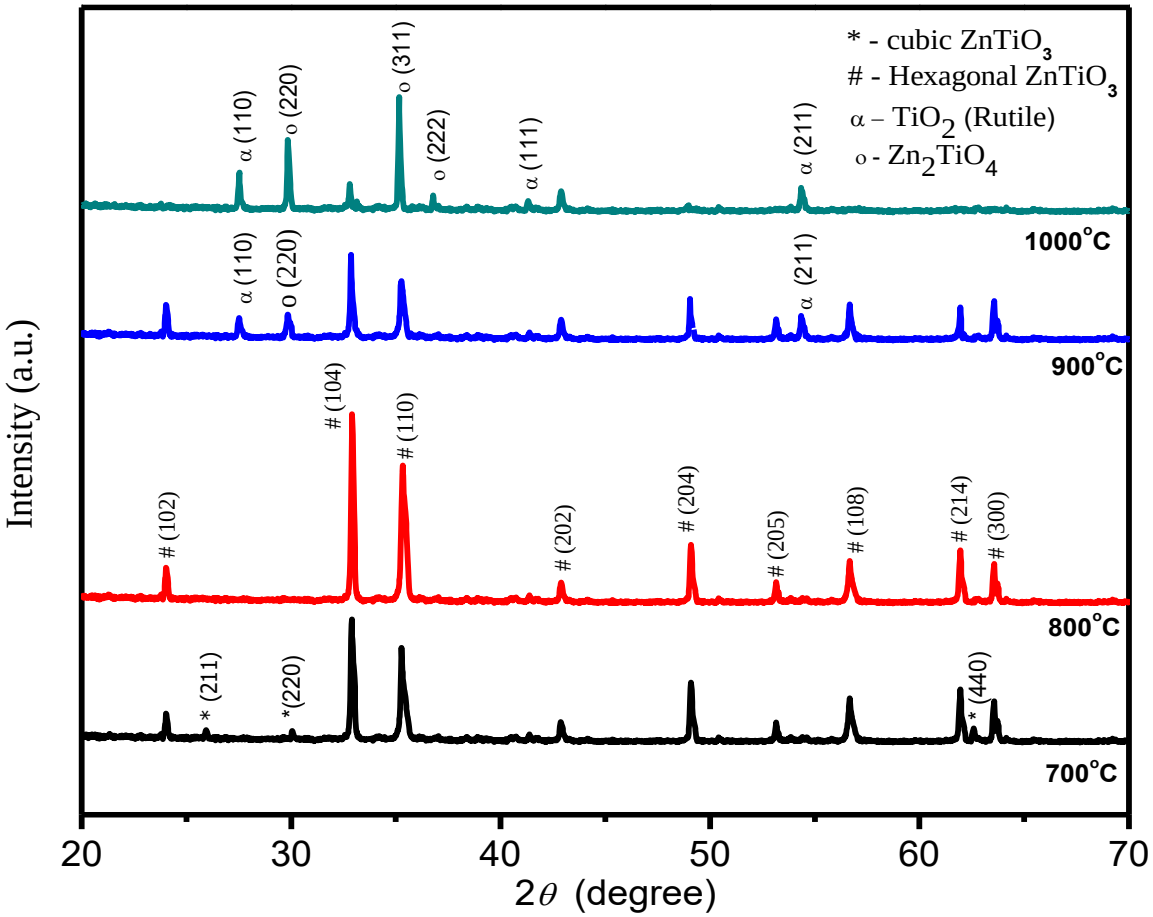

Fig.5.1: XRD patterns of $ZnTiO_3$ pallet obtained at different sintering temperatures.

Fig. 5.2 shows the XRD patterns of the $ZnTiO_3$ thin films at different substrate temperatures varying from room temperature to 550 ^oC. At room temperature film was amorphous nature, only single peak appears of substrate. When we increase the substrate temperature from room temperature to 300 ^oC hexagonal phases starts to appear and become more intense at 400^oC. Further increases in substrate temperature the XRD pattern shows the coexistence of both cubic and hexagonal-phases.

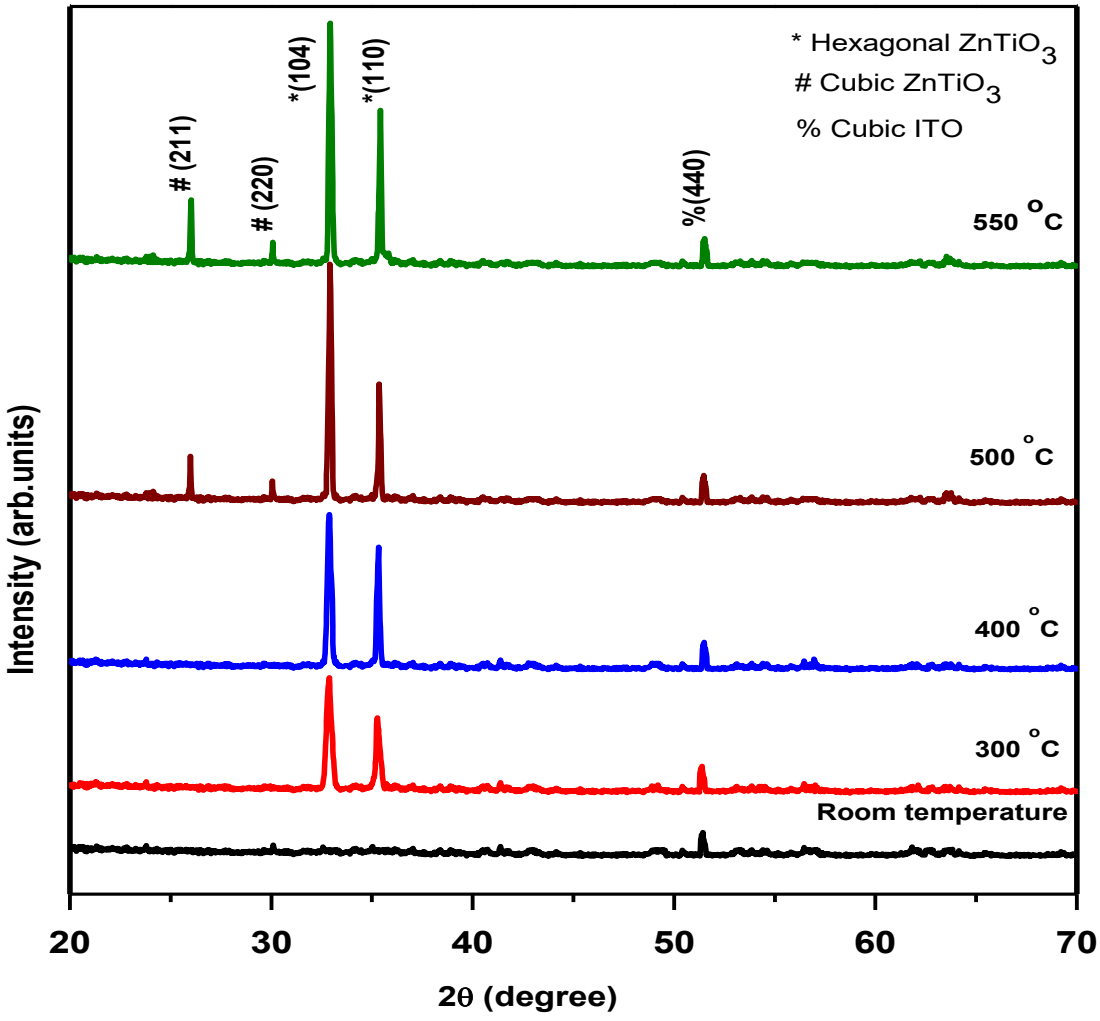

Fig.5.2: XRD patterns of $ZnTiO_3$ thin film at different substrate temperatures

The crystallite size of these samples was calculated along the (104) orientation of hexagonal $ZnTiO_3$ phase using the Scherrer's formula [165]. The crystallite size of the thin films at various substrate temperature calculated using Scherrer's formula are shown in Table 1 and the variation of FWHM and crystallite size are shown in Fig. 5.3 (a). It is observed as the substrate temperature increases the crystallite size increases

and FWHM decreases. This is because of the Ostwald ripening [170], according to that particle size increases due to the amalgamation of the smaller particles into larger ones and is a result of the potential energy difference between larger and smaller particles. This can occur through solid state diffusion.

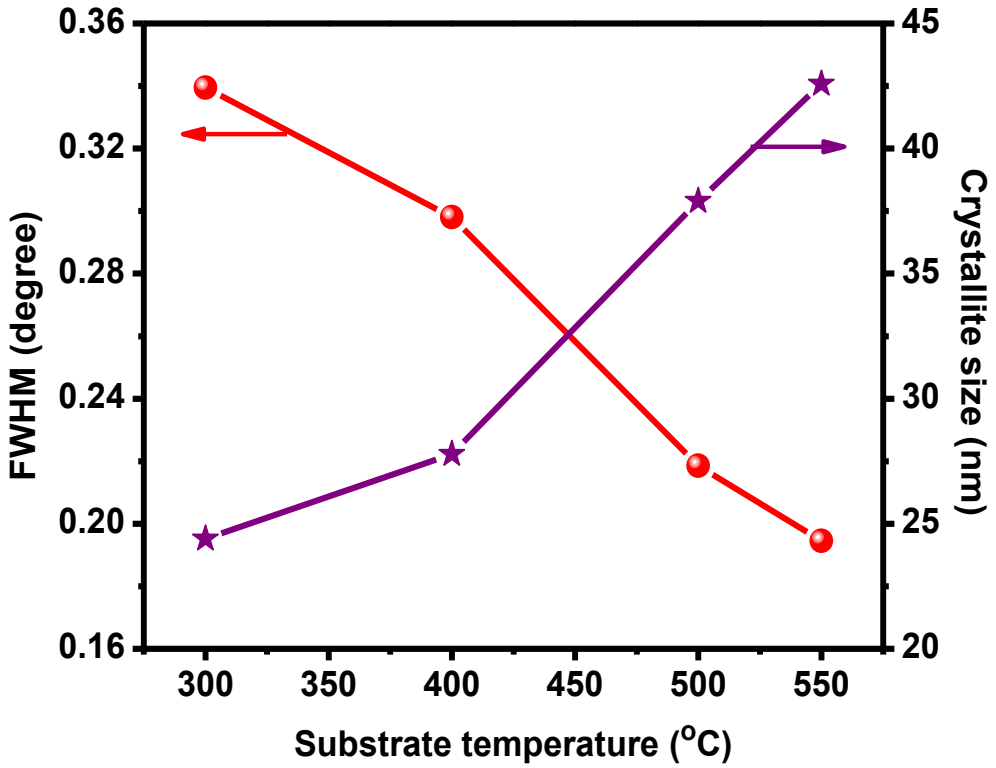

Fig. 5.3(a): Variation of FWHM and crystallite size with substrate temperature.

The approximate percentage of hexagonal-phase was calculated from the ratio of areas under the hexagonal-phase peaks to the areas of all peaks using the equation as follows:

$$H(\%) = \frac{A_h}{A_{all}} \times 100 \qquad (5.1)$$

Here, A_h and A_{all} denote the areas of hexagonal-phase of $ZnTiO_3$ and the areas of all peaks of $ZnTiO_3$, respectively. The results are listed in Table 1.

Fig. 5.3(b) demonstrates the variation of unit cell volume and lattice parameter with substrate temperature. It is found that lattice parameter and unit cell volume decreases with substrate temperature. This is because of shifting the (104) peak to the larger angle representing the existence of residual stress. The residual stress occurs due to different thermal expansion coefficients between substrate and $ZnTiO_3$ film after cooling down [28]. Compared to the unstressed bulk value of a=5.077 Å , the large

value of lattice constant for $ZnTiO_3$ film grown at room temperature shows that the unit cell is elongated along the *a* axis, and compressive force acts on the plane of the film. As substrate temperature increases, the compressive force decreases, however, as the substrate temperature reaches to 400^0C, the lattice constant of the $ZnTiO_3$(104) films becomes shorter than that of bulk $ZnTiO_3$, which indicates that the compressive stress in the film plane changes to a tensile one with a substrate temperature increasing.

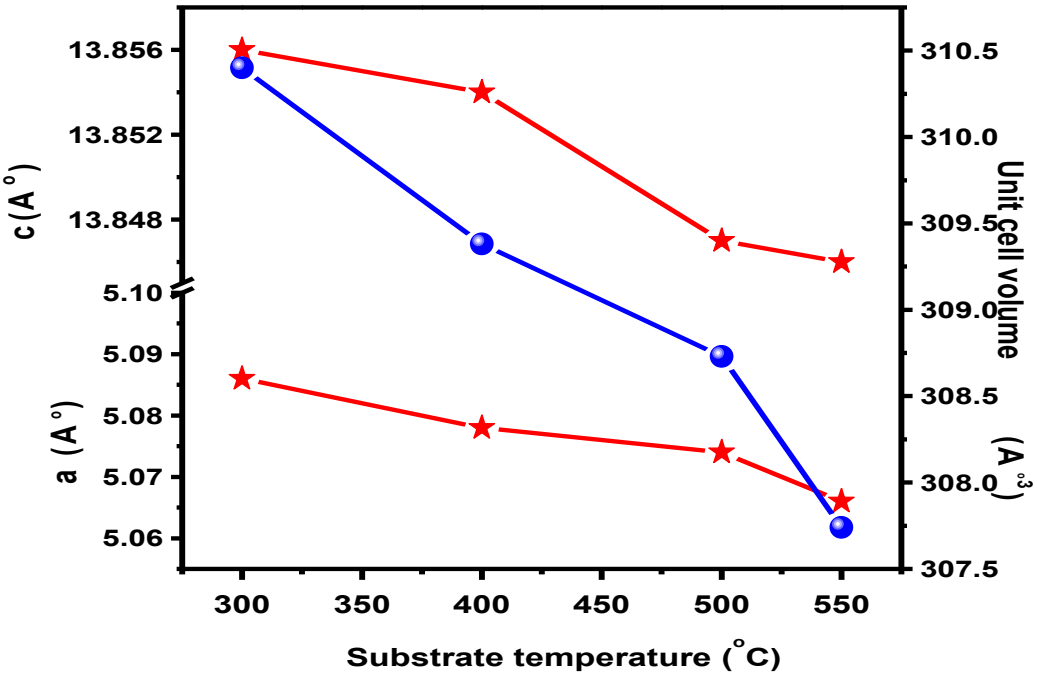

Fig. 5.3(b): Variation of lattice parameter and unit cell volume with substrate temperature

Table 5.1: Various parameters of $ZnTiO_3$ thin films deposited at different substrate temperature.

Substrate temperature (°C)	Lattice Constants		Unit cell volume ($Å^3$)	Hexagonal phase percentage (%)	FWHM (degree)	Crystallite Size (nm)	Grain size AFM (nm)
	a (Å)	*c* (Å)					
300	5.086	13.856	310.40	100	0.3395	24.39	43
400	5.078	13.854	309.38	100	0.2981	27.78	61
500	5.074	13.847	308.73	64.65	2.7191	37.90	85
550	5.066	13.846	307.74	59.33	0.1945	42.58	102

Fig. 5.4 shows the surface morphology of the $ZnTiO_3$ thin film prepared at different substrate temperature. The the average columnar grain size and RMS roughness were computed from the AFM images. It has been found that the average value of grain size increases from 43 nm to 102 nm and roughness of surface increases from 5 nm to 10 nm over the substrate temperature range.

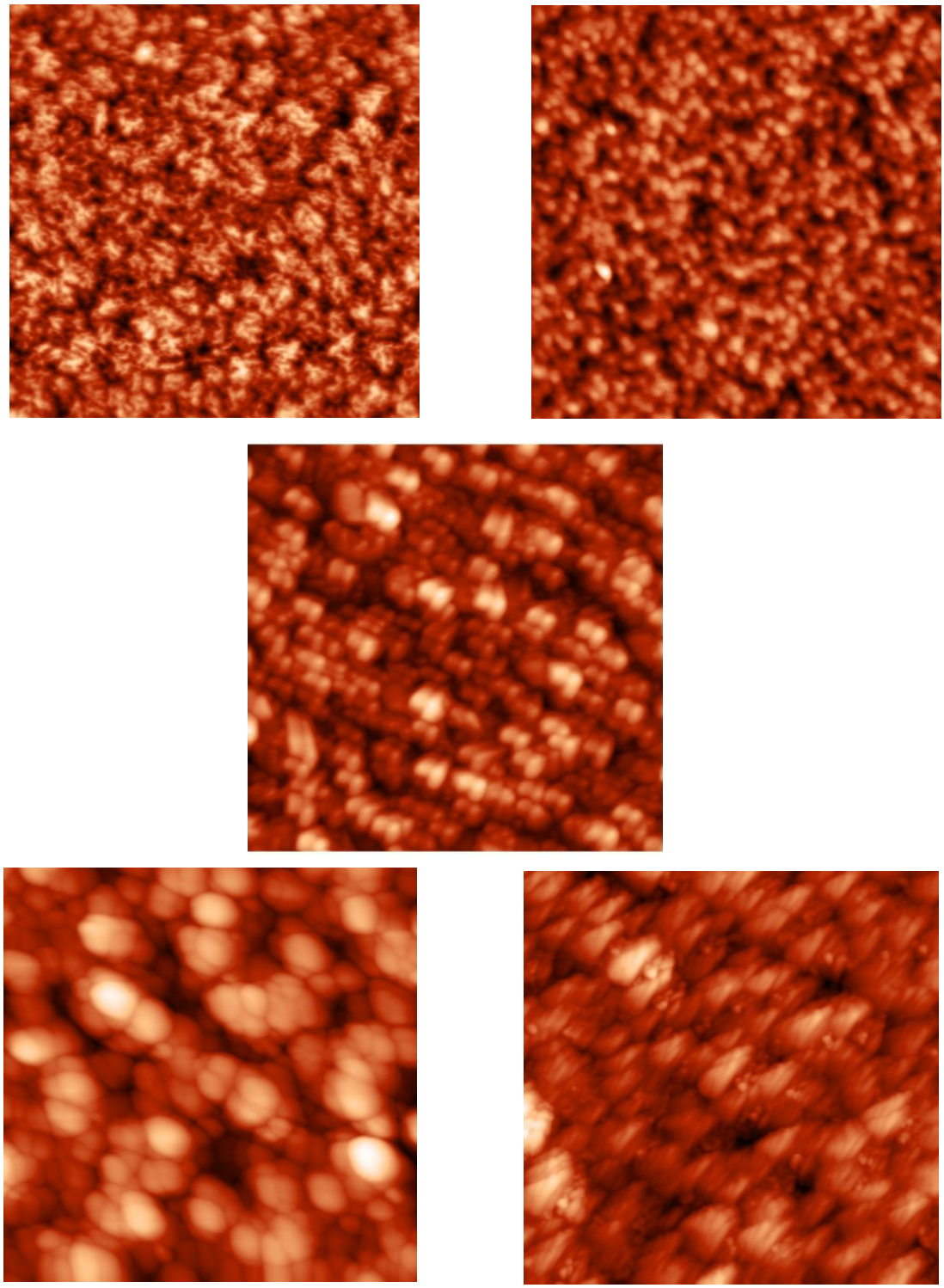

Fig.5.4: AFM image for $ZnTiO_3$ thin film deposited at various substrate temperatures

It is believed that high temperature provided sufficient energy to the atoms to obtain high surface mobility, which endorse the formation of the larger columnar structure grains. The surface roughness increases due to the increase in the average grain size.

5.3.2 Optical Properties

The optical absorption spectra of $ZnTiO_3$ thin film deposited at different substrate temperature are shown in Fig.5.5 (a).

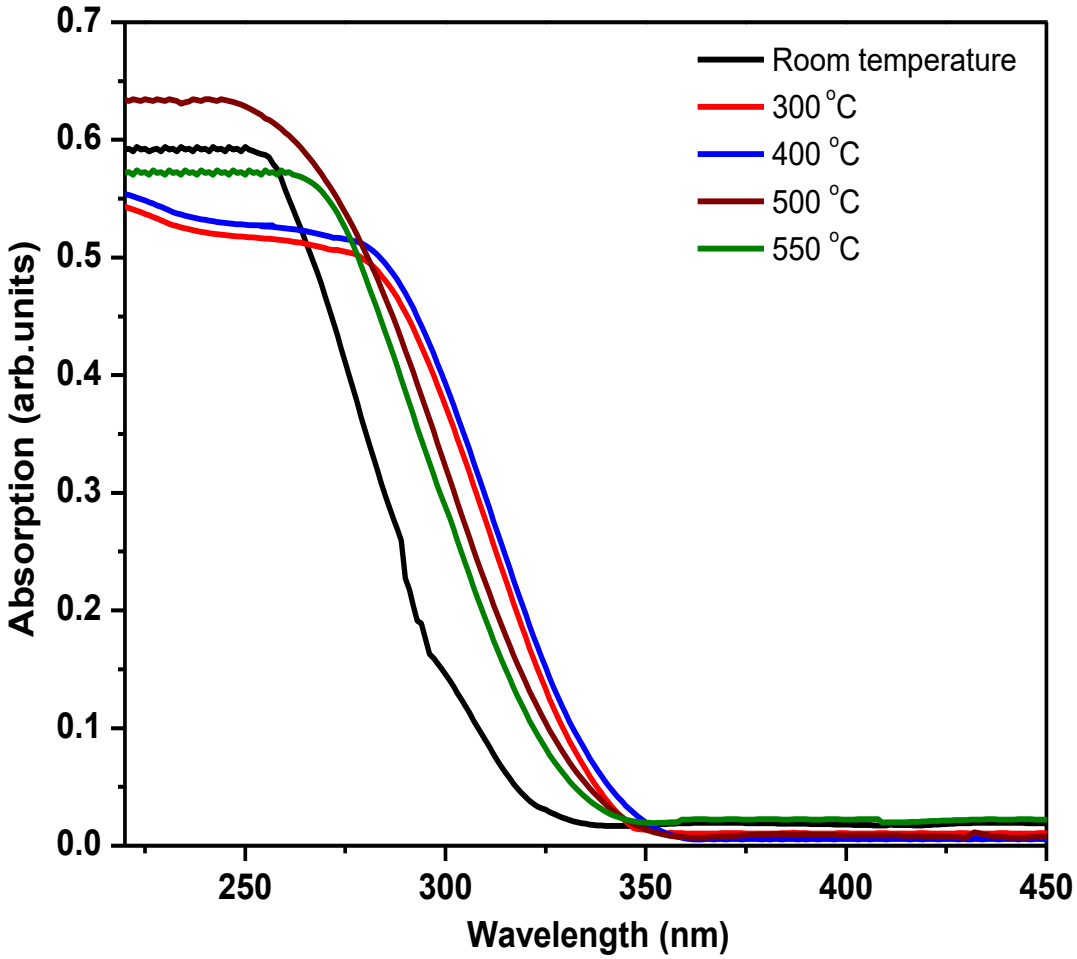

Fig.5.5 (a): Optical absorption spectra of $ZnTiO_3$ thin film deposited at different substrate temperature

One can see that the absorption edge of the crystalline thin film moves to longer wavelength as compared with that of amorphous film. It is also observed that the ultraviolet absorption edge of single hexagonal-phase $ZnTiO_3$ has a red-shift, compared with that of cubic/hexagonal mixed phase $ZnTiO_3$.

The relation between photon energy ($h\nu$) and the absorption edge for the indirect band-gap semiconductor can be expressed as follows [171]:

$$\alpha h\nu = A\left(h\nu - E_g\right)^2 \qquad (5.2)$$

where A is a constant , α is the absorption coefficient, E_g is the optical band gap, h is Planck's constant, ν is the photon frequency. The plot of hν vs $(\alpha h\nu)^{1/2}$ of thin films prepared at different substrate temperature is demonstrated in Fig. 5.5 (b). The value of optical band gap E_g was measured from an extrapolation of the linear region of the plot of $(\alpha h\nu)^{1/2}$ on the y-axis versus photon energy (hν) on the x-axis. $ZnTiO_3$ thin films showing indirect band gap which is arises from the best fitting of $(\alpha h\nu)^{1/2}$ versus (hν) plot. It is also consistent with the reported in literature [172]. The variation of band gap with substrate temperature is shown in inset of Fig.5.5 (b). We have observed the blue shift in absorption edge is caused by the poor crystallinity of $ZnTiO_3$ thin films prepared at low temperature. The crystallinity of the $ZnTiO_3$ thin films prepared below 400 °C was poor and reveal polycrystalline structure. The physical model of the structure can be viewed as various nanocrystalline islands embedded in a matrix of amorphous $ZnTiO_3$. Qualitatively, the interatomic spacing of amorphous structure would be relatively long and more disordered than crystalline structure due to the absence of long-range translational periodicity. As the fraction of amorphous $ZnTiO_3$ phase increases in the films grown at low temperature, the extended localization in the conduction and valence bands increases [173]. As a result, the absorption of photon is mainly contributed by amorphous $ZnTiO_3$ and hence the absorption edge blue shifted. When the substrate temperature increases from 300 ^oC to 400 ^oC the band gap decreases due to strong hexagonal phase, but more increment in substrate temperature increases the band gap causes by change of phase from hexagonal to cubic.

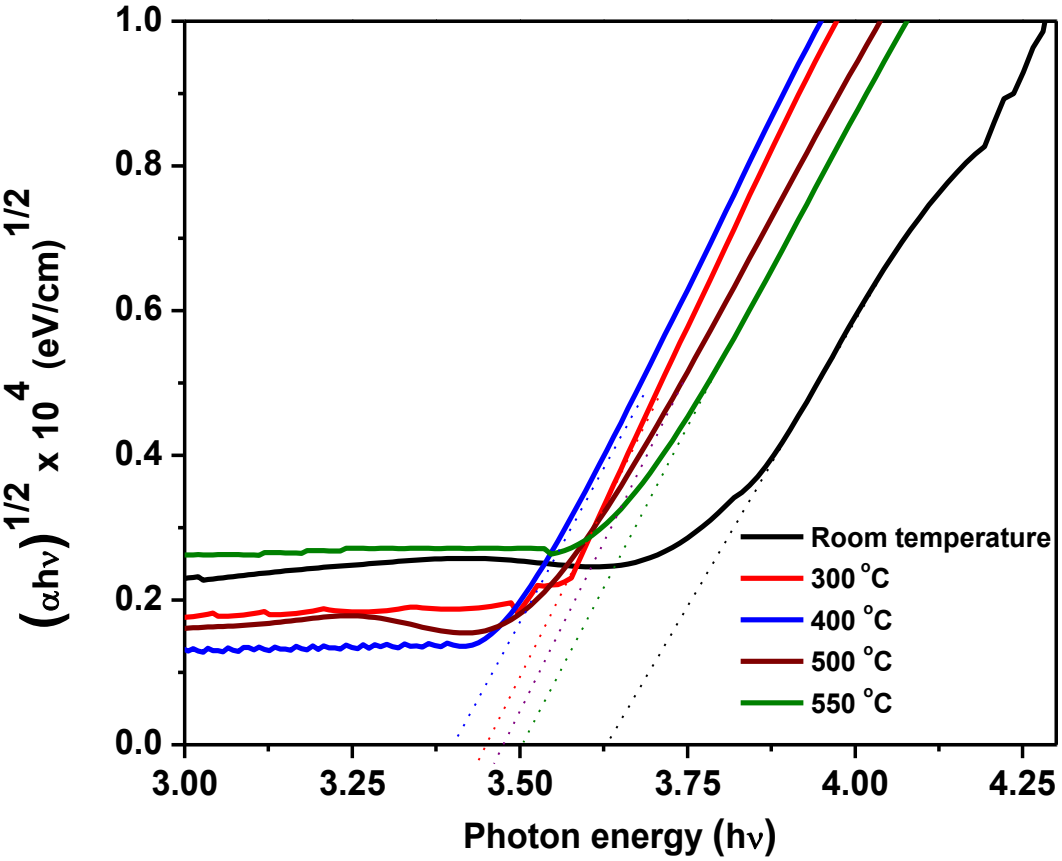

Fig.5.5 (b): $(\alpha h\nu)^{1/2}$ versus hν plot of ZTO sintered at different substrate temperature.

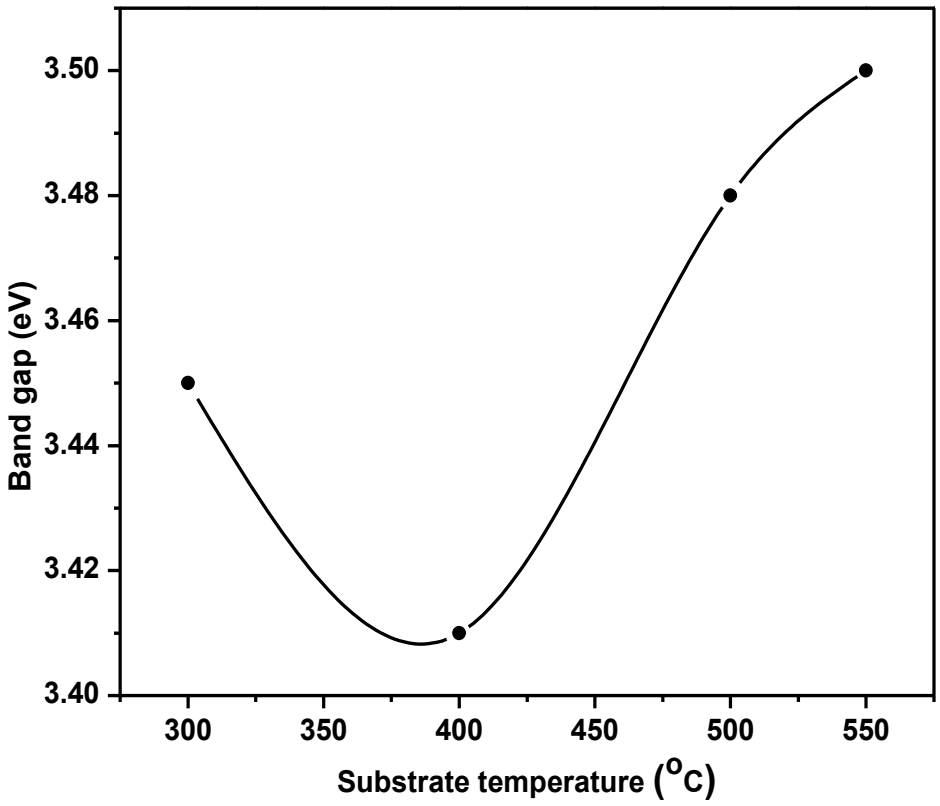

Fig. 5.5 (c): The variation of band gap with substrate temperature

5.3.3 Dielectric Properties

Fig. 5.6 (a-c) shows the measured capacitance, loss tangent and relative dielectric constant as a function of frequency in the range 500 Hz to 5 MHz of the $ZnTiO_3$ thin films deposited at different substrate temperature. Dielectric constant ε_r is calculated from the measurement of capacitance value which can be obtained using the following equations:

$$\varepsilon_r = \frac{t \times C_p}{A \times \varepsilon_0} = \frac{t \times C_p}{\pi \left(\frac{d}{2}\right)^2 \times \varepsilon_0} \qquad (5.3)$$

where, C_p= equivalent parallel capacitance which is obtained from the measurement data, t = film thickness, d = diameter of the electrode, ε_0 = permittivity of vacuum.

It has been observed that in high frequency region dielectric constant remains constant; while for lower frequencies a steep decrease in the dielectric constant with increase in frequency has been observed. The dielectric loss tangent is also found to almost constant at higher frequency region but decreasing in the lower frequency region. This indicates that frequency dispersion in the dielectric properties are negligible at higher frequency region for $ZnTiO_3$ thin film, which is an important property suitable for many applications.

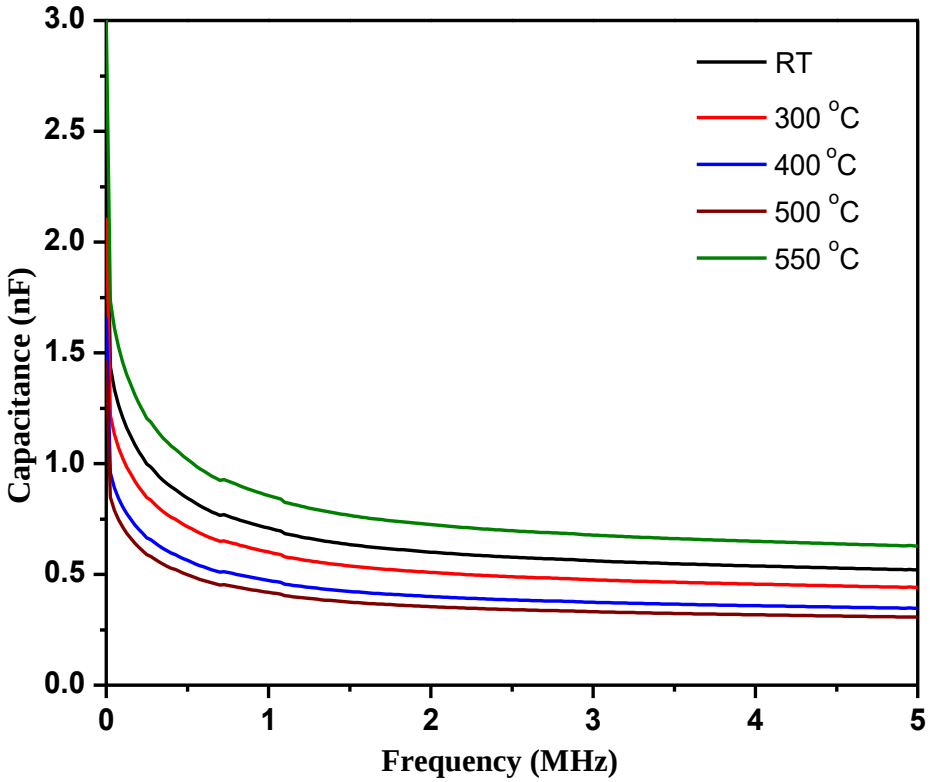

Fig. 5.6 (a): The capacitance as a function of frequency $ZnTiO_3$ thin films deposited at different substrate temperatures

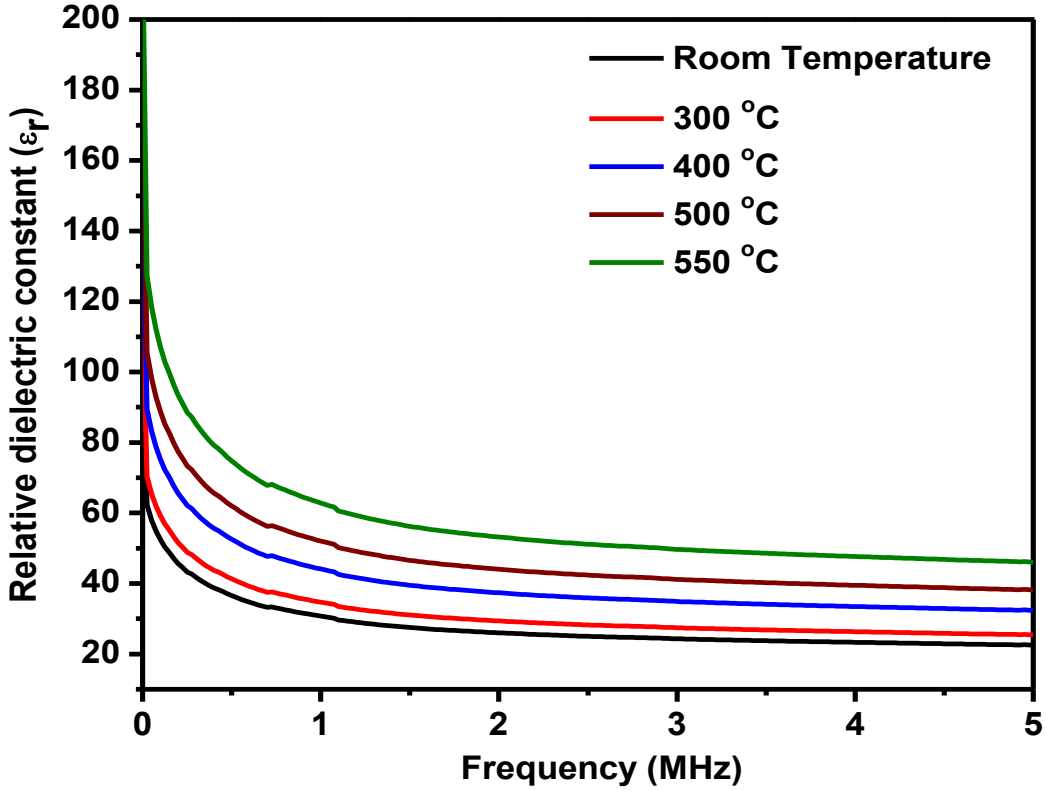

Fig. 5.6 (b): The relative dielectric constant *as a function of frequency $ZnTiO_3$ thin films deposited at different substrate temperatures*

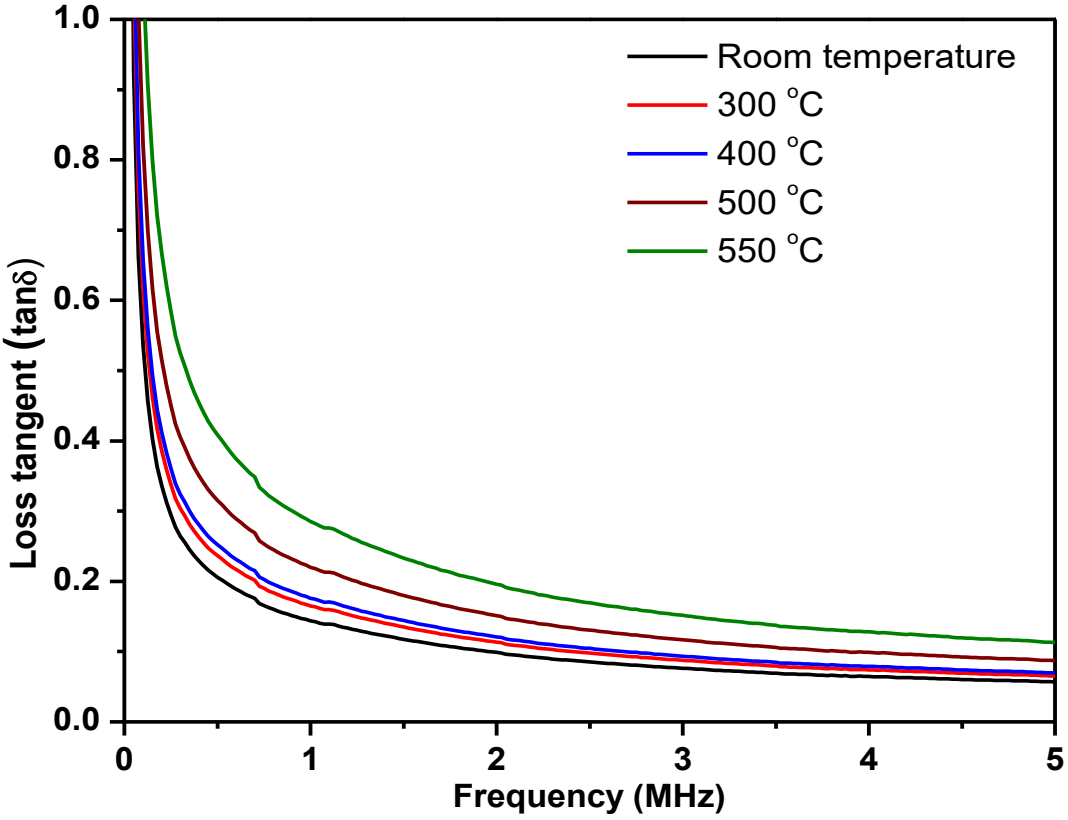

Fig. 5.6 (c): The loss tangent *as a function of frequency $ZnTiO_3$ thin films deposited at different substrate temperatures*

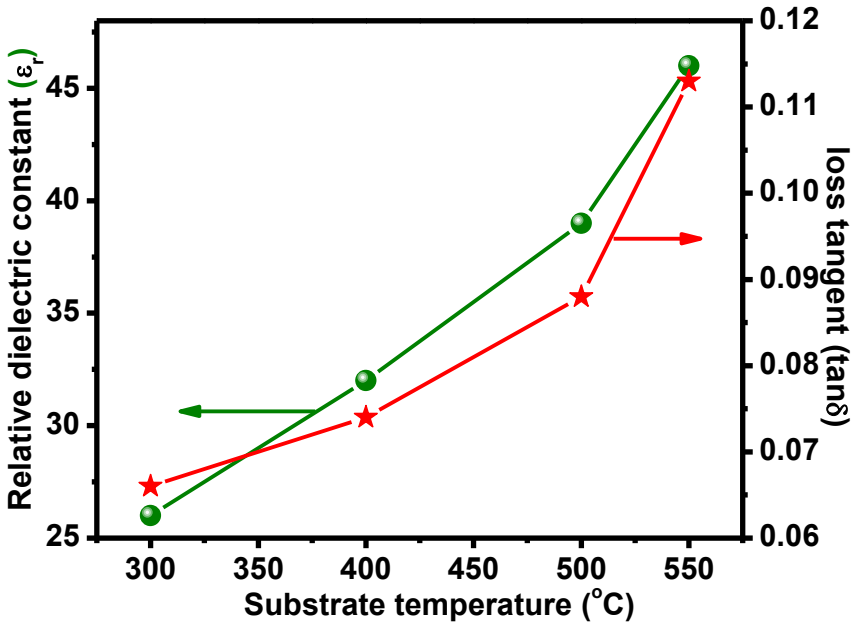

Fig. 5.7: Variation of relative dielectric constant and loss tangent with substrate temperature

The high value of dielectric constant at lower frequency is associated with the contributions from ionic, space charge and interface polarization. At higher frequency, dielectric constant becomes independent of frequency. It is due to the inability of electric dipoles to follow the fast variation of the applied electric field. Fig. 5.7 shows the variation of relative dielectric constant and loss tangent with substrate temperature. The dielectric constant of $ZnTiO_3$ thin film deposited at room temperature is lowest due to its amorphous nature. When the substrate temperature increases, dielectric constant increases due to the enhancement in crystallinity. The improved film morphology by the increment in substrate temperature might also contribute to the enhancement of dielectric properties.

5.4. Conclusion

Pure phase $ZnTiO_3$ thin films were prepared by pulsed laser deposition using ZnO-TiO_2 composite ceramic which was sintered at 800°C. At room temperature film was amorphous in nature, when we increase the substrate temperature hexagonal phase starts to appear. Further increases in substrate temperature film shows the coexistence of both cubic and hexagonal-phases. It is also observed that the ultraviolet absorption edge of single hexagonal-phase $ZnTiO_3$ has a red-shift, compared with that of cubic/hexagonal mixed phase $ZnTiO_3$. The dielectric constant and loss tangent is steeply decreasing in the lower frequency region and has an almost constant value at the higher frequency region.

CHAPTER 6

Switching Characteristics in TiO_2/ZnO Double Layer Resistive Switching Memory Device

The uniform and reliable resistive switching characteristics of the ZnO based RRAM device with thin TiO_2 layer are successfully investigated. In this study, the effect of the thickness of TiO_2 layer on switching characteristics has been investigated. Compared with different thicknesses of thin TiO_2 layers, the remarkable improved resistive switching parameters such as lower forming voltage and the narrower variation of endurance are achieved for TiO_2 layer of thickness 2 nm.

6.1 Introduction

The modern electronic technologies/devices require high speed and denser memories. The use of non-volatile memory (NVM) devices is continuously increasing for recent microprocessor-based devices e.g. mobile phones, computer, digital cameras, cars, portable electronic gadgets and so many other wireless products. Current nonvolatile memory technology, such as flash memory, is based on charge storage and this technology is rapidly reaching its physical limits. Therefore, non-charge based nano-scale memories e.g. magnetic random access memory (MRAM), ferroelectric random access memory (FeRAM), resistive random access memory (RRAM) and phase change random access memory (PCRAM) are being intensively studied for upcoming nonvolatile memory applications. Recently, RRAM has fascinated great consideration due to its potential for the replacement of flash memory in next-generation NVM applications [60-63]. The RRAM devices composed of a simple metal-insulator-metal (MIM) structure has the merits of high speed operation, low power consumption and high density integration. The current-voltage (*I-V*) characteristics of the MIM structure exhibit an intense change of resistance between the high resistance state (HRS) and the low resistance state (LRS) for logic signal (off and on states). The conductive mechanism of the resistive switching (RS) phenomenon is due to the formation and rupture of conductive filament consisting of oxygen vacancies. A number of metal oxides such as HfO_2 [103], TiO_2 [100], ZrO_2 [101], Al_2O_3 [105], $SrTiO_3$ [174], Ga_2O_3 [175], SiO_2 [176], ZnO [102] etc. have been studied for RRAM applications. Among them, ZnO is one of the promising materials in semiconductor foundry, which has been extensively studied for RRAM application because of its simple constitution and compatibility with the standard CMOS technology. In addition, some reports indicated

that the multilayer-based RRAM devices could obtain excellent resistive switching (RS) performance, such as high HRS/LRS ratio, fast switching speed, great scalability and low power.

In this study, the RS behaviors of double layer TiO_2/ZnO films in RRAM structure are investigated. A thin TiO_2 layer with different thickness deposited on the ZnO RS layer leads the significantly different resultant switching curve form that without TiO_2 layer. The TiO_2/ZnO double layer structure with 2 nm TiO_2 thin films can improve the resistive switching behavior compared to the single ZnO layer. Moreover, the bipolar switching behavior with high performance was demonstrated in this structure. It could be expected in future that this kind of double layer metal oxide based RRAM device would open a new way to the research and development of RRAM and what is more, to the exploration of the mechanism of RS.

6.2 Experimental Details

In First step the cleaning of p-type Si (100) wafer was done using the standard RCA cleaning process for device fabrication. An isolation thick layer of SiO_2 with 200 nm was grown on the Si wafer at the 950 ^oC by wet oxidation to avoid the leakage current from Si wafer. After that adhesion layer of Ti metal film with thickness 20 nm was deposited on the SiO_2 substrate. Further inert bottom electrode (Pt) with thickness 50 nm was deposited on the Ti adhesion layer. Both Pt and Ti layers were deposited at room temperature using the e-beam evaporation technique. The ZnO thin film with thickness 10 nm and TiO_2 thin film with thickness 2 nm, 5 nm and 10 nm were deposited at 200 ^oC and room temperature, respectively, by using radio frequency magnetron sputtering. Finally, top electrode and capping layer of Ti with 50 nm thickness and Pt with 20 nm thicknesses, respectively, were deposited by electron beam evaporation at room temperature to form the Ti/TiO_2/ZnO/Pt RRAM structure. Besides, the control sample without the TiO_2 thin film was fabricated by the same processes described above. The switching characteristic of the all devices was measured using an Agilent B1500A semiconductor parameter analyzer. Thermo Scientific Theta Probe Angle-Resolved X-ray Photoelectron Spectrometer System used for the measurement of oxygen vacancies in ZnO and TiO_2 thin films using Al K_α X-ray source (1486.6 eV). *The facility of RRAM device fabrication and characterization techniques provided by the Department of Electronics Engineering and Institute of Electronics, National Chiao Tung University, Taiwan*.

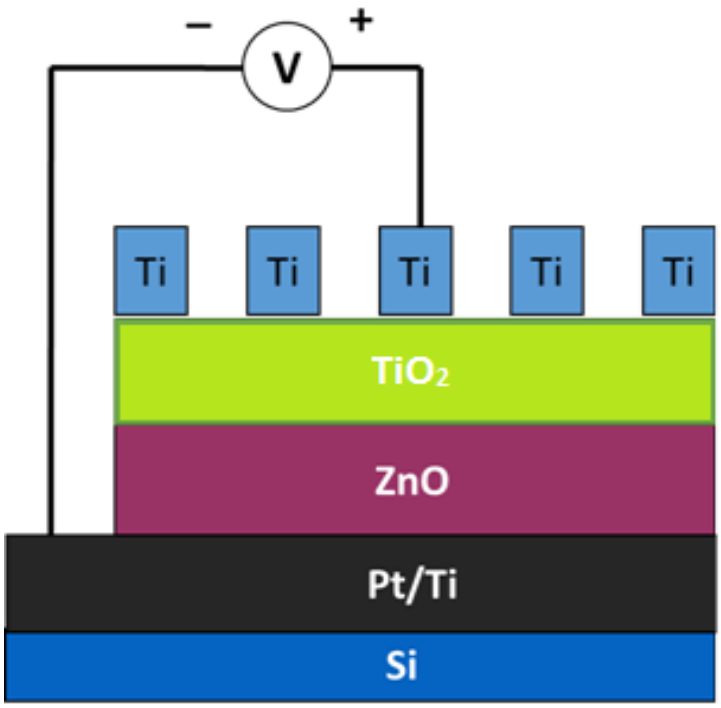

Fig. 6.1(a): Schematic structure of the fabricated RRAM device

RCA Clean of p-type Si (100) substrate

↓

Wet oxide (SiO_2 growth), Isolation layer of 200-nm

↓

20-nm Ti Layer (adhesion layer) and then bottom electrode (Pt layer of 50 nm) deposited by electron beam evaporation

↓

10 nm-ZnO and TiO_2 (different thickness varying from 2 nm to 10 nm) deposited by sputtering at 200 ^oC

↓

50 nm-Ti as top electrode were deposited by electron beam evaporation

Fig. 6.1(b): Experimental flow diagram for fabrication of RRAM device

6.3 Results and Discussion

Fig. 6.1 (a-b) shows schematic diagram and experimental flow of the Ti/TiO_2/ZnO/Pt device architecture. For the I–V measurements, the voltage was applied to the top active electrode while the bottom electrode was grounded. To evaluate the memory effects, I–V characteristics of these device structures were studied by dc voltage sweep measurements. The forming process of devices are needed to activate the RS properties, as shown in Fig. 6.2 (a).

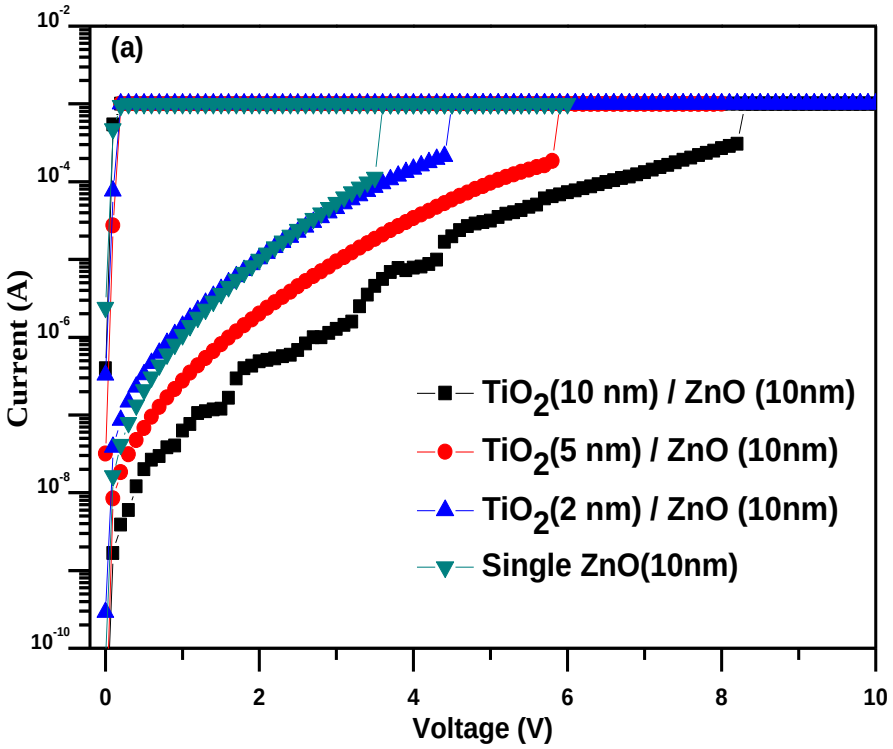

Fig. 6.2 (a) Forming processes of Ti/ZnO (10 nm)/Pt and Ti/TiO_2 (2 nm, 5 nm and 8 nm)/ ZnO (10 nm)/Pt devices structure.

After the initial forming process, the Ti/ZnO/Pt device was switched from HRS (OFF state) to LRS (ON state). The forming voltage (V_F) increases linearly with the film thickness of TiO_2 as shown in Fig. 6.2 (b). A large forming voltage (V_F) of about 8 V is observed for the Ti/TiO_2 (10nm)/ZnO/Pt structure, while only about 3.5 V is need to switch the Ti/ZnO/Pt structure from initial HRS to LRS. The linearly dependence of V_F on the TiO_2 film thickness supports the idea that forming process are governed by dielectric breakdown like phenomenon [177].

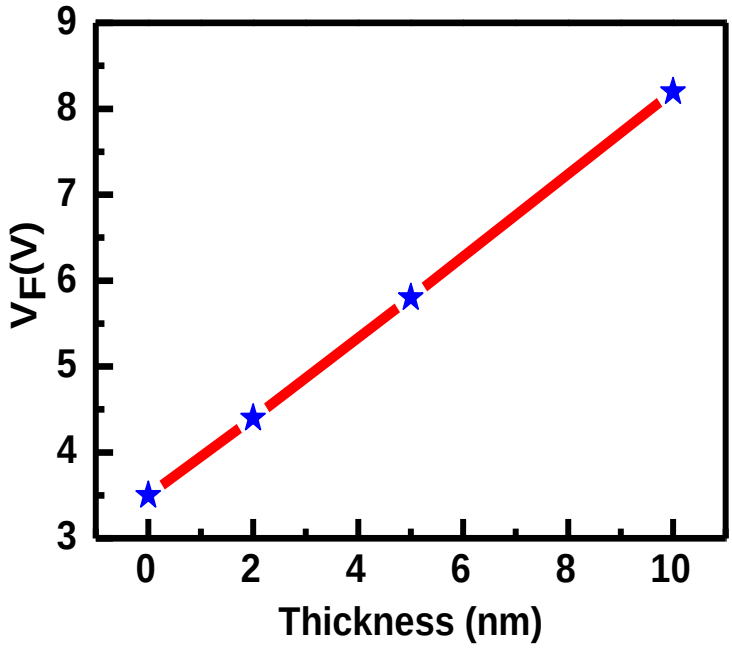

Fig 6.2 (b): The variation in forming voltage with TiO_2 thickness

Fig.6.3 shows the typical bipolar RS process of the Ti/ZnO/Pt and Ti/TiO_2 (2nm, 5nm, 10nm)/ZnO/Pt devices, both devices show bipolar resistive switching behaviors. The compliance current was set as 1 mA. To further study the conduction and switching mechanism of the RRAM devices between HRS and LRS, the I–V characteristics are re-plotted in log–log scale and fitted the positive voltage region. As shown in Fig.6.4, the slopes of current (log I) vs. voltage (log V) in LRS of the ZnO/TiO_2 double layer RRAM devices with different thickness of TiO_2 are around one, which indicates that the LRS is dominated by Ohmic conduction mechanism. The conduction mechanism of LRS suggests that our devices belong to conductive filament formation/rupture model. The HRS shows linear fitting with slope around 2, this suggests that the current conduction mechanism of our memory device is dominated by a trap-controlled space-charge-limited current conduction mechanism. Oxygen vacancies might be serving as the trap sites [178-179].

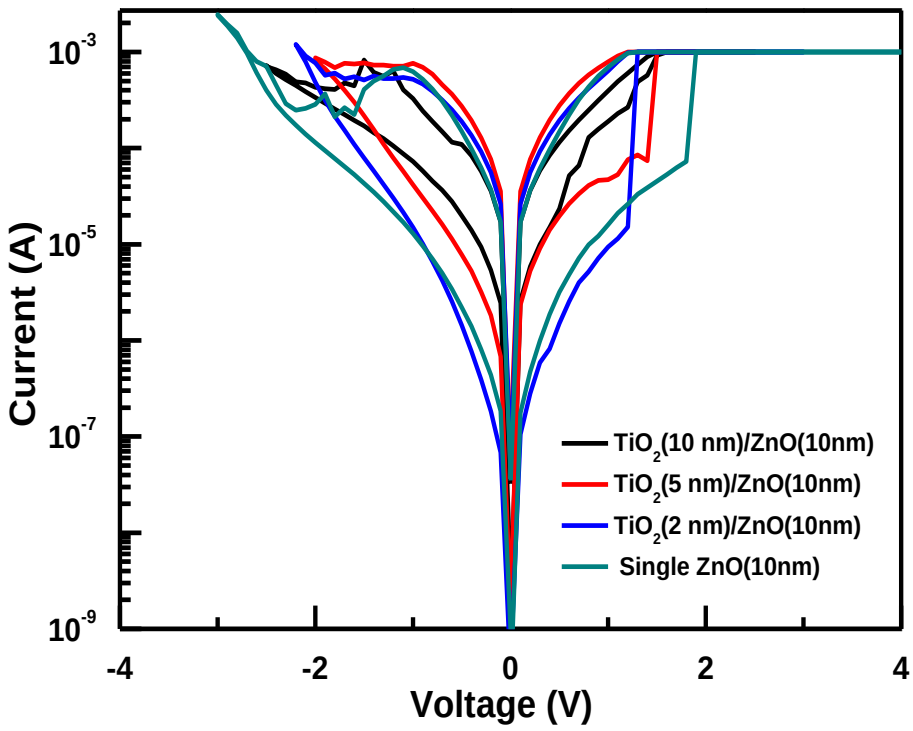

Fig. 6.3: Typical DC sweep I-V characteristics of all the devices.

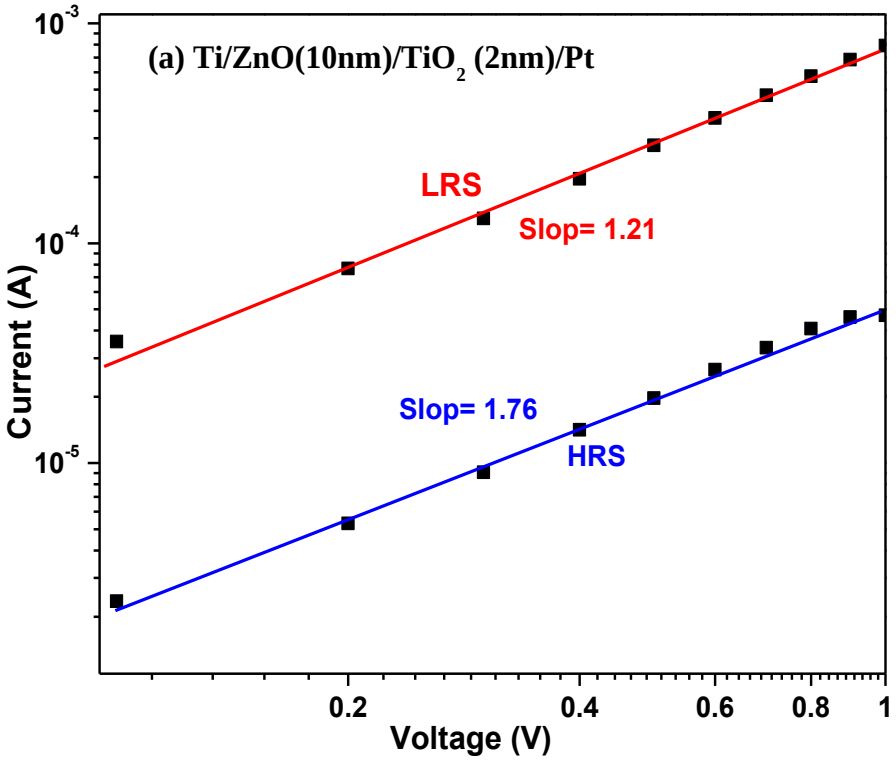

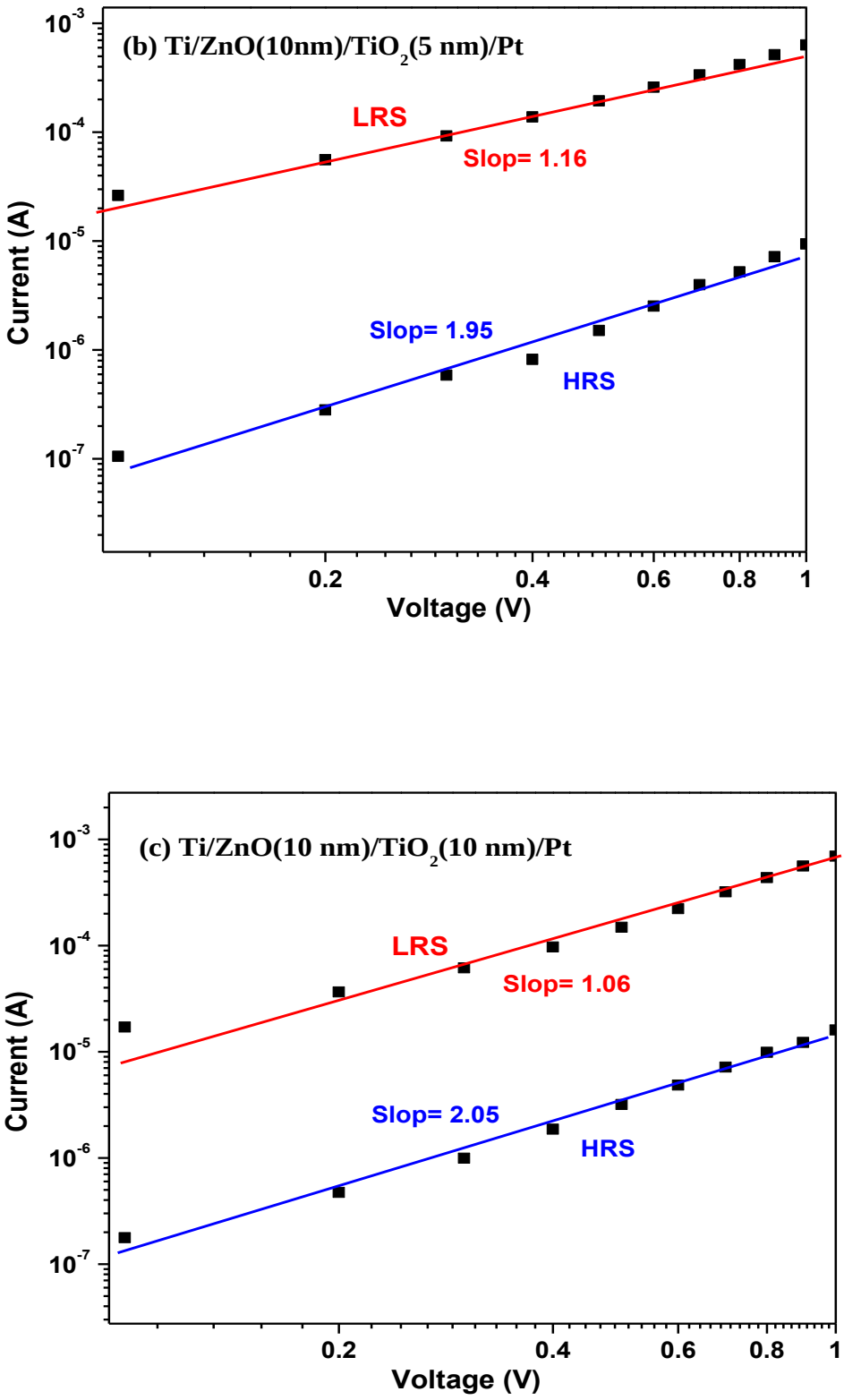

Fig. 6.4: I–V characteristics curve of the RRAM devices in log-log scale of the HRS and LRS (a) Ti/ ZnO (10nm)/ TiO_2 (2nm)/Pt (b)) Ti/ ZnO (10nm)/ TiO_2 (5nm)/Pt (c)) Ti/ ZnO (10nm)/ TiO_2 (10nm)/Pt

To confirm the reliability of the device, the RS characteristics of the devices during continuous switching cycles are measured and the results are shown in Fig. 6.5. The resistances in high and low resistance states are measured at 0.3V read voltage. Significantly fluctuations of both HRS and LHS states are observed in the Ti/ZnO/Pt device structure as shown in Fig.6.5 (a). But when we apply thin layer of TiO_2 (2nm) between ZnO and Ti, it shows narrower distribution and the resistance ratio between HRS and LRS can well maintain for more than 10^3 cycles without any degradation as shown in Fig.6.5 (b). These results indicate that the formation and rupture of conductive filament can be easily performed in the interface between Ti and TiO_2 film comparison to that in the Ti/ZnO interface. In addition, the effect of the different thicknesses of TiO_2 layer on the RS characteristics is also studied. As the thickness of TiO_2 layer increases to 5 nm and 10 nm as shown in Fig 6.5(c-d), device exhibit the unstable RS behavior and switching cycles less than 10^2. When the TiO_2 thickness increases, it increases the variation of formation and rupture of the conducting filament. The large variation may be caused by the random rupture of the conducting filaments implying that the region for filament rupture might be large. The endurance test suggests that the Ti/TiO_2(2nm)/ZnO (10 nm)/Pt structure is reliable for nonvolatile memory application.

To obtain further information on oxygen vacancies, the X-ray photoelectron spectroscopy (XPS) measurements were taken for ZnO and TiO_2 thin film as shown in Fig.6.6. For the ZnO thin film, the O1s peak is located at around 530.eV, while for TiO_2 thin film the O1s peak is located at higher binding energy at around 530.3 eV. The results reveals that more defect (more oxygen vacancies) are available in TiO_2 thin film as compare to ZnO, which indicate that the TiO_2 layer exhibit a highly non-stoichiometric property than ZnO layer [180]. The higher oxygen vacancies inside TiO_2 film favorable stable switching cycles [181]. Therefore, the Ti/TiO_2 (2nm)/ZnO (10 nm)/Pt device shows the better RS property than Ti/ ZnO (10 nm)/Pt.

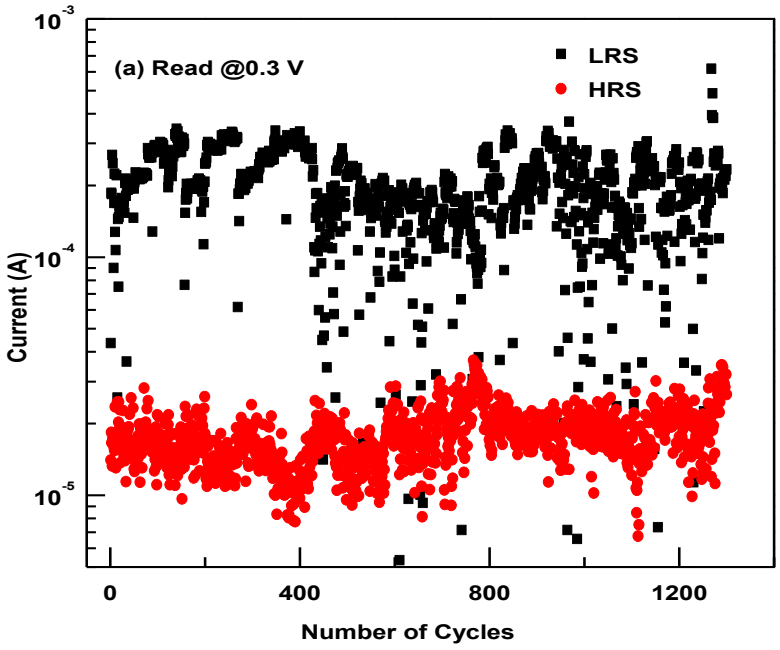

Fig.6.5 (a) DC endurance test for device with Single ZnO (10nm) layer measured at room temperature with a read voltage of 0.3 V.

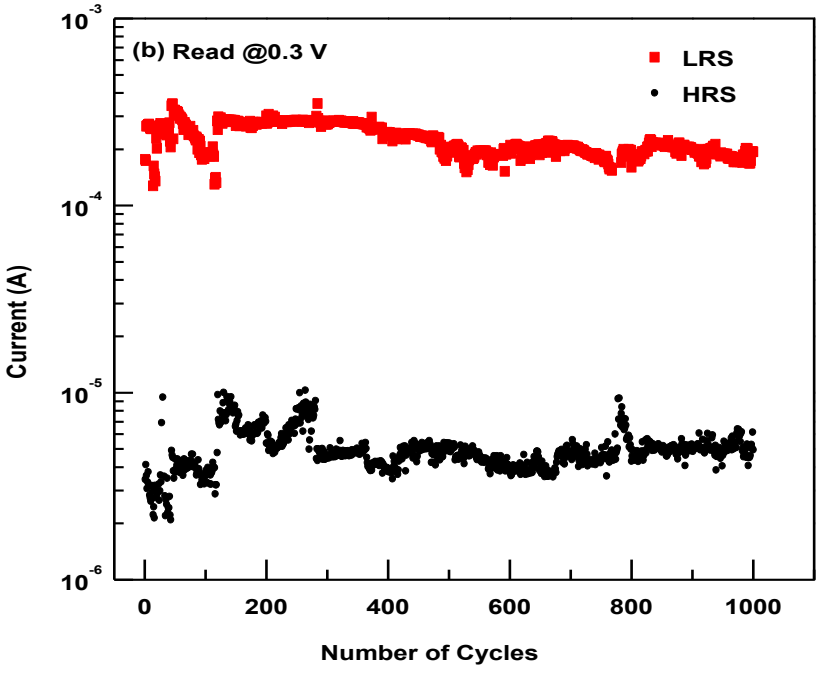

Fig.6.5 (b) DC endurance test for device with TiO_2 (2nm)/ ZnO (10nm) layer measured at room temperature with a read voltage of 0.3 V.

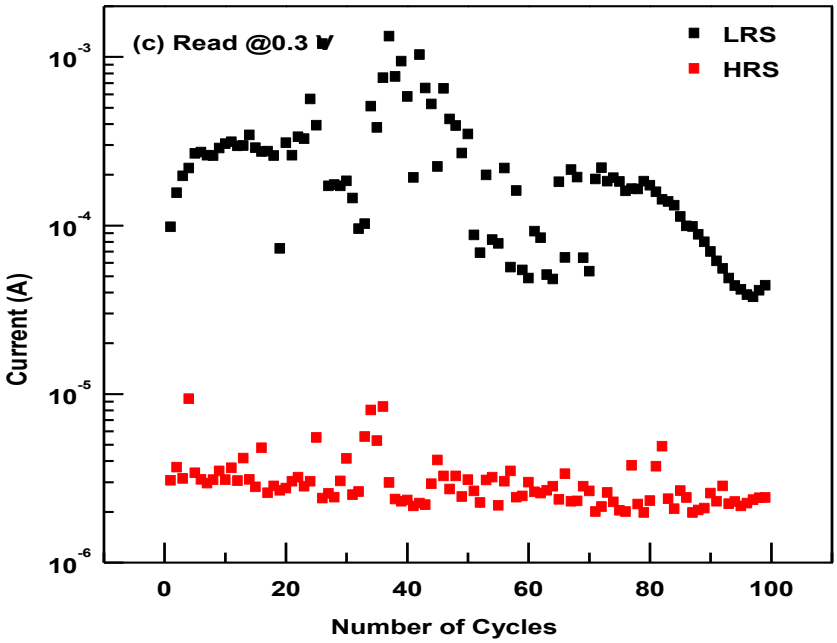

Fig.6.5 (c) DC endurance test for device with TiO_2 (5 nm)/ ZnO (10 nm) layer measured at room temperature with a read voltage of 0.3 V.

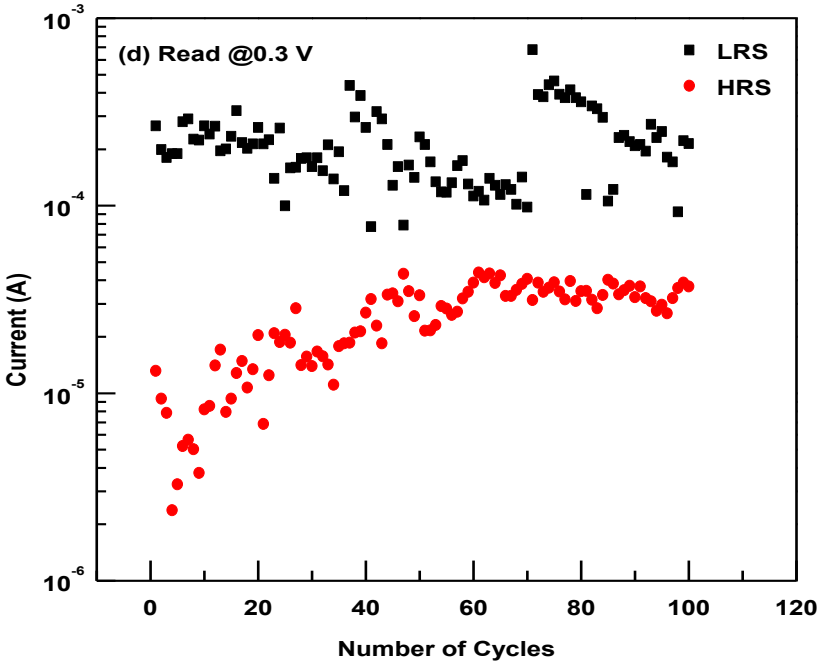

Fig.6.5 (d) DC endurance test for device with TiO_2 (10 nm)/ ZnO (10 nm) layer measured at room temperature with a read voltage of 0.3 V.

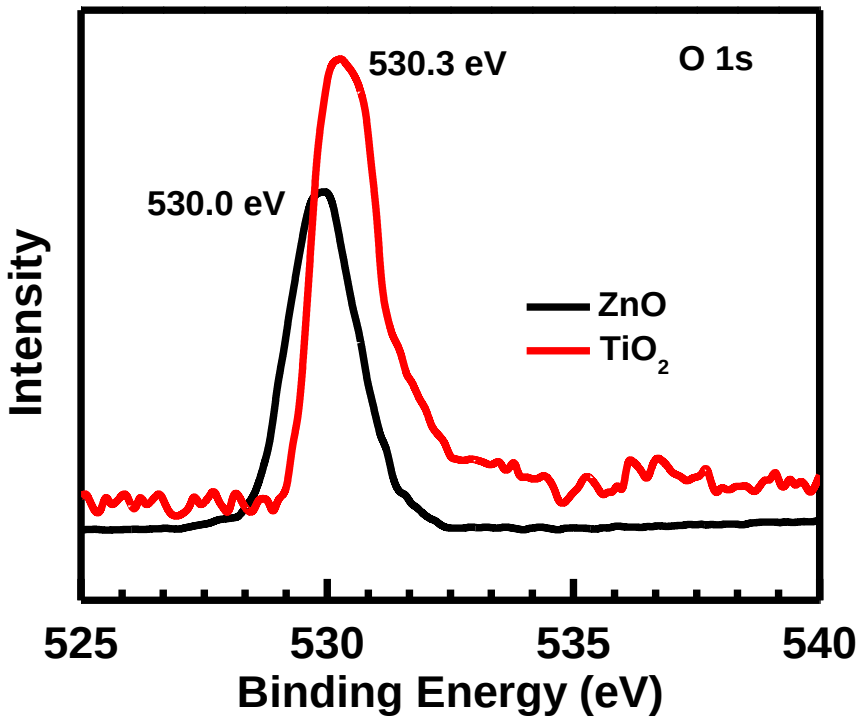

Fig. 6.6: The O 1s XPS spectra of ZnO and TiO_2 layer

The RS mechanism of the demonstrated devices is schematically illustrated in fig. 6.7 and fig. 6.8. The conducting filaments are composed of the oxygen vacancies, hence, as for the conducting filaments model, the forming process has been known as the defect-induced dielectric soft breakdown and oxygen vacancies are created by external electric field and lined up to form the low resistance conducting filaments in the resistive switching thin film. Moreover, it is believed that the formation and rupture of conducting filament occurs in a specific, confined, and local area of resistive switching layer, rather than in homogeneous one. Hence, the resistance of LRS is dependent of device area.

The defect generate inside the switching layer to form a conductive filament between the bottom electrode and the top electrode under applied high positive voltage. The device exhibits the bipolar resistive switching behavior due to the active Ti metal as the top electrode modifying the distribution of the oxygen vacancies in the resistive switching layer. The active Ti metal can easily attract oxygen from non-stoichiometric (more oxygen vacancies) TiO_2 layer rather than that from stoichiometric ZnO layer, which is confirmed by XPS spectra.

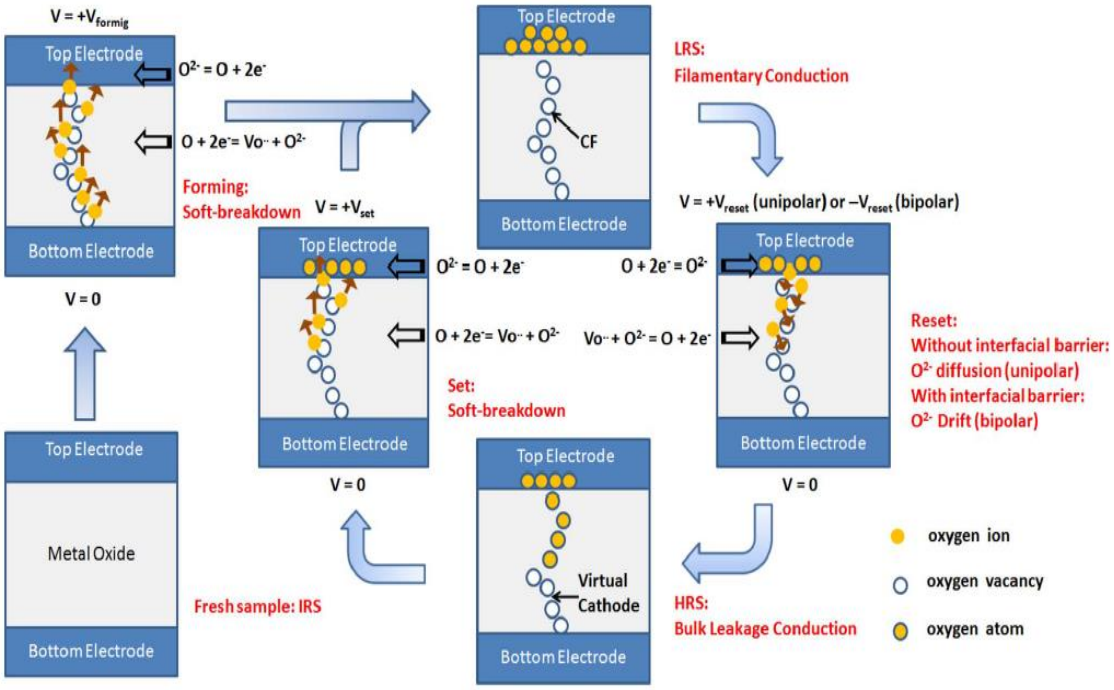

Fig. 6.7: Schematic illustration of the switching process in the simple binary metal-oxide RRAM [183]

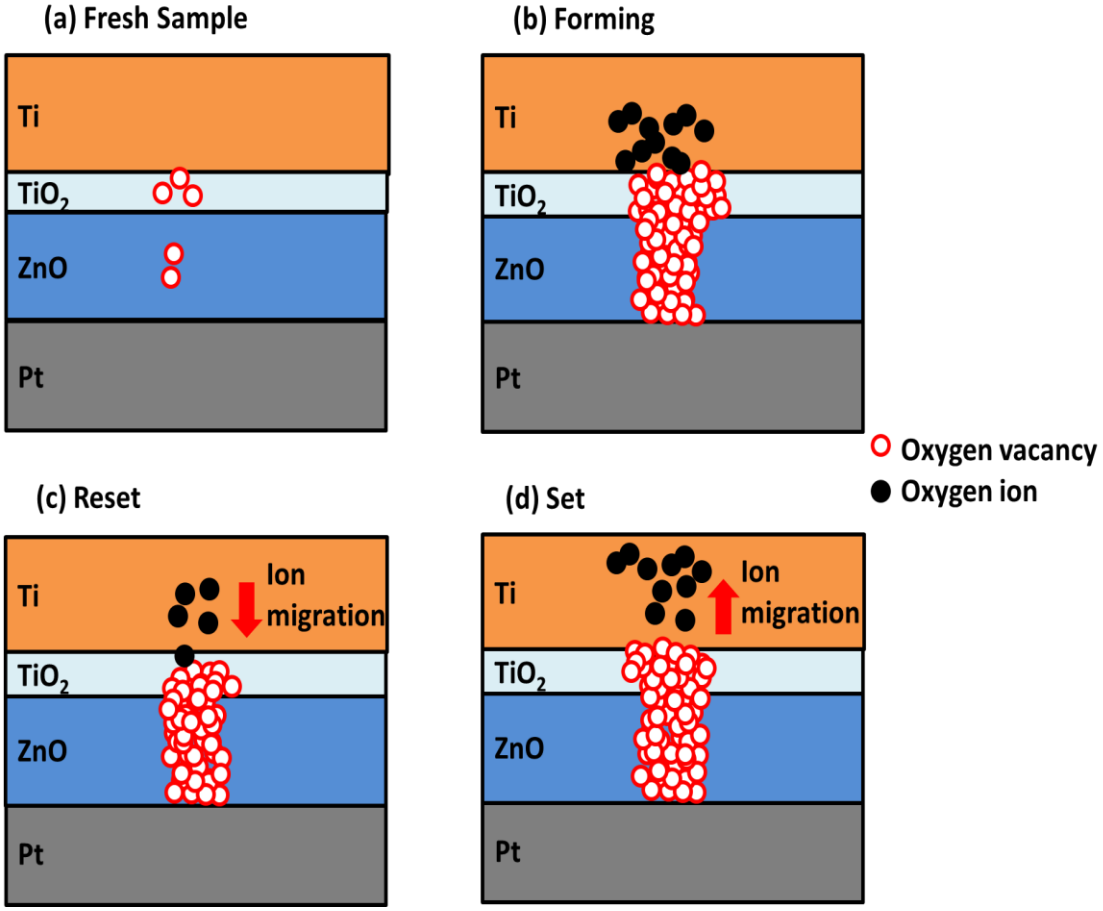

Fig.6.8: (a)-(d) Schematic diagrams for the conduction mechanism of resistive switching in Ti/TiO_2/ZnO/Pt device.

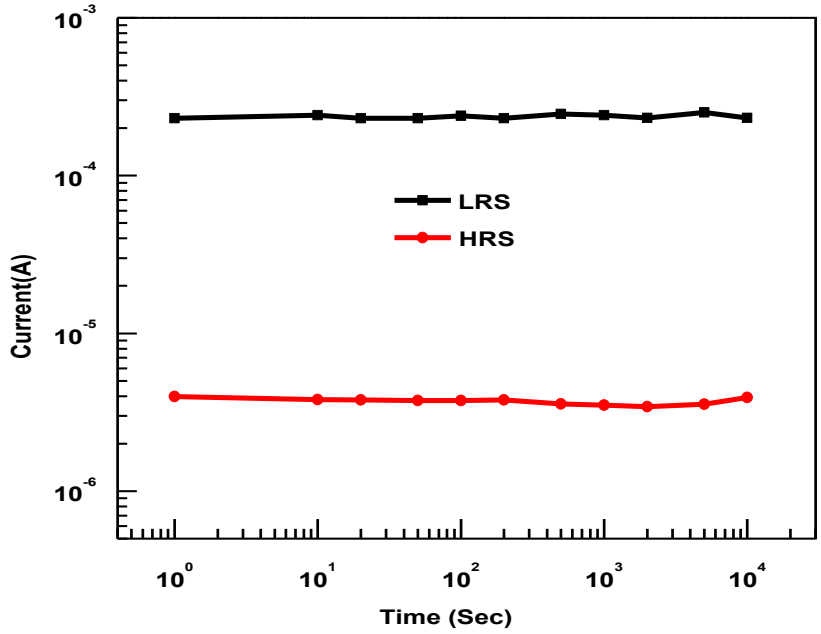

Fig.6.9(a) Retention behavior of both resistance states measured at room temperature for Ti/TiO_2(2nm)/ZnO(10nm)/Pt.

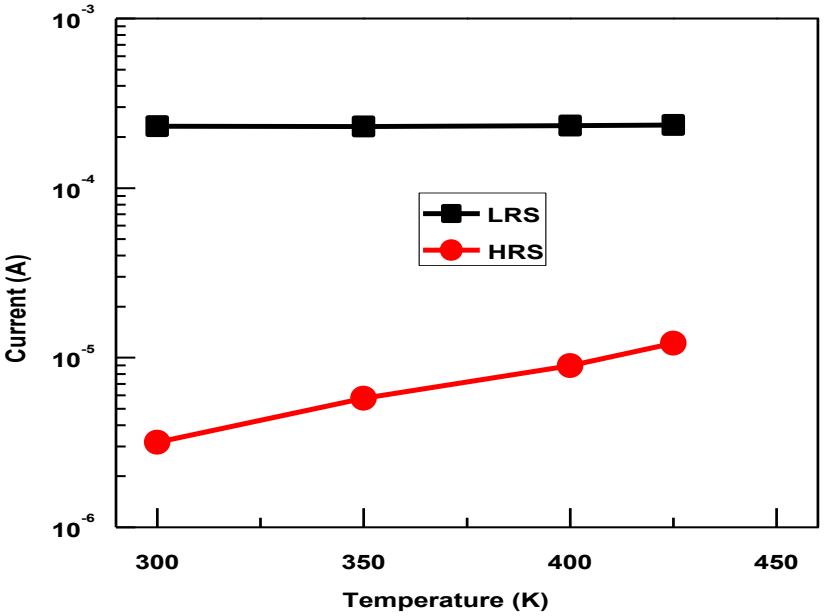

Fig. 6.9 (b) Temperature dependence of the current for LRS and HRS of Ti/TiO_2 (2nm)/ZnO(10nm)/Pt.

The conductive filament forms and rupture at the interface between Ti electrode and TiO_2 interface due to the active Ti metal as the top electrode [182], which modifies the distribution of the oxygen vacancies in the TiO_2 layer, and then the device is in LRS to HRS (ON-state to OFF state). On the other hand, the fluctuation in ZnO device is attributed to that the Ti metal is not easy to oxidize and reduction with the ZnO film due to its more stoichiometric property than TiO_2 film. Therefore, the inserting TiO_2 thin film between Ti top electrode and the ZnO switching layer can stable the endurance property.

The non-volatility of data storage for Ti/TiO_2 (2nm)/ZnO (10 nm)/Pt device is further confirmed by retention test measured at room temperature is shown in Fig.6.9 (a). It is clearly observed that both HRS and LRS do not exhibit any degradation for more than 10^4 s. The temperature dependence of the electrical conductivity is used to study the current transport mechanism during the RS of fabricated device as shown in Fig 6.9 (b). The LRS current is constant with temperature ranges from 300 K to 425 K, which also shows a metallic ohmic behavior [184]. On the other hand, the conduction of the HRS current strongly relies on temperature exhibits a semiconductor – like behavior [185], where the current increase with an increase in temperature. The semiconductor - like Ohmic conduction is expressed as [186]

$$J \approx V \exp(\frac{-C}{T}) \tag{6.1}$$

where T is the absolute temperature and C is a constant. This result indicates that the conduction path is composed of oxygen vacancies rather than metal atoms.

6.4 Conclusion

The switching characteristics in TiO_2/ZnO double layer resistive switching memory device with different thickness of TiO_2 (2 nm, 5 nm and 10 nm) are demonstrated. A remarkable switching uniformity improvement was demonstrated in the TiO_2 layer for 2 nm-thick. The lower forming voltage and more stable RS characteristics were obtained in the double layer for 2 nm thickness of TiO_2. In addition, Ti/TiO_2 (2nm)/ZnO (10nm)/Pt structure demonstrates the stable DC sweep endurance upto 10^3 cycles, satisfactory retention are achieved. From the electrical characteristics, the present device exhibits the potential for future nonvolatile memory applications. The proposed technical solution to achieve the uniform RS behaviors could provide a guideline for the optimization of future generation oxide based RRAM technology.

Chapter-7

Investigation of Photocurrent Efficiency of ZnO/CdTe based Inorganic Thin Film Solar Cell

In this chapter the investigation of photocurrent efficiency of ZnO/CdTe based solar cell has been presented. The effect of ZnO thickness on the solar cell performance has been reported. For further improvement in the solar cell performance, TiO_2 buffer layer was used.

7.1 Introduction

CdTe is II–VI semiconductor compound, which shows the optical band-gap of 1.5 eV that is nearly optimally matched to the solar spectrum for photovoltaic (PV) energy conversion, has been recognized as a potential material for thin film solar cells. High absorption coefficient, more than $5x10^5$/cm also make it suitable for the application in solar cell, i.e. maximum photons with energy greater than the band-gap (E_g) can be absorbed within 2 µm of CdTe film [187-189] Another benefit is that CdTe is a binary compound; therefore it is easier to maintain stochiometry than ternary or quaternary compounds .

CdS thin film has been frequently used as a window layer in the CdTe solar cell due to its wide band gap. But the use of CdS thin film as a window layer limits the device permanence. To improve the blue spectral response, CdS thickness reduced, it improve the J_{sc} but adversely impact V_{oc} and FF. To resolve this issue, high-resistivity ZTO (zinc stannate) buffer layer was used between CdS and CdTe thin film to minimize these unfavorable effects [190]. On the other hand, the lattice mismatching between CdS and CdTe thin film is about 10 %, which causes the high defect density at the junction region. High temperature device fabrication method must be used to improve the inter diffusion of the CdS and CdTe films and form an intermixed layer ($CdTe_{1-x}S_x$), which again causes the new defects that limits the improvement of device performance. Therefore, The best way to solve these issue is to find new window material that has both the higher optical band-gap and a better lattice match with the CdTe absorber, for further improving CdTe cell performance [191].

ZnO is suitable for the production of light emitting devices and a promising candidate for the next generation of electronic devices due to its wide band gap (3.37 eV) and large exciton binding energy (60 meV). ZnO thin films play an important role in solid-state display devices, solar cells and exciting acoustic waves at microwave

frequencies. ZnO is referred to as a window layer or a transparent conducting oxide (TCO) material for solar cell application [23, 25]. In this work, we report ZnO/CdTe based inorganic solar cell in which ZnO layer work as window layer as well as antireflection layer. The main objective of this work is to study the effect of ZnO layer thickness on the efficiency of solar cell. For further improvement in the solar cell performance, TiO_2 buffer layer was used before ZnO layer.

7.2 Experimental Details:

The ZnO film on ITO glass substrate was grown by the RF sputtering system (Company: Advanced Process Technologies, India) at room temperature. The distance between the sputtering target and the deposition substrates was kept at 5.5 cm. High-purity argon (99.999%) was used as during the process. The thickness of ZnO thin film was varied from 50 nm to 150 nm for different device structure. CdSe, MoO_3 and metal contacts were prepared using thermal evaporation technique (Model: BC-300 HHV). The thickness of CdTe was kept at 1 µm. The surface topography and microstructure were examined by atomic force microscope (Multimode -8 Scanning Probe Microscope from Bruker) and FE-SEM (Model: Nova Nano FESEM 450). Current density-voltage characteristics of the devices were measured with Keithley electrometer with illuminating the devices with solar simulator (Xe- source of light). The light intensity was adjusted to 100 mW/cm^2. *The facility of Solar Cell device fabrication and characterization techniques provided by Materials Research Centre, MNIT Jaipur and Department of Electronics Engineering and Institute of Electronics, National Chiao Tung University, Taiwan*

7.3 Effect of ZnO Layer Thickness on the Photocurrent Efficiency

The schematic structure of fabricated ZnO/CdTe based solar cell is shown in Fig. 7.1. The experimental flow for fabrication of device is shown in fig. 7.2. The fabricated solar cells have five layers as follows:

1. Transparent conducting oxides layer (ITO), which is also work as front contact due to its higher conductivity. The main features of this layer are: highly transparent for visible region, highly conducting at room temperature and good adhesion to glass substrate.

2. Window layer (ZnO), which also work as antireflection coating for incident light and electron transport layer for separating the excitons. The main features of this layer are: n-type semiconductor, relatively high transparency, thin layer so that maximum absorption take place in the CdTe absorber layer, to avoid short circuiting this layer

should not much less, It should have higher photoconductivity so that it may not able to change the spectral response of solar cell.

3. Absorber layer (CdTe): This layer is made on top of ZnO layer and is used as p-type semiconductor. CdTe has an ideal band gap (1.5 eV) and high absorption coefficient. These make it suitable material for absorbing layer. A thin layer of CdTe is enough to absorb maximum incoming sunlight.

4. Hole transport layer (MoO_3): This layer provide the barrier to electrons and easier path to hole. So that holes can effectively collected at electrode.

5. Metal contact layer (Al), which is also known as the back contact and is deposited on top of the hole transport layer. This layer must have high work function (>4.5 eV) to form ohmic contact with CdTe layer.

Fig. 7.3 shows the band alignment with respect to the vacuum of the designed solar cell structure. It is clear that ZnO layer and MoO_3 layer works as electron transport layer and hole transport layer, respectively. The normal incident light will penetrate glass, ITO, and ZnO layers before entering in the active CdTe absorber layer. Through this path, a part of the incident light will be lost in these layers due to reflection from air-glass, glass-ITO, ITO-ZnO and ZnO-CdTe interfaces and absorb in glass, ITO, and ZnO layers. The reflectivity from the interface between two layers depends on the values of refractive index (n) and extinction coefficient (k) of the contacting materials. The spectral dependence of refractive index and extinction coefficient of glass, ITO, ZnO and CdTe layers on wavelength.

When one of the ITO, ZnO and CdTe layers is used as a single layer (i.e., the interfaces are between air-ITO, air-ZnO, and air-CdTe), the calculated reflection dependence on wavelength. The absorption coefficient $\alpha(\lambda)$ can be calculated using the data of extinction coefficient $k(\lambda)$ according to the following equation [192]:

$$\alpha(\lambda) = 4\pi\kappa/\lambda \qquad (7.1)$$

The losses caused by recombination process is determined by the width (W) of the space charge region i.e. depletion layer. It is mainly depends on the uncompensated concentration of acceptors (N_a-N_d). It is also used to determine the efficiency of photoelectric conversion for CdTe layer. The electronic processes take place in the CdTe depletion layer is similar to the depletion layer of the Schottky diode, due to the high photo conduction of ZnO layer. The depletion layer (the space–charge region) of the ZnO/CdTe formation is nearly placed in CdTe and band bending also falls onto CdTe [193].

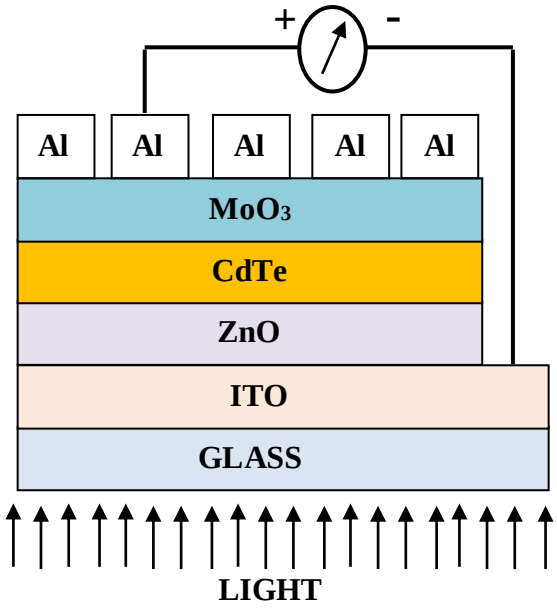

Fig. 7.1: Schematic diagram of Designed Solar cell

Cleaning of ITO coated glass substrate, ITO used as cathode

↓

RF sputtered ZnO thin film, antireflection coating and electron transport layer, thickness varied from 50 nm to 150 nm

↓

Thermal Evaporated CdTe thin film, light absorbing layer thickness 1µm

↓

Thermal Evaporated MoO_3 Thin film, Hole transporting layer 50 nm

↓

Thermal evaporated metal (Al) contact, used a anode

Fig. 7.2: Experimental flow for fabrication of Solar cell

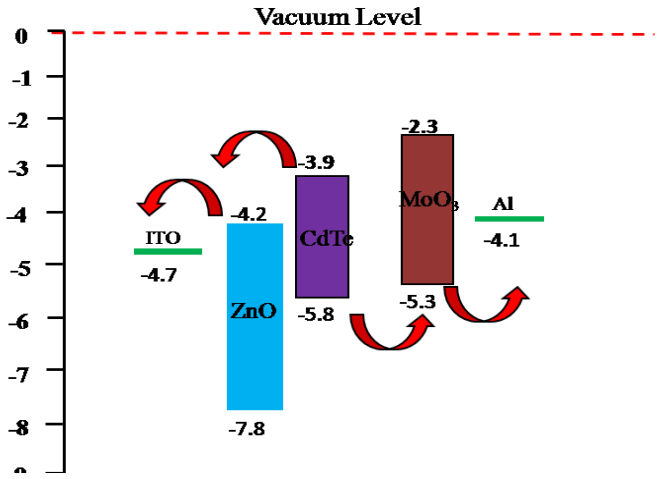

Fig. 7.3: Band alignment of the designed solar cell structure

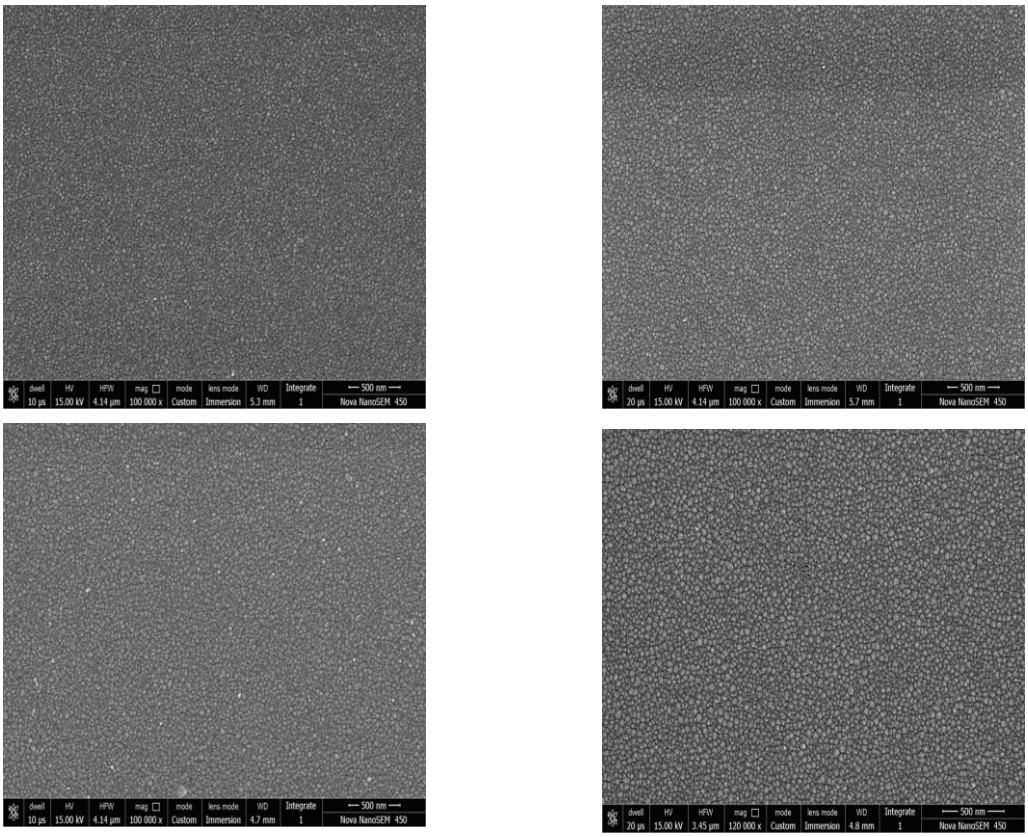

Fig. 7.4: SEM image of ZnO thin film with different thickness

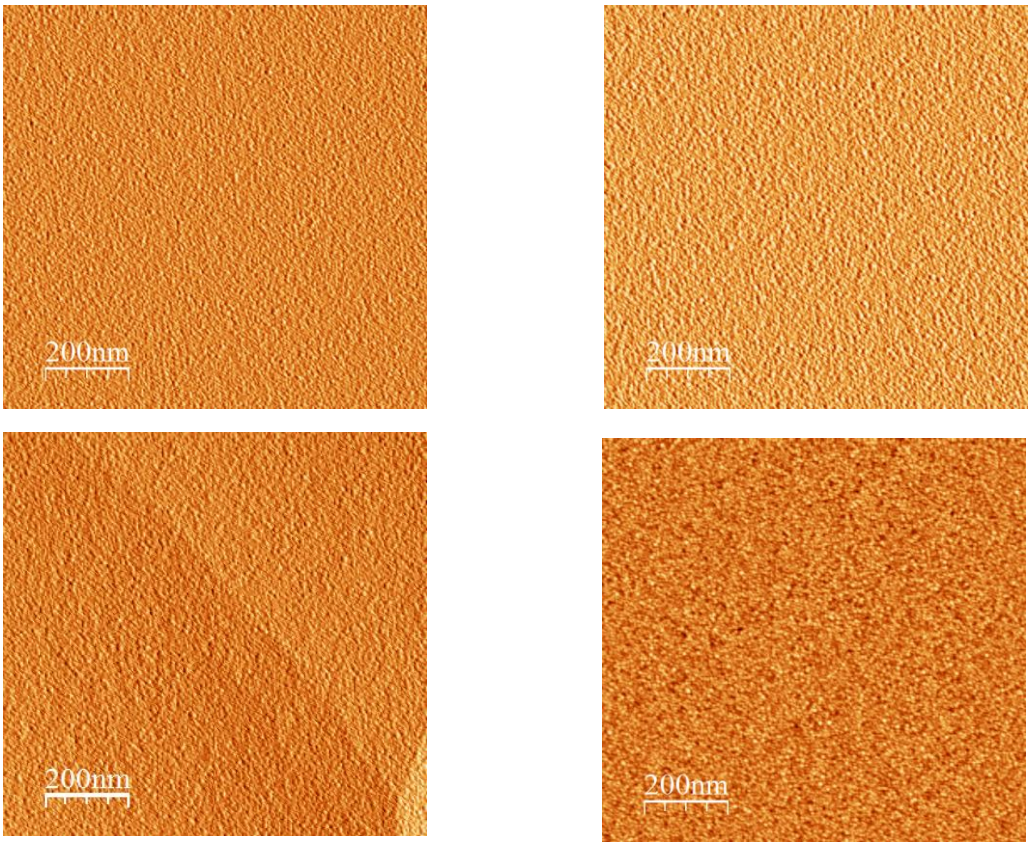

Fig. 7.5: AFM image of ZnO thin film with different thickness

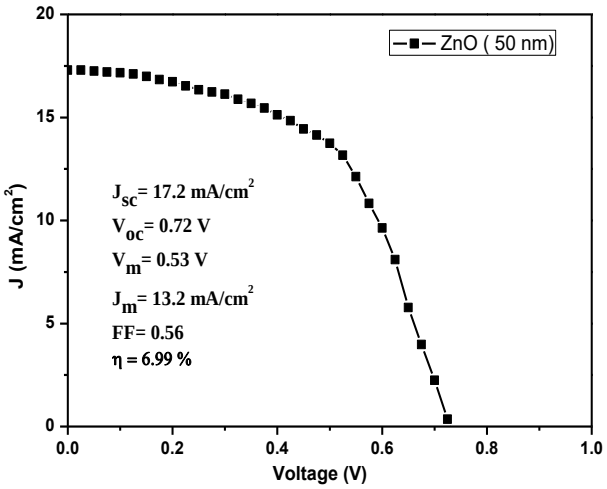

Fig. 7.6(a): J-V characteristics of solar cell with ZnO thickness of 50 nm

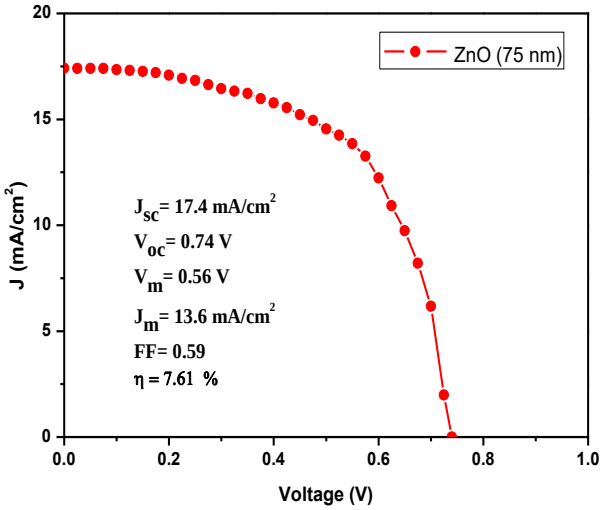

Fig. 7.6(b): J-V characteristics of solar cell with ZnO thickness of 75 nm

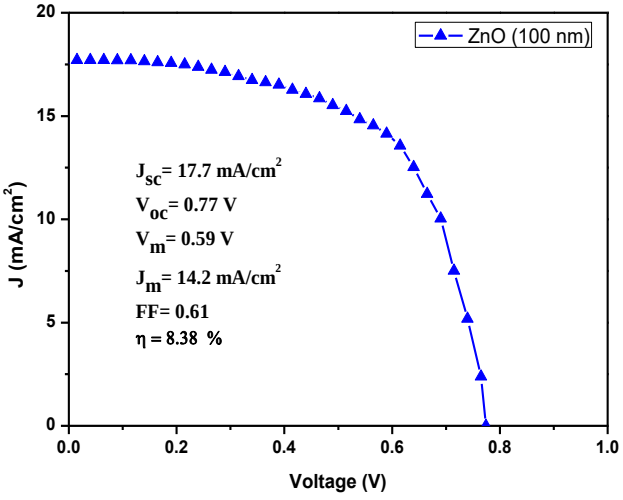

Fig. 7.6(c): J-V characteristics of solar cell with ZnO thickness of 100 nm

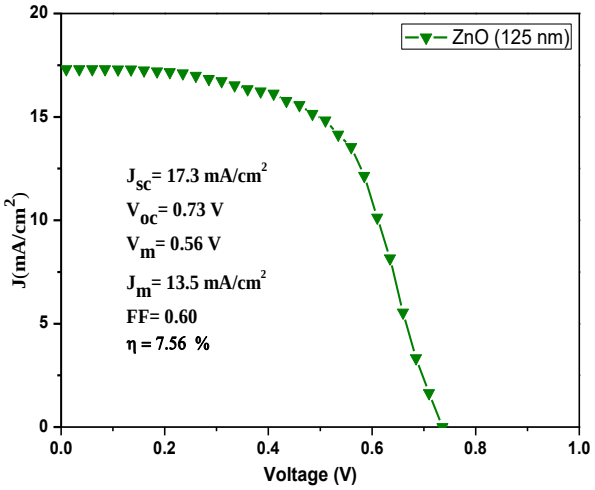

Fig. 7.6(d): J-V characteristics of solar cell with ZnO thickness of 125 nm

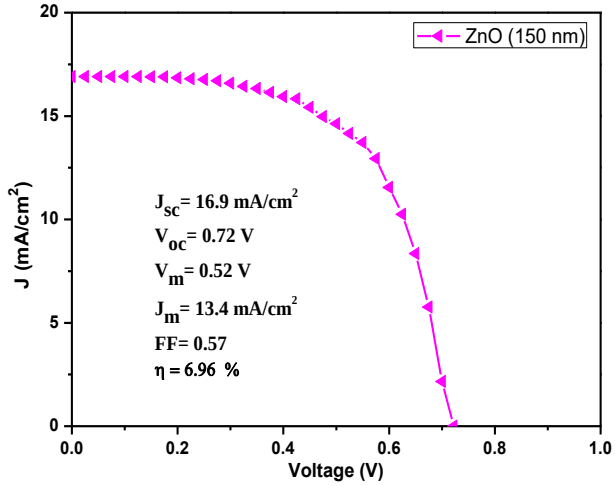

Fig. 7.6(e): J-V characteristics of solar cell with ZnO thickness of 150 nm

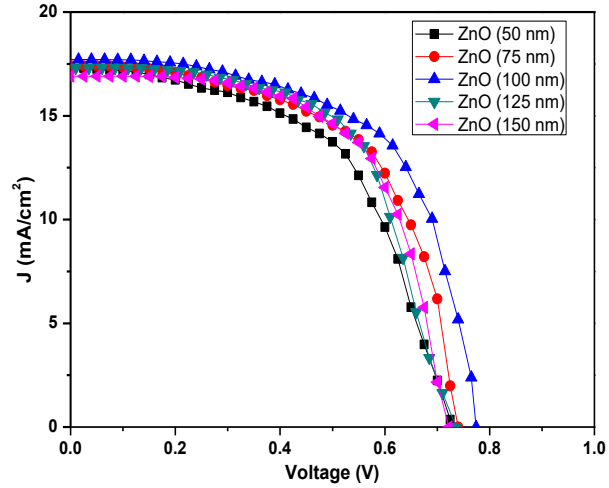

Fig. 7.6(f): Comparison of J-V characteristics of solar cell with different thickness of ZnO layer

Table 7.1: Various characteristics parameters of solar cell with different ZnO layer thickness

Thickness of ZnO layer (nm)	J_{sc} (mA/cm^2)	V_{oc} (V)	Fill Factor (FF)	V_m (V)	J_m (mA/cm^2)	Efficiency η (%)
50	17.2	0.72	0.56	0.53	13.2	6.99
75	17.4	0.74	0.59	0.56	13.6	7.61
100	17.7	0.77	0.61	0.59	14.2	8.38
125	17.3	0.73	0.60	0.56	13.5	7.56
150	16.9	0.72	0.57	0.52	13.3	6.96

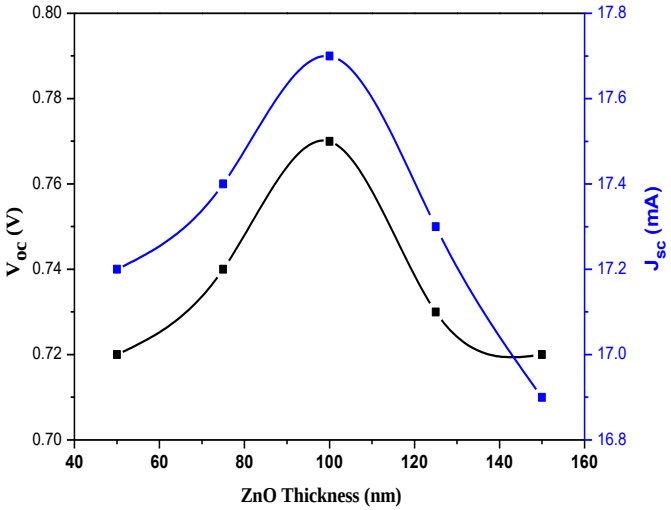

Fig.7.7: Variation of V_{oc} and J_{sc} with different ZnO layer thickness

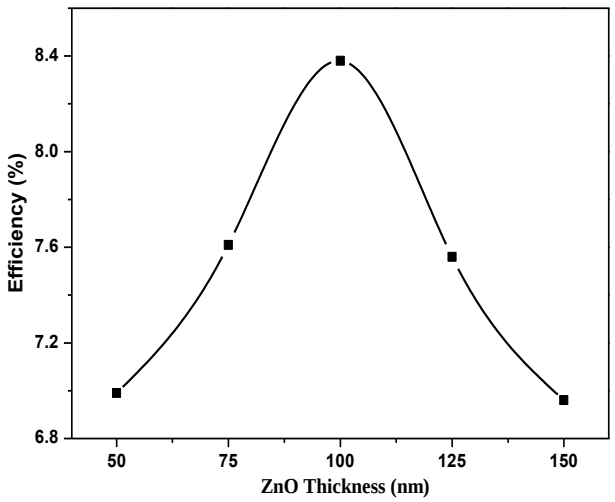

Fig.7.8: Variation of photo conversion efficiency with different ZnO layer thickness

The surface morphology of the ZnO thin films were characterized using AFM and SEM. The observed images of ZnO thin films with different thickness from AFM and SEM are shown in fig. 7.4 and fig. 7.5, respectively. It is clearly seen from images that the uniformity of grains and quality of films are good. The roughness observed from AFM is between 2-3 nm. The J-V characteristics of the fabricated solar cells are shown in fig. 7.6 (a-f). The calculated characteristics parameters of solar cells from J-V characteristics are listed in Table 7.1.

The internal and external quantum efficiency is the main parameters to determine the performance of PV solar cell. The internal quantum efficiency is observed more than 80% using thin film device technology but reported maximum external efficiency for Si solar cell is about 25%. The poor light entering capacity of the solar cell structure which results from the Fresnel reflections causes this large difference between these two efficiencies.

The intensity of Fresnel reflected light is dependent on the refractive index of two layers [194], given as:

$$I_R = [n_2 - n_1]^2 / [n_2 + n_1]^2 \quad (7.2)$$

Antireflection coating is used to reduce Fresnel refection, which is based on the Interference of light in thin film. The thickness of antireflection coating and refractive index should satisfy the following equation [194]:

$$d = \lambda / (4 \times n_f) \quad (7.3)$$

$$n_f = \sqrt{(n \times n_0)} \quad (7.4)$$

Where, λ is the light wavelength and n_0 is the refractive index of the air.

Initially, short circuit current increases with ZnO thicknesses from 50 nm to 100 nm but more increment in the thickness causes the reduction in the short circuit current. The maximum value is achieved at 100 nm; this is due to satisfaction of destructive interference condition more properly.

The variation of J_{sc}, V_{oc} and efficiency with respect to ZnO layer thickness is shown in fig. 7.7 and fig. 7.8, respectively. Initially as we increase the thickness of ZnO layer, the more the excitons encouraged by light absorption. This increases the efficiency of solar cell. The thickness of ZnO ranging from 75-100 nm also support for perfect antireflection coating which increases the absorption of light. However, more

increment in the ZnO thickness causes the longer pathway due to the weaker build-in-electric field for transporting the opposite charge carriers. At the same time, the weaker exiciton separation to their corresponding electrode is also lower.

7.4 Effect of TiO_2 Layer Thickness on the Photocurrent Efficiency

A buffer layer in a heterojunction solar cell is used to form a junction with the absorber layer/window layer to provide maximum amount of light to the junction region and absorber layer. Additionally, buffer layer should also have minimal absorption losses and capable of separating the photo generated carries with minimal electrical resistance and with minimum recombination losses. The main features of this layer are: (i) For high optical transmission, it should have large energy band gap, (ii) Optimal band discontinuities, it increase the probability of the interface cross-recombination, (iii) Lattice mismatching should be less and (iv) sufficient doping density to confine the space charge region at absorber. As we have mentioned the properties of TiO_2, TiO_2 fufill the above mentioned requirements. So we have used the TiO_2 buffer layer for ZnO layer in order to improve the performance of the solar cell.

The schematic structure of fabricated TiO_2/ZnO/CdTe based solar cell is shown in Fig. 7.9. The experimental flow for fabrication of device is shown in fig. 7.10. The TiO_2 film on ITO glass substrate was grown by the RF sputtering system (Company: Advanced Process Technologies, India) at room temperature. The distance between the sputtering target and the deposition substrates was kept at 5.5 cm. High-purity argon (99.999%) was used as during the process. The thickness of TiO_2 thin film was varied from 20 nm to 40 nm for different device structure. After that ZnO thin film of 100 nm (which gives the best result in above section) was prepared using sputtering technique. The Band alignment of the designed solar cell structure is shown in fig. 7.11. It is clear from that TiO_2 layer provides the path to electrons for collecting at the electrode. The J-V characteristics of the fabricated solar cells are shown in fig. 7.12 (a-c). The calculated characteristics parameters of solar cells from J-V characteristics are listed in Table 7.2.

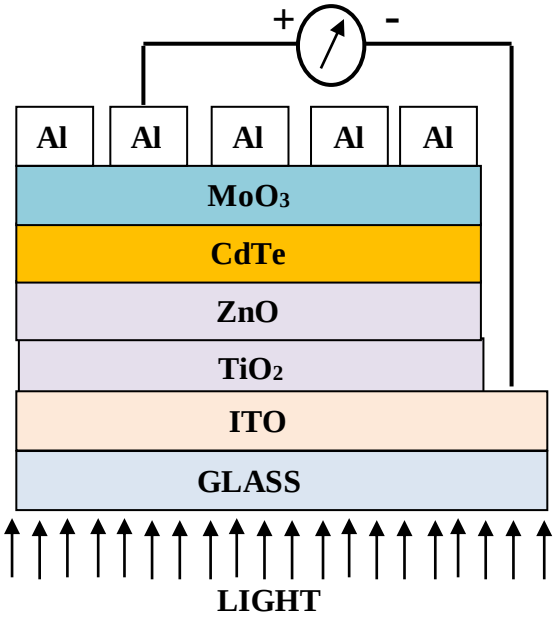

Fig. 7.9: Schematic diagram of Designed Solar cell

Cleaning of ITO coated glass substrate, ITO used as cathode

↓

RF sputtered TiO_2 thin film of thickness varied from 20 nm to 50 nm

↓

RF sputtered ZnO thin film of thickness 75 nm

↓

Thermal Evaporated CdTe thin film, light absorbing layer thickness 1µm

↓

Thermal Evaporated MoO_3 Thin film, Hole transporting layer 50 nm

↓

Thermal evaporated metal (Al) contact, used a anode

Fig. 7.10: Experimental flow for fabrication of Solar cell

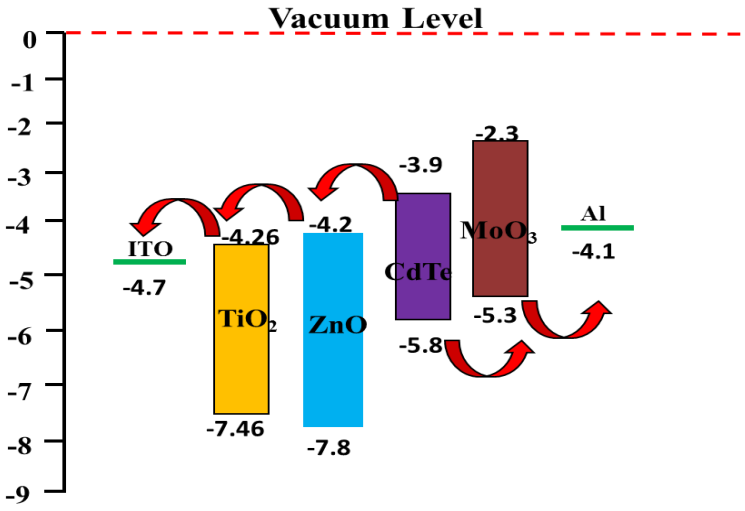

Fig. 7.11: Band alignment of the designed solar cell structure

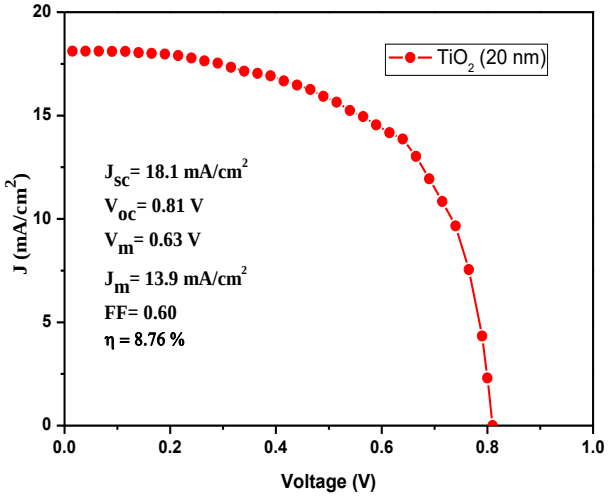

Fig. 7.12(a): J-V characteristics of solar cell with TiO_2 thickness of 20 nm

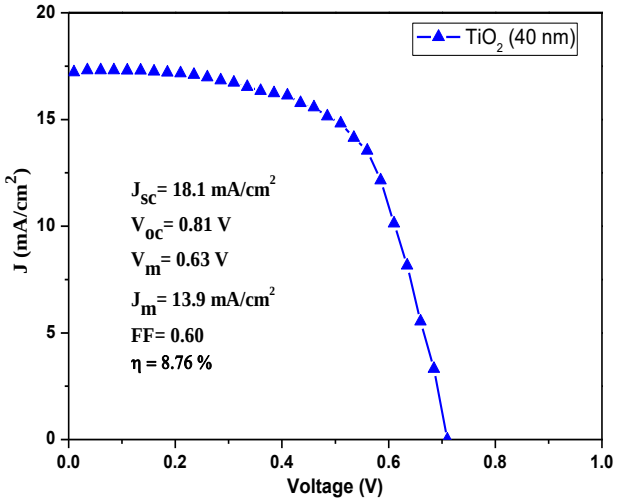

Fig. 7.12(b): J-V characteristics of solar cell with TiO_2 thickness of 40 nm

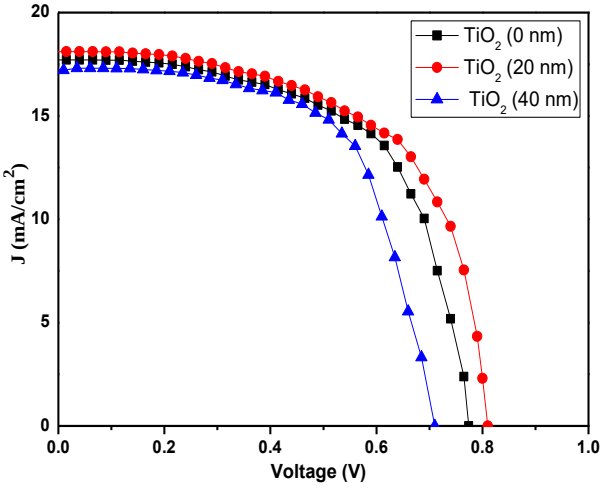

Fig. 7.12(c): Comparison of J-V characteristics of solar cell with different thickness of TiO_2 layer

Table 7.2: Various characteristics parameters of solar cell with different TiO_2 layer thickness

Thickness of TiO_2 layer (nm)	**J_{sc} (mA/cm^2)**	**V_{oc} (V)**	**Fill Factor (FF)**	**V_m (V)**	**J_m (mA/cm^2)**	**Efficiency η (%)**
0	17.7	0.77	0.61	0.59	14.2	8.38
20	18.1	0.81	0.60	0.63	13.9	8.76
40	17.2	0.71	0.60	0.55	13.4	7.37

The results indicate that thin TiO_2 layer between ITO and ZnO improves device performance while excessive thickness degrades the performance of the device. This is because of the reduce mobility and increases series resistance in thick TiO_2 film. Additionally, as concluded in chapter 4, the use of TiO_2 buffer layer increases the crystallinity of ZnO layer. This results the easier transportation of charge carriers and consequently increase performance of the solar cell. But more increment in TiO_2 layer causes the longer pathway for the charge carriers causes the reduced performance of the solar cell.

7.5 Conclusion

Glass/ITO/ZnO/CdTe/MoO_3/Al structured inorganic thin film solar cell was successfully fabricated. The effect of ZnO thickness varying from 50 nm to 150 nm on the performance parameters of solar cell (open circuit voltage, short circuit current, fill factor and power conversion efficiency) was investigated. The maximum efficiency of about 8.39% was observed for the 100 nm thickness of ZnO layer. For further improvement in the efficiency, thin layer of TiO_2 (20 nm) before ZnO layer was used and efficiency was improved upto 8.76%.

Chapter-8

Conclusions and Future Scope

This Chapter presents the summary and conclusions of the entire work and also proposes the future directions in which these studies can be extended.

The main aim of the present work was to fabricate high quality ZnO and TiO_2 nanocrystalline thin films and to use these films for solar cell and resistive random access memory. Following is a brief summary and conclusion of the entire work done and the directions in which it can be pursued further.

8.1 Conclusions

ZnO and TiO_2 thin films, with and without buffer layer, were deposited on single crystal Si (100) substrate using pulsed laser deposition (PLD) technique with KrF excimer laser source. Structural properties of the deposited thin films were characterized using XRD and AFM. It has been observed that ZnO thin film with TiO_2 buffer layer exhibited higher crystallinity along (002) diffraction peak. ZnO thin film deposited on TiO_2 buffer layer possesses small compressive strain and stress. Therefore, it shows better optical properties as compared to ZnO thin films grown directly on Si substrates. TiO_2 thin film deposited on a Si substrate showed pure anatase phase while the films deposited with ZnO buffer was found to have improved crystallinity than bared TiO_2 thin film. A TiO_2 and ZnO buffer layer respectively enhances the ultraviolet emissions of the ZnO and TiO_2 thin films to a larger extent. The optical band gap of ZnO and TiO_2 thin film with buffer layer found to decrease as compared to bared ZnO and TiO_2 thin films due to the improved crystallinity.

Perovskite materials ($ZnTiO_3$type materials) exhibit many interesting and intriguing properties from both the theoretical and the application point of view. Recently, much attention has been focused on the synthesis of ***single phase perovskite materials*** (because of their unique properties). In the present work, single phase $ZnTiO_3$ thin film were successfully fabricated on ITO coated glass substrate through pulsed laser deposition (PLD). Substrate temperature has significant effect on transformation of hexagonal phase to cubic phase. Therefore, effect of substrate temperature on optical and dielectric properties was studied. The pure hexagonal phase of $ZnTiO_3$was observed upto 400 ^oC substrate temperature and more increment in temperature leads to transformation of hexagonal phase to cubic phase.When the substrate temperature

increases from 300 to 400 ^{o}C the band gap decreases due to strong hexagonal phase, but further increment in substrate temperature increases the band gap. This increase in band gap is due to change of phase from hexagonal to cubic. The dielectric constant of $ZnTiO_3$ thin film increases as the substrate temperature increases due to improved crystallinity and morphology. The dielectric constant and loss tangent shows a steep decrease in the lower frequency region while a constant value was observed at the higher frequency region.

The resistive switching characteristics of ***TiO_2/ZnO double layer RRAM device*** were successfully investigated. The effect of thickness of TiO_2 layer (2 nm, 5 nm and 10 nm) on switching characteristics was studied using Agilent B1500A semiconductor parameter analyzer. It was observed that device with 2 nm thickness of TiO_2 layer show stable resistive switching characteristics. The forming voltages of the fabricated RRAM devices were dependent on the TiO_2thickness which supports the idea that forming process is governed by dielectric breakdown. It was observed that the RRAM device with the 2 nm TiO_2 layer exhibits good dc endurance up to 10^3 cycles. Moreover, both low resistance state (LRS) and high resistance state (HRS) do not exhibit any degradation for more than 10^4 s. The study of electrical characteristics reveals that the present device exhibits the potential for future nonvolatile memory applications. The proposed technical solution to achieve the uniform RS behaviors could provide a guideline for the optimization of future generation oxide based RRAM technology.

The sputtering and thermal evaporation method was employed to fabricate ***ZnO/CdTe based inorganic thin film solar cell.*** The SEM and AFM image indicate good crystallinity and less roughness of the thin films thus suggesting the good quality of thin films. The J-V characteristics of solar cell were measured using Keithley electrometer with illuminating the device with solar simulator (Xe-Source of light and AM 1.5G filter). The effect of ZnO thickness varying from 50 nm to 150 nm was investigated and maximum efficiency of about 8.39 % was observed for the 100 nm thickness of ZnO layer. For further improvement in the efficiency, thin layer of TiO_2 between ZnO and ITO layer was introduced. It has been observed that the efficiency was improved upto 8.76 % with 20 nm thickness of TiO_2 layer. It may be concluded that thin TiO_2 layer improves device performance while the excessive thickness degrades the performance of the device due to reduced mobility and increase in series resistance.

8.2Future Scope

The quality of ZnO and TiO_2 thin film is an important determining factor of the device performance for thin film based devices. An experimental study may be performed on the effect of variation of thickness of ZnO and TiO_2 buffer layer on TiO_2 and ZnO thin films, respectively. There is a scope for extending the research to perform the investigation on the ZnO/TiO_2multilayer.The single phase $ZnTiO_3$ thin films may be prepared on different substrates like glass, Si, silica wafer, Al_2O_3etc. and the role of substrate matrix on the growth of film could be investigated.Electrical studies, like I-V characterization and Hall measurement could be carried out for the above prepared samples.

We have addressed the key problems of the relatively poor uniformity and large variability of the resistive switching properties in RRAM devices, and its solutions through innovations in device materials and structures. Transition metal oxide (TMO) based resistive random access memory (RRAM) reveals high performance memory behavior, such as large endurance, long retention, and low operation voltage. However, the small on/off ratios and large variation during endurance characteristic in TMO based RRAM are big challenges that need to be solved. Recently, the conductive bridge switching memory (CBRAM) is seen as a major contender for future memory replacement with large on/off ratio and good retention property. The major challenge is cycle to cycle variation as well as device to device variation. To acheive this, it is necessary to have a complete understanding of the conduction and resistive switching mechanism. The solution may come from a combination of insulator-electrode material and device structures.

The solar cell may be designed and fabricated using other II-VI compounds like ZnS, CdSe, CdTe, ZnO etc. Doping and reduce particle size may enhance optical absorption and making it more efficient. To increase the electrical property, quantum assembly and conducting polymer may be used to conduct single electron from dot to dot through matrix and increase the quantum efficiency of the device.So far, most of the solar cells are entirely made of inorganic semiconductors, but these materials are not as energy efficient as organic semiconductors. The new method lies in the groundwork for building a new generation of solar cells made up of both organic and inorganic materials.

References/Bibiography

[1] G. Decher, J. B. Schlenoff, "Multilayer Thin Films: Sequential Assembly of Nanocomposite Materials", Wiley-2nd Ed, 2012.

[2] Catherine Picart, Frank Caruso, Jean-Claude Voegel, Gero Decher, "Layer-by-Layer Films for Biomedical Applications", Wiley-VCH, 2003

[3] Y. S. Lim, J. S. Jeong, J. Bang, J. Kim "CaO buffer layer for the growth of ZnO thin film", Journal of Solid State Communications, vol. 150, 2010, pp. 428-430.

[4] Yan Xu, Jingjie Jin, Xianliang Li, Yide Han, Hao Meng, Tianyu Wang, Xia Zhang, "Simple synthesis of ZnO nanoflowers and its photocatalytic performances toward the photodegradation of metamitron", Materials Research Bulletin, vol. 76, 2016, pp. 235-239.

[5] Liqing Liu, Kunquan Hong, Xing Ge, Dongmei Liu, Mingxiang Xu, "Controllable and Rapid Synthesis of Long ZnO Nanowire Arrays for Dye-sensitized Solar Cells", *J. Phys. Chem. C*, vol. 118, 2014, pp. 15551–15555.

[6] Laurent Schlur, Anne Carton, Patrick Lévêque, Daniel Guillon, Geneviève Pourroy "Optimization of a New ZnO Nanorods Hydrothermal Synthesis Method for Solid State Dye Sensitized Solar Cells Applications", *J. Phys. Chem. C*,117, 2013, pp. 2993–3001.

[7] K. Koike, T. Aoki, R. Fujimoto, S. Sasa, M. Yano, S. Gonda, R. Ishigami, K. Kume, "Radiation hardness of single-crystalline zinc oxide films" J. Phys. Status Solidi C, vol. 9, 2012, pp.1577–1579.

[8] Shashikant Sharma, Bernhard C. Bayer; Viera Skakalova; Ghanshyam Singh, Chinnamuthan Periasamy, "Structural, Electrical, and UV Detection Properties of ZnO/Si Heterojunction Diodes" IEEE Transactions on Electron Devices, vol. 63, 2016, pp.1949-1956.

[9] R.Pietruszka. B.S.Witkowski, P.Caban, E.Zielony, K.Gwozdz, P.Bieganski, E.Placzek-Popko, "New efficient solar cell structures based on zinc oxide nanorods Solar Energy Materials and Solar Cells", Journal of Solar Energy Materials and Solar Cells, vol. 143, 2015, pp. 99-104.

[10] J. C. Sun, J. M. Bian, H. W. Liang, J. Z. Zhao, L. Z. Hu, Z. W. Zhao, W. F. Liu, and G. T. Du, "Realization of controllable etching for ZnO film by NH_4Cl

aqueous solution and its influence on optical and electrical properties", Appl. Sur. Sci, vol. 253, 2007, pp.5161-5165.

[11] L. Znaidi, S. Illia, S. Benyahia, C. Sanchez, A. V. Kanaev, "Oriented ZnO thin films synthesis by sol–gel process for laser application" Thin Solid Films, vol. 428, 2003, pp. 257-262.

[12] M. Karthika, V. Manoj, S. Boomadevi, K. Jeyadheepan, R. K. Karn, R. John, S. K. Pandiyan, "Gas Sensing Studies on Nanocrystalline ZnO Thin Films Prepared by Dip Coating" Asian Journal of Applied Sciences, vol. 7, 2014, pp. 786-791.

[13] Mazran Esro, George Vourlias, Christopher Somerton, William I. Milne, George Adamopoulos, "High-Mobility ZnO Thin Film Transistors Based on Solution-processed Hafnium Oxide Gate Dielectrics", J. of Advanced Functional Materials vol. 25, 2015, pp. 134–141.

[14] Charles Opoku, Abhishek Singh Dahiya, Christopher Oshman, Frederic Cayrel, Guylaine Poulin-Vittrant, Daniel Alquier, Nicolas Camara, "Fabrication of ZnO Nanowire Based Piezoelectric Generators and Related Structures", Physics Procedia, vol. 70, 2015, pp. 858-862.

[15] Kanwal Preet Bhatti, Vivek Kumar Malik, Sujeet Chaudhary, "Cobalt substituted ZnO thin films: a potential candidate for spintronics", J Mater. Sci: Mater. in Electron, vol. 19, 2008, pp. 849-854.

[16] Van-Son Dang, Harish Parala, Jin Hyun Kim, Ke Xu, Nagendra B. Srinivasan, Eugen Edengeiser, Martina Havenith, Andreas D. Wieck, Teresa de los Arcos, Roland. A. Fischer, Anjana Devi, "Electrical and optical properties of TiO_2 thin films prepared by plasma-enhanced atomic layer deposition", Physica Status Solidi(a), vol. 211, 2014, pp. 416-424.

[17] M. I. Khan, K. A. Bhatti, Rabia Qindee, Hayat Saeed Althobaiti, Norah Alonizan "Structural, electrical and optical properties of multilayer TiO_2 thin films deposited by sol–gel spin coating" Results in Physics, vol. 7, 2017, pp. 1437-1439.

[18] Najla Ghrairi, Mongi Bouaicha, "Structural, morphological, and optical properties of TiO_2 thin films synthesized by the electro phoretic deposition technique", Nanoscale Research Letters, vol.7, 2012, pp. 357-360.

[19] B. Karunagaran, Periyayya Uthirakumar, S. J. Chung, S. Velumani, E.-K.Suh, "TiO_2 thin film gas sensor for monitoring ammonia" Materials Characterization, vol. 58, 2007, pp. 680-684.

[20] Nathalie Demarest, Damien Deubel, Jean-Claude Keromnes, Claude Vaudry, Fabien Grasset, Ronan Lefort, Maryline Guilloux-Viry, "Optimization of bandpass optical filters based on TiO2 nanolayers", Optical Engineering SPIE, vol. 54, 2015, pp. 015101 (1-7)

[21] P. Singh, D. Kaur, "Room temperature growth of nanocrystalline anatase TiO_2 thin films by dc magnetron sputtering", Physica B: Condensed Matter, vol. 405, 2010, pp.1258-1266.

[22] Narumi Inoue, Hiromitsu Yuasa, Masayuki Okoshi, "TiO_2 thin films prepared by PLD for photocatalytic applications", Applied Surface Science, vol. 197-198, 2002, pp. 393-397.

[23] G. San Vicente, A. Morales, M. T. Gutierrez, "Preparation and characterization of sol–gel TiO_2 antireflective coatings for silicon", Thin Solid Films, vol. 391, 2001, pp. 133-137.

[24] Christopher C. Evans, Chengyu Liu, Jin Suntivich, "TiO_2 Nanophotonic Sensors for Efficient Integrated Evanescent Raman Spectroscopy", ACS Photonics, vol. 3, 2016, pp. 1662-1669.

[25] Jiajie Fan, Zhenzhen Li, Wenyuan Zhou, Yucong Miao, Yaojia Zhang, Junhua Hu, Guosheng Shao, "Dye-sensitized solar cells based on TiO_2 nanoparticles/ nanobelts double-layered film with improved photovoltaic performance", A. Surface Sci., vol. 319, 2014, pp. 75-82.

[26] Yu. M. Evtushenko, S.V. Romashkin, N.S. Trofimov, T.K. Chekhlova, "Optical Properties of TiO_2 Thin Films", Physics Procedia, vol. 73, 2015, pp. 100-107.

[27] Zu Rong Dai, Zheng Wei Peng, Zhong L. Wang, "Novel nanostructures of functional oxides synthesized by thermal evaporation", Adv. Functional Mater., vol. 13, 2003, pp. 9-24.

[28] Duncan W. Bruce, Dermot O'Hare, Richard I. Walton, "Functional Oxides", WILEY, June 2010

[29] Jitendra N. Tiwari, Rajanish N. Tiwari, Kwang S. Kim, "Zero-dimensional, one-dimensional, two-dimensional and three-dimensional nanostructured

materials for advanced electrochemical energy devices", Progress in Materials Sci., vol. 57, 2012, pp.724–803.

[30] Serge Zhuiykov, Toshikazu Kawaguchi, Zhenyin Hai, Mohammad Karbalaei Akbari, Philippe M. Heynderickx, "Interfacial engineering of two-dimensional nano-structured materials by atomic layer deposition", Applied Surface Sci., vol. 392, 2017, pp. 231-243.

[31] P. Singh, A. K. Chawla, D. Kaur, R Chandra, "Effect of oxygen partial pressure on the structural and optical properties of sputter deposited ZnO nanocrystalline thin films", Materials Letters, vol. 61, 2007, pp.2050-2053.

[32] Stephen Pearton, "GaN and ZnO-based Materials and Devices", Springer Science & Business Media, 2012.

[33] S. Logothetidis,, A. Laskarakis, S. Kassavetis, S. Lousinian, C. Gravalidis, G. Kiriakidis, "Optical and structural properties of ZnO for transparent electronics", Thin Solid Films, vol. 516, 2008, pp. 1345-1349.

[34] R. L. Hoffman, B. J. Norris and J. F. Wager, "ZnO-based transparent thin-film transistors", Applied Physics Letters, vol. 82, 2003, pp. 733-735.

[35] Nandhinee R Shanmugam, Sriram Muthukumar & Shalini Prasad, "A review on ZnO-based electrical biosensors for cardiac biomarker detection", Future Sci. OA (2017), FSO196.

[36] Sebastian C. Dixon, David O. Scanlon, Claire J. Carmalt, Ivan P. Parkin, "n-Type doped transparent conducting binary oxides: an overview", J. Mater. Chem. C, vol. 4, 2016, pp. 6946-6961.

[37] Nasrin Sarmadian, Rolando Saniz, Bart Partoens, Dirk Lamoen, "Easily doped n-type, low hole effective mass, transparent oxides", Scientific Reports, vol.6, 2016, pp.20446.

[38] Zhong Lin Wang, "Zinc oxide nanostructures: growth, properties and applications", J. Phys.: Condens. Matter, vol. 16, 2004, pp. R829–R858.

[39] N. Nagarani, V. Vasu, "Structural and Optical Characterization of ZnO thin films by Sol- Gel Method", Journal on Photonics and Spintronics, vol.2, 2013, pp. 19-21.

[40] Xiaoli Mao, Ru Zhou, Shouwei Zhang, Liping Ding, Lei Wan, Shengxian Qin, Zhesheng Chen, Jinzhang Xu, Shiding Miao, "High Efficiency Dye-sensitized Solar Cells Constructed with Composites of TiO_2 and the Hot-

bubbling Synthesized Ultra-Small SnO_2 Nanocrystals", Scientific Reports, vol. 6, 2016,19390.

[41] Azhar Ali Haidry, Peter Schlosser, Pavol Durina, "Hydrogen gas sensors based on nanocrystalline TiO_2 thin films", Central European Journal of Physics, vol. 9, 2011, pp. 1351-1354.

[42] D. Hocine, M. S. Belkaid, L. Escoubas, P. Torchio, A. Moreau, "Characterization of TiO_2 antireflection coatings elaborated by APCVD for monocrystalline silicon solar cells", Phys. Status Solidi C, vol. 212, 2015, pp. 323–326

[43] Pradeepan Periyat, Nigel Leyland, Declan E. McCormack, John Colreavy, David Corr, Suresh C. Pillai,"Rapid microwave synthesis of mesoporous TiO_2 for electrochromic displays", J. Mater. Chem., vol. 20, 2010, pp. 3650-3655.

[44] Hyunwoong Park, Hyoung-il Kim, Gun-hee Moon, Wonyong Choi, "Photoinduced charge transfer processes in solar photocatalysis based on modified TiO_2", Energy Environ. Sci., vol. 9, 2016, pp.411-433.

[45] Paola Russo, Robert Liang, Rui Xiu He, Y. Norman Zhou, "Phase transformation of TiO_2 nanoparticles by femtosecond laser ablation in aqueous solutions and deposition on conductive substrates", Nanoscale, vol. 9, 2017, pp. 6167-6177.

[46] Mo S. D., Ching W. Y., "Electrical and optical properties of three phases of titanium dioxide: Rutile, anatase and brookite", Phys. Rev. B, vol. 51, 1995, 13023.

[47] P. Singh, A. Kumar, Deepak, D. Kaur, "ZnO nanocrystalline powder synthesized by ultrasonic mist-chemical vapour deposition", Optical Materials, vol.30, 2008, pp.1316-1322.

[48] P. Singh, A. Kumar and D. Kaur, "Substrate effect on texture properties of nanocrystalline TiO_2 thin films", Physica B: Condensed Matter, vol. 403, 2008, pp. 3769-3773.

[49] M. Perez-Gonzalez, S.A. Tomas, M. Morales-Luna, M.A. Arvizu, M.M. Tellez-Cruz, "Optical, structural and morphological properties of photocatalytic TiO_2–ZnO thin films synthesized by the sol–gel process", Thin Solid Films, vol. 594, 2015, pp. 304–309.

[50] R. Ben Belgacem, M. Chaari, A. Matoussi, "Studies on structural and electrical properties of ZnO/TiO_2 composite materials", J. of Alloys Comp., vol. 651, 2015, pp.49-58.

[51] F. H. Dulin, D. E. Rase, "Phase Equilibria in the System ZnO-TiO_2", J. Am. Ceram. Soc., vol. 43, 1960, pp.125-131.

[52] S. K. Manik, S.K. Pradhan, "Preparation of nanocrystalline microwave dielectric Zn_2TiO_4 and $ZnTiO_3$ mixture and X-ray microstructure characterization by Rietveld method", Physica E vol. 33, 2006, pp.69-76.

[53] A. Chaouchi, S. Astorg, S. Marinel, M. Aliouat, "$ZnTiO_3$ ceramic sintered at low temperature with glass phase addition for LTCC applications", Mater. Chem. Phys., vol.103, 2007, pp.106-111.

[54] Sarra Ayed, Raoudha Ben Belgacem, Jaafar Othman Zayani, Adel Matoussi, "Structural and optical properties of ZnO/TiO_2 composites", Superlattices and Microstructures, vol. 91, 2016, pp. 118-128.

[55] S.F. Wang, M.K. Lu, F. Gu, C.F. Song, D. Xu, D.R. Yuan, S.W. Liu, G.J. Zhou, Y.X. Qi, "Photoluminescence characteristics of Pb^{2+} ion in sol–gel derived ZnTiO3 nanocrystals", Inorg. Chem. Commun. vol. 6, 2003, pp.185–188.

[56] C. Ye, Y. Wang, Y. Ye, J. Zhang, G. H. Li, "Preparation and photoluminescence of undoped $ZnTiO_3$ thin films", J. App. Phy., vol. 106, 2009, 033520.

[57] H. E. Maes, G. Groeseneken, H. Lebon, J. Witters, "Trends in semiconductor memories", Microelectronics Journal, vol. 20, 1989, pp. 9-58.

[58] W. W. Zhuang, W. Pan, B. D. Ulrich, J. J. Lee, L. Stecker, A. Burmaster, D. R. Evans, S. T. Hsu, M. Tajiri, A. Shimaoka, K. Inoue, T. Naka, N. Awaya, K. Sakiyama, Y. Wang, S. Q. Liu, N. J. Wu, and A. Ignatiev, "Novell colossal magnetoresistive thin film nonvolatile resistance random access memory (RRAM)", IEDM Tech. Dig., San Francisco, USA, 2002, pp. 193-196.

[59] K. Kim, J. H. Choi, and H.-S. Jeong, "The future prospect of nonvolatile memory", Proc. VLSI-TSA-Tech., 2005, pp. 88-94

[60] J. M. Slaughter, R. W. Dave, M. Durlam, G. Kerszykowski, K. Smith, K. Nagel, B. Feil, J. Calder, M. DeHerrera, B. Garni, and S. Tehrani, "High speed toggle MRAM with MgO-based tunnel junctions", IEDM Tech. Dig., 2005, pp. 873-876.

[61] R. Moazzami, "Ferroelectric thin film technology for semiconductor memory", Semicond. Sci. Technol., vol.10, 1995, 375.

[62] I. H. Inoue, S. Yasuda, H. Akinaga, and H. Takagi, “Nonpolar resistance switching of metal/binary-transition-metal oxides/metal sandwiches: Homogeneous/inhomogeneous transition of current distribution”, Phys. Rev. B, Condens. Matter, vol. 77, 2008, 035105.

[63] A. Pirovano, A. L. Lacaita, D. Merlani, A. Benvenuti, F. Pellizzer, and R. Bez, “Electronic switching effect in phase-change memory cells”, IEDM Tech. Dig., 2002, pp. 923-926.

[64] G. Muller, T. Happ, M. Kund, G. Y. Lee, N. Nagel, R. Sezi, “Status and outlook of emerging nonvolatile memory technologies,” IEDM Tech. Dig. (2004), pp. 567-570.

[65] A. Odagawa, Y. Katoh, Y. Kanzawa, Z. Wei, T. Mikawa, S. Muraoka, and T. Takagi, “Electroforming and resistance-switching mechanism in a magnetite thin film”, Appl. Phys. Lett. vol. 91, 2007, 133503.

[66] R. Waser, M. Aono, “Nanoionics-based resistive switching memories”, Nature Materials, vol. 6, 2007, pp. 833–840.

[67] K. L. Chopra**,** S.R. Das, “Thin Film Solar Cells”, Springer US, 1983

[68] Jef Poortmans , Vladimir Arkhipov, “Thin Film Solar Cells: Fabrication, Characterization and Applications”, WILEY, 2006

[69] B. Gao, H. Zhang, B. Chen, L. Liu, R. Han, J. Kang, Z. Fang, H. Yu, B. Yu, and D. L. Kwong, “Modeling of Retention Failure Behavior in Bipolar Oxide-Based Resistive Switching Memory”, IEEE Electron Device Lett., vol. 32, 2011, pp. 276-278.

[70] S. Yu, Y. Yin Chen, X Guan, H. S. Philip Wong, J. A. Kittl, “A Monte Carlo study of the low resistance state retention of HfO_x based resistive switching memory”, Appl. Phys. Letter, vol. 100, 2012, 043507.

[71] A.V. Desai, M.A. Haque, “Mechanical properties of ZnO nanowires”, Sensors and Actuators A Phys, vol. 134, 2007, pp. 169-176.

[72] Y. Zhang, M. K. Ram, E. K. Stefanakos, D. Y. Goswami, “Synthesis, characterization, and applications of ZnO nanowires”, Journal of Nanomaterials, vol. 2012 (2012), pp. 1-22.

[73] N. K. Hassan, M. R. Hashim, M. Bououdina, “One-dimensional ZnO nano structure growth prepared by thermal evaporation on different substrates: ultraviolet emission as a function of size and dimensionality”, Ceram Int, vol. 39, 2013, pp. 7439-7444.

[74] J. Luo, S.Y. Ma, A.M. Sun, L. Cheng, G.J. Yang, T. Wang, "Ethanol sensing, enhancement by optimizing ZnO nanostructure: from 1D nanorods to 3D nanoflower" Materials Letters, vol.137, 2014, pp. 17-20.

[75] L. Qi, H. Li, L. Dong, "Simple synthesis of flower-like ZnO by a dextran assisted solution route and their photocatalytic degradation property", Materials Letters, vol.107, 2013, pp.354-356.

[76] F. Xie, A. Centeno, B. Zou, M. P. Ryan, D. J. Riley, N. M. Alford, "Tunable synthesis of ordered zinc oxide nanoflower-like arrays", J Colloid Interface Sci, vol. 395, 2013, pp. 85-90.

[77] Jian-Fu Tang, Zong-Liang Tseng, Lung-Chien Chen, Sheng-Yuan Chu, "ZnO nanowalls grown at low-temperature for electron collection in high-efficiency perovskite solar cells", Solar Energy Materials and Solar Cells, vol.154, 2016, pp. 18-22.

[78] Megan M. Brewster, Ming-Yen Lu, Sung Keun Lim, Matthew J. Smith, Xiang Zhou, and Silvija Gradečak,"The Growth and Optical Properties of ZnO Nanowalls" Nanoparticles and Nanostructures, vol. 2, 2011, pp. 1940-1945.

[79] J. M. Gracia Jiménez J. Cembrero, M. Mollar, B.Marí, "Photoluminescent properties of electrochemically synthesized ZnO nanotubes", Materials Characterization, vol.119, 2016, pp. 152-158.

[80] Jian-Fu Tang, Zong-Liang Tseng, Lung-Chien Chen, Sheng-Yuan Chu, "ZnO nanowalls grown at low-temperature for electron collection in high-efficiency perovskite solar cells", Solar Energy Materials and Solar Cells, vol. 154, 2016, pp. 18-22.

[81] M.I. Khan, K.A. Bhatti, Rabia Qindeel, Norah Alonizan, Hayat Saeed Althobaiti, "Characterizations of multilayer ZnO thin films deposited by sol-gel spin coating technique", Results in Physics, vol. 7, 2017, pp. 651-655.

[82] Rungroj Tuayjaroen, Tula Jutarosaga, "The influence of oxygen partial pressure on the shape transition of ZnO microstructure by thermal evaporation", Thin Solid Films, vol. 631, 2017, pp. 213-218.

[83] Jianfeng Su, Chunjuan Tang, Qiang Niu, Chunhe Zang, Yongsheng Zhang, Zhuxi Fu, "Microstructure, optical and electrical properties of Al-doped ZnO films grown by MOCVD", Applied Surface Science, vol. 258, 2012, pp. 8595-8598.

[84] Ajay Kaushal, Davinder Kaur, "Pulsed laser deposition of transparent

ZnO/MgO multilayers", Journal of Alloys and Compounds, vol. 509, 2011, pp. 200-205.

[85] A.A. Othman, M.A. Osman, E.M.M. Ibrahim, Manar A. Ali, A.G. Abd-Elrahim, "Mn-doped ZnO nanocrystals synthesized by sonochemical method: Structural, photoluminescence, and magnetic properties", Materials Science and Engineering: B, vol. 219, 2017, pp. 1-9.

[86] C. Supatutkul, S. Pramchu, A.P. Jaroenjittichai, Y. Laosiritaworn, "Density functional theory investigation of surface defects in Sn-doped ZnO", Surface and Coatings Technology, vol.306, 2016, pp. 364-368.

[87] R. Dhahri, M. Hjiri, L. El Mir, H. Alamri, A. Bonavita, D. Iannazzo, S.G. Leonardi, G. Neri, "CO sensing characteristics of In-doped ZnO semiconductor nanoparticles", Journal of Science: Advanced Materials and Devices, vol. 2, 2017, pp 34-40.

[88] Marin Cernea, Valentina Mihalache, Elisabeta Corina Secu, Roxana Trusca, Vasile Bercu, Lucian Diamandescu, "Structural, morphological, ferromagnetic and photoluminescence properties of Fe-doped ZnO", prepared by hydrothermal route, Superlattices and Microstructures, vol. 104, 2017, pp. 362-373.

[89] Guifeng Chen, Xiaoli Zhao, Hui Zhang, He Wang, Feifei Liu, Xiaoqiang Zhang, Jianbo Gao, Yanmin Zhao, Chao Zhang, Junguang Tao, "Effect of substrate temperature on the structure, electrical and optical properties of Mo doped ZnO films", Materials Science and Engineering: B, vol. 211, 2016, pp. 135-140.

[90] Y.S. Lim, J.S. Jeong, J. Bang, J. Kim, "CaO buffer layer for the growth of ZnO thin film", Solid State Communications, vol.150, 2010, pp. 428-430.

[91] Y. S. Chang, Y. H. Chang, I. Chen, Y. L. Chai, "Synthesis, formation and characterization of ZnTiO3 ceramics", International Journal of Ceramic, vol. 30, 2004, pp.2183-2188.

[92] L. Hou, Y. D. Hou, M. K. Zhu, J. Tang, J. Liu, H. Yan, "Formation and transformation of $ZnTiO_3$ prepared by sol–gel process", Material Letter, vol. 59, 2005, pp.197-200

[93] H.T. Kim, "Microstructure and microwave dielectric properties of modified zinc titanates", Mater. Res. Bull., vol. 33, 1998, pp. 963-973.

[94] Y.S. Chang, Y.H. Chang, J. Alloys Compd., "The structure and properties of zinc titanates doped with strontium", vol. 354, 2003, pp. 303-309.

[95] Q. L. Zhang, H. Yang, J. L. Zoul, H. P. Wang, "Sintering and microwave dielectric properties of LTCC-zinc titanate multilayers", Materials Letters, vol. 59, 2005, pp. 880-884

[96] P. K. Jain, D. Kumar, A. Kumar, D. Kaur, "Structural, optical and dielectric properties of $ZnTiO_3$ ceramics", J. Opto. Adv. Mater., vol. 4, 2010, pp.299-304

[97] T. W. Hickmott, "Low frequency negative resistance in thin anodic oxide films", J. Appl. Phys., vol. 33, 1962, pp. 2669–2682

[98] I. G. Baek, M. S. Lee, S. Seo, M. J. Lee, D. H. Seo, D.-S. Suh, J. C. Park, S. O. Park, H. S. Kim, I. K. Yoo, U-In Chung and I. T. Moon, "Highly scalable nonvolatile resistive memory using simple binary oxide driven by asymmetric uni-polar voltage pulses", IEDM Tech. Dig., 2004, pp. 587–590.

[99] S. Seo, M. J. Lee, D. H. Seo, E. J. Jeoung, D.-S. Suh, Y. S. Joung, I. K. Yoo, I. R. Hwang, S. H. Kim, I. S. Byun, J.-S. Kim, J. S. Choi, and B. H. Park, "Reproducible resistance switching in polycrystalline NiO films", Applied Physics Letters, vol. 85, 2004, pp. 5655–5657.

[100] B. J. Choi, D. S. Jeong, S. K. Kim, C. Rohde, S. Choi, J. H. Oh, H. J. Kim, C. S. Hwang, K. Szot, R. Waser, B. Reichenberg, and S. Tiedke, "Resistive switching mechanism of TiO_2 thin films grown by atomic-layer deposition", Journal of Applied Physics, vol. 98, 2005, 033715.

[101] S. Y. Wang, D. Y. Lee, T. Y. Tseng, and C. Y. Lin, "Effects of Ti top electrode 164 thickness on the resistive switching behaviors of rf-sputtered ZrO_2 memory films," Appl. Phys. Lett., vol. 95, 2009, 112904.

[102] N. Xu, L. Liu, X. Sun, X. Liu, D. Han, Y. Wang, R. Han, J. Kang, and B. Yu, "Characteristics and mechanism of conduction/set process in TiN⁄ZnO⁄Pt resistance switching random-access memories", Applied Physics Letters, vol. 92, 2008, pp. 232112.

[103] S. Yu, B. Gao, H. Dai, B. Sun, L. Liu, X. Liu, R. Han, J. Kang, and B. Yu, "Improved uniformity of resistive switching behaviors in HfO2 thin films with embedded Al layers," Electrochem, Solid-State Lett. vol. 13,2010, H36.

[104] Z. Wei, Y. Kanzawa, K. Arita, Y. Katoh, K. Kawai, S. Muraoka, S. Mitani, S. Fujii, K. Katayama, M. Iijima, T. Mikawa, T. Ninomiya, R. Miyanaga, Y. Kawashima, K. Tsuji, A. Himeno, T. Okada, R. Azuma, K. Shimakawa, H.

Sugaya, T. Takagi, R. Yasuhara, K. Horiba, H. Kumigashira, and M. Oshima, "Highly reliable TaO_x ReRAM and direct evidence of redox reaction mechanism", IEEE IEDM, 2008, pp. 293–296.

[105] W. Kim, S. I. Park, Z. Zhang, Y. Y. Liauw, D. Sekar, H.-S. P. Wong, and S. S. Wong, "Forming-free nitrogen-doped AlO_x RRAM with sub-μA programming Current", IEEE Symposium on VLSI Technology, 2011, pp. 22-23.

[106] B. Strukov, G. S. Snider, D. R. Stewart, and R. S. Williams, "The missing memristor found", Nature, vol. 453, 2008, pp. 80–83.

[107] C. Y. Lin, C. Y. Wu, C. Y. Wu, T. Y. Tseng, and C. Hu, "Modified resistive switching behavior of ZrO_2 memory films based on the interface layer formed by using Ti top electrode", J. Appl. Phys., vol. 102, 2007, 094101.

[108] H. Y. Lee, P. S. Chen, T. Y. Wu, Y. S. Chen, C. C. Wang, P. J. Tzeng, C. H. Lin, F. Chen, C. H. Lien, and M. J. Tsai, "Low power and high speed bipolar switching with a thin reactive Ti buffer layer in robust HfO_2 based RRAM", IEEE IEDM, 2008, pp. 1–4.

[109] A. Odagawa, H. Sato, I. H. Inoue, H. Akoh, M. Kawasaki, and Y. Tokura, "Colossal electroresistance of a $Pr_{0.7}Ca_{0.3}MnO_3$ thin film at room temperature", Phys. Rev. B, vol. 70, 2004, 224403.

[110] X. Chen, N. J. Wu, J. Strozier, and A. Ignatiev, "Direct resistance profile for an electrical pulse induced resistance change device", Appl. Phys. Lett., vol. 87, 2005, 233506.

[111] A. Sawa, T. Fujii, M. Kawasaki, and Y. Tokura, "Interface transport properties and resistance switching in perovskite-oxide heterojunctions", in Proc. SPIE, 2005, 59322C

[112] S. X. Wu, L. M. Xu, X. J. Xing, S. M. Chen, Y. B. Yuan, Y. J. Liu, Y. P. Yu, X. Y. Li, and S. W. Li, "Reverse-bias-induced bipolar resistance switching in $Pt/TiO_2/SrTi_{0.99}Nb_{0.01}O_3/Pt$ devices", Appl. Phys. Lett., vol. 93, 2008, 043502.

[113] K. M. Kim, B. J. Choi, Y. C. Shin, S. Choi, and C. S. Hwang, "Anode-interface localized filamentary mechanism in resistive switching of TiO_2 thin films", Appl. Phys. Lett., vol. 91, 2007, 012907.

[114] R. Waser, "Electrochemical and thermochemical memories", IEEE IEDM Tech. Dig., 2008, pp. 289-292.

[115] Ting-Chang Chang, Kuan-Chang Chang, Tsung-Ming Tsai, Tian-Jian Chu and Simon M. Sze, "Resistance random access memory", Materials Today , vol. 19, 2016, pp. 254-264

[116] H. S. Philip Wong, Heng-Yuan Lee, Shimeng Yu, Yu-Sheng Chen, Yi Wu, Pang-Shiu Chen, Byoungil Lee, Frederick T. Chen, and Ming-Jinn Tsai, "Metal–Oxide RRAM" Proceedings of the IEEE , vol. 100, 2012, pp.1951-1970.

[117] Firman Mangasa Simanjuntak, Debashis Panda, Kung-Hwa Wei and Tseung-Yuen Tseng, "Status and Prospects of ZnO-Based Resistive Switching Memory Devices", Nanoscale Research Letters, vol. 368, 2016, pp.1-31.

[118] H. Y. Lee, Y. S. Chen, P. S. Chen, T. Y. Wu, F. Chen, C. C. Wang, P. J. Tzeng, M.-J. Tsai, C. Lien, "Low-power and nanosecond switching in robust hafnium oxide resistive memory with a thin Ti cap", IEEE Electron Device Lett., vol. 31, 2010, pp. 44-46.

[119] M. Kawai, K. Ito, N. Ichikawa, and Y. Shimakawa, "Thermally formed conducting filaments in a single-crystalline NiO thin film", Appl. Phys. Lett., vol. 96, 2010, 072106.

[120] I. G. Baek, D. C. Kim, M. J. Lee, H. J. Kim, E. K. Yim, M. S. Lee, J. E. Lee, S. E. Ahn, S. Seo, J. H. Lee, J. C. Park, Y. K. Cha, S. O. Park, H. S. Kim, I. K. Yoo, U. I. Chung, J. T. Moon, and B. I. Ryu, "Multi-layer cross- point binary oxide resistive 154 memory (O_xRRAM) for post-NAND storage application", IEDM Tech. Dig., 2005, pp. 750-753.

[121] D. C. Kim, M. J. Lee, S. E. Ahn, S. Seo, J. C. Park, I. K. Yoo, I. G. Baek, H. J. Kim, E. K. Yim, J. E. Lee, S. O. Park, H. S. Sim, U-In Chung, J. T. Moon and B. I. Ryu, "Improvement of resistive memory switching in NiO using IrO_2", Appl. Phy. Lett., vol. 88, 2006, 232106.

[122] C. Y. Lin, M. H. Lin, M. C. Wu, C. H. Lin, and T. Y. Tseng, "Improvement of resistive switching characteristics in $SrZrO_3$ thin films with embedded Cr layer", IEEE Electron Device Lett., vol.29, 2008, 1108.

[123] R. Jung, M.-J. Lee, S. Seo, D. C. Kim, G.-S. Park, K. Kim, S. Ahn, Y. Park, I.-K. Yoo, J.-S. Kim, and B. H. Park, "Decrease in switching voltage fluctuation of Pt/NiO_x/Pt structure by process control", Appl. Phys. Lett., vol. 91, 2007, 022112.

[124] S. Seo, M. J. Lee, D. H. Seo, S. K. Choi, D.-S. Suh, Y. S. Joung, I. K. Yoo, I. S. Byun, I. R. Hwang, S. H. Kim, and B. H. Park, "Conductivity switching characteristics and reset currents in NiO films", Appl. Phys. Lett., vol.86, 2005, 093509.

[125] K. Kinoshita, T. Tamura, M. Aoki, Y. Sugiyama, and H. Tanaka, "Lowering the switching current of resistance random access memory using a hetero junction structure consisting of transition metal oxides", J. Jpn. Appl. Phys., vol. 45, 2006, L991.

[126] D. Lee, D. Seong, H. J. Choi, I. Jo, R. Dong, W. Xiang, S. Oh, M. Pyun, S. Seo, S. Heo, M. Jo, D. K. Hwang, H. K. Park, M. Chang, M. Hasan, and H. Hwang, "Excellent uniformity and reproducible resistance switching characteristics of doped binary metal oxides for non-volatile resistance memory applications", IEEE IEDM Tech. Dig., 2006, pp. 797-800.

[127] Liu Z-J, Chou J-C, Wei S-Y, Gan J-Y, Yew T-R, "Improved resistive switching of textured ZnO thin films grown on Ru electrodes", IEEE Electron Device Lett., vol. 32, 2011, pp. 1728–1730.

[128] Muhammad NM, Duraisamy N, Rahman K, Dang HW, Jo J, Choi KH, "Fabrication of printed memory device having zinc-oxide active nano-layer and investigation of resistive switching", Curr Appl Phys, vol. 13, 2013, pp. 90–96.

[129] Lin C-L, Tang C-C, Wu S-C, Juan P-C, Kang T-K, "Impact of oxygen composition of ZnO metal-oxide on unipolar resistive switching characteristics of Al/ZnO/Al resistive RAM (RRAM)", Micro electron Eng, vol. 136, 2015, pp. 15–21.

[130] Younis A, Chu D, Li S, "Bi-stable resistive switching characteristics in Ti doped ZnO thin films", Nanoscale Res Lett, vol.8, 2013, 154.

[131] Kim M-S, Hwan Hwang Y, Kim S, Guo Z, Moon D-I, Choi J-M, Seol M-L, Bae B-S, Choi Y-K , "Effects of the oxygen vacancy concentration in InGaZnO-based resistance random access memory", Appl Phys Lett, vol. 101, 2012, 243503.

[132] Chen G, Song C, Chen C, Gao S, Zeng F, Pan F, "Resistive switching and magnetic modulation in cobalt-doped ZnO", Adv Mater, vol. 24, 2012, pp. 3515–3520.

[133] Murali S, Rajachidambaram JS, Han S-Y, Chang C-H, Herman GS, Conley JF, "Resistive switching in zinc–tin-oxide", Solid State Electron, vol. 79, 2013, pp.248–252.

[134] Xu Z, Yu L, Xu X, Miao J, Jiang Y, "Effect of oxide/oxide interface on polarity dependent resistive switching behavior in ZnO/ZrO_2 heterostructures", Appl Phys Lett., vol.104, 2014, 192903.

[135] Xu D, Xiong Y, Tang M, Zeng B, Xiao Y, Li J, Liu L, Yan S, Tang Z, Wang L, Zhu X, Li R, "Improvement of resistive switching performances in ZnLaO film by embedding a thin ZnO buffer layer", ECS Solid State Lett., vol. 2, 2013, pp. Q69–Q71.

[136] Zhao J-W, Sun J, Huang H-Q, Liu F-J, Hu Z-F, Zhang X-Q, "Effects of ZnO buffer layer on GZO RRAM devices", Appl Surf Sci., vol. 258, 2012, pp.4588–4591.

[137] Simanjuntak FM, Panda D, Tsai T-L, Lin C-A, Wei K-H, Tseng T-Y, "Enhancing the memory window of AZO/ZnO/ITO transparent resistive switching devices by modulating the oxygen vacancy concentration of the top electrode", J Mater Sci., vol. 50, 2015, pp. 6961–6969.

[138] Seo JW, Park J-W, Lim KS, Yang J-H, Kang SJ, "Transparent resistive random access memory and its characteristics for nonvolatile resistive switching", Appl Phys Lett, vol. 93, 2008, 223505.

[139] Chen M-C, Chang T-C, Huang S-Y, Chen S-C, Hu C-W, Tsai C-T, Sze SM, "Bipolar resistive switching characteristics of transparent indium gallium zinc oxide resistive random access memory", Electrochem Solid-State Lett, vol. 13, 2010, H191.

[140] Peter Würfel, "Physics of Solar Cells: From Basic Principles to Advanced Concepts", Wiley-VCH (2^{nd} Ed.), 2009

[141] K.L. Chopra, S.R. Das, "Thin Film Solar Cells", Springer Science & Business Media, 1983

[142] Choubey, P.C., Oudhia, A. and Dewangan, R., "A Review: Solar Cell Current Scenario and Future Trends", Recent Research in Science and Technology, vol. 4, 2012, pp.99-101

[143] X. Wu, "High-efficiency polycrystalline CdTe Thin–Film Solar Cells", Solar Energy, vol.77, 2004, pp. 803-814.

[144] V. Avrutin, N. Izyumskaya and H. Morko, "Semiconductor solar cells: recent progress in terrestrial applications", Super- lattices and Microstructures, vol. 49, 2011, pp. 337-364.

[145] Hui Li, Xiangxin Liu, "Improved performance of CdTe solar cells with CdS treatment", Solar Energy, vol. 115, 2015, pp. 603-612.

[146] Kai Shen, RuilongYang, Dezhao Wang, Mingjer Jenge, Sumit Chaudhary, Deliang Wang, "Stable CdTe solar cell with V_2O_5 as a back contact buffer layer", Solar Energy Materials and Solar Cells, vol. 144, 2016, pp. 500-508.

[147] J. M. Kephart, J. W. McCamy, Z. Ma, A. Ganjoo, F. M. Alamgir W. S. Sampath, "Band alignment of front contact layers for high-efficiency CdTe solar cells", Solar Energy Materials and Solar Cells, vol. 157, 2016, pp. 266-275

[148] H. A. Mohamed, "Optimized conditions for the improvement of thin film CdS/CdTe solar cells", Thin Solid Films, vol. 589, 2015, pp. 72-78.

[149] H. A. Mohamed, N. M. A. Hadia, "Theoretical analysis of ZnO and ZnO based alloys as front electrode in CdS/CdTe solar cells", Optik - International Journal for Light and Electron Optics, vol. 126, 2015, pp. 1976-1980.

[150] E. Hernandez-Rodriguez, V.Rejon, R.Mis-Fernandez, J. L. Pena, "Application of sputtered TiO_2 thin films as HRT buffer layer for high efficiency CdS/CdTe solar cells", Solar Energy, vol. 132, 2016, pp. 64-72

[151] Chen Li, Jonathan Poplawsky, Yanfa Yan, Stephen J. Pennycook, "Understanding individual defects in CdTe thin-film solar cells via STEM: From atomic structure to electrical activity", Materials Science in Semiconductor Processing, vol. 65, 2017, pp. 64-76.

[152] Chen Li, Yelong Wu, Timothy J. Pennycook, Andrew R. Lupini, Donovan N. Leonard, Wanjian Yin, Naba Paudel, Mowafak Al-Jassim, Yanfa Yan, and Stephen J. Pennycook, "Carrier Separation at Dislocation Pairs in CdTe", Phys. Rev. Lett., vol. 111, 2013, 096403.

[153] Chen Li, Yelong Wu, Jonathan Poplawsky, Timothy J. Pennycook, Naba Paudel, Wanjian Yin, Sarah J. Haigh, Mark P. Oxley, Andrew R. Lupini, Mowafak Al-Jassim, Stephen J. Pennycook, and Yanfa Yan, "Grain-Boundary-Enhanced Carrier Collection in CdTe Solar Cells", Phys. Rev. Lett., vol. 112, 2014, 156103.

[154] Xiaoyan Yang, Run Luo, Ping Tang, Jingquan Zhang, Wei Li, Lianghuan Feng, "Preparation and characterization of pulsed laser deposited CdS/CdSe bi-layer films for CdTe solar cell application", Materials Science in Semiconductor Processing, vol. 48, 2016, pp 27-32.

[155] V. V. Brus, P. D. Maryanchuk, M. I. Ilashchuk, J. Rappich, I. S. Babichuk, Z. D. Kovalyuk, "Graphitic carbon/n-CdTe Schottky-type heterojunction solar cells prepared by electron-beam evaporation, Solar Energy", vol. 112, 2015, pp 78-84.

[156] Ohring M., "Materials Science of Thin Films", Academic Press, New York (2006)

[157] Yuldashev Sh. U., Panin G. N., Kang T. W., Nusretov R. A., Khvan I. V., "Electrical and optical properties of ZnO thin films grown on Si substrates", J. Appl. Phys., vol. 100, 2006, 013704.

[158] Jin Z., Fukumura T., Kawasaki M., "High throughput fabrication of transition- metal - doped epitaxial ZnO thin films: A series of oxide-dilute magnetic semiconductors and their properties", Appl. Phys. Lett., vol. 78, 2001, 3824.

[159] Singh R. K., Narayan J., "Pulsed-laser evaporation technique for deposition of thin films: Physics and theoretical model", Phys. Rev. B, vol. 41, 1991, 8843.

[160] Cullity B. D. and Stock S. R., "Elements of X-Ray Diffraction", Prentice Hall 3rd Ed., New Jersey 2001.

[161] Fleger S. L., Heckman J. W., Karen Jr., Klomparens L., "Scanning and Transmission Electron Microscopy: An Introduction", Oxford University Press, New York (1993).

[162] G.C. Yi, C.R. Wang, W.I. Park, "ZnO nanorods: synthesis, characterization and applications", Semicond. Sci. Technol., vol. 20, 2005, pp. S22-S34.

[163] Debashis Panda, Tseung-Yuen Tseng, "Growth, dielectric properties, and memory device applications of ZrO_2 thin films", Thin Solid Films, vol. 531, 2013, pp. 1–20.

[164] X.M. Fan, J.S. Lian, Z.X. Guo, H.J. Lu, "Microstructure and photoluminescence properties of ZnO thin films grown by PLD on Si (1 1 1) substrates", Appl. Surf. Sci., vol. 239, 2005, pp. 176-181.

[165] H. Xu, W. Liu, L. Cao, G. Su, R. Duan, "Preparation of porous TiO2/ZnO composite film and its photocathodic protection properties for 304 stainless steel" Appl. Surf. Sci., vol. 301, 2014, pp. 508-514

[166] L. Xu, L. Shi, X. Li, "Effect of TiO2 buffer layer on the structural and optical properties of ZnO thin films deposited by E-beam evaporation and sol–gel method", Appl. Surf. Sci., vol. 255, 2008, pp. 3230–3234

[167] Y. Zhang, B. Lin, Z. Fu, C. Liu, W. Han, "Strong ultraviolent mission and rectifying behavior of nanocrystalline ZnO films", Opt. Mater., vol.28, 2006, 1192-1196.

[168] H.Y. Lin, Y.Y. Chou, C.L. Cheng, Y.F. Chen, "Giant enhancement of band edge emission based on ZnO/TiO_2 nanocomposites", Opt. Express, vol. 15, 2007, pp. 13832-13837.

[169] Yuanbing Mao, Hongjun Zhou, Stanislaus S. Wong, "Synthesis, Properties, and Applications of Perovskite-Phase Metal Oxide Nanostructures", Material Matters, vol. 5, 2010, pp.50-54.

[170] P. Singh, A. Kumar, Deepak, D. Kaur, "Growth and characterization of ZnO nanocrystalline thin films and nanopowder via low-cost ultrasonic spray pyrolysis", Journal of Crystal Growth, vol. 306, 2007, pp. 303-310.

[171] J. Tauc, "Amorphous and Liquid Semiconductors", Plenum Press, New York, 1974.

[172] C. Ye, Y. Wang, Y. Ye, J. Zhang, G. H. Li, "Preparation and photoluminescence of undoped $ZnTiO_3$ thin films", J. App. Phy., vol. 106, 2009, 033520.

[173] S. T. Tan, B. J. Chen, X. W. Sun, W. J. Fan, H. S. Kwok, X. H. Zhang and S. J. Chua, "Blue shift of Optical Band Gap in ZnO Thin Films Grown by Metal-Organic Chemical-Vapor Deposition," Journal of Applied Physics, Vol. 98, 2005, 013505.

[174] X. B. Yan, K. Lia, J. Yin, Y. D. Xia, H. X. Guo, L. Chen, and Z. G. Liu, "The Resistive Switching Mechanism of $Ag/SrTiO_3/Pt$ Memory Cells Semiconductor Devices, Materials, and Processing", Electrochemical and Solid-State Letters, vol. 13, 2010, pp. H87-H89.

[175] X. B. Yan, H. Hao, Y. F. Chen, Y. C. Li, and W. Banerjee, "Highly transparent bipolar resistive switching memory with In-Ga-Zn-O semiconducting electrode in In-Ga-Zn-O/Ga_2O_3/In-Ga-Zn-O structure", Applied Physics Lett., vol. 105, 2014, 093502

[176] X. B. Yan, Z. Zhou, B. Ding, J. Zhao, and Y. Zhang, "Superior resistive switching memory and biological synapse properties based on a simple TiN/SiO_2/p-Si tunneling junction structure", Journal of Materials Chemistry C, vol. 5, 2017, pp. 2259-2267.

[177] J. J. O. Dwyer, "The theory of electrical conduction and breakdown in solid dielectrics", Clarendon Press, Oxford (1973).

[178] Ming Hua Tang , Bo Jiang, Yong Guang Xiao, Zheng Qiu Zeng, Zi Ping Wang, Jian Cheng Li, John He, "Top electrode-dependent resistance switching behaviors of ZnO thin films deposited on Pt/Ti/SiO_2/Si substrate", Microelectronic Engineering, vol. 93, 2012, pp. 35–38.

[179] Siddheswar Maikap, Debanjan Jana, Mrinmoy Dutta, Amit Prakash, "Self-compliance RRAM characteristics using a novel W/TaO_x /TiN structure", Nanoscale Res Lett., vol. 9, 2014, 292.

[180] J. C. Dupin, D. Gonbeau, P. Vinatier, and A. Levasseur , "A. Systematic XPS studies of metal oxides, hydroxides and peroxides", Phys. Chem. Chem. Phys., vol. 2, 2000, pp. 1319-1324.

[181] X. B. Yan, Y. C. Li, J. Zhao, Y. Li, G. Bai, and S. Zhu, **"**Roles of grain boundary and oxygen vacancies in $Ba_{0.6}Sr_{0.4}TiO_3$films for resistive switching device application", Applied Physics Lett.vol. 108, 2016, 033108 .

[182] U. Chand, C.Y. Huang and T. Y. Tseng, "Mechanism of high temperature retention property (up to 200 ^oC) in ZrO_2-based memory device with inserting a ZnO thin layer", IEEE Electron Device Lett., vol. 35, 2104, pp.1019-1021.

[183] S. Yu, B. Lee, and H. S. Wong, "Metal oxide resistive switching memory in Functional Metal Oxide Nanostructures", New York: Springer-Verlag, 2011.

[184] X. A. Tran, H. Y. Yu, Y. C. Yeo, L. Wu, W. J. Liu, Z. R. Wang, Z. Fang, K. L. Pey,X. W. Sun, A. Y. Du, B. Y. Nguyen, and M. F. Li, "A High-Yield HfO_x-Based Unipolar Resistive RAM Employing Ni Electrode Compatible With Si-Diode Selector for Crossbar Integration", IEEE Electron Device Lett., vol.32, 2011, pp. 396-398.

[185] X. B. Yan, Y. D. Xia, H. N. Hu, X. Gao, H. T. Li, R. Li, J. Yin, and Z. G. Liu, "Effects of the electroforming polarity on bipolar resistive switching characteristics of $SrTiO_{3-\delta}$ films", Applied Physics Lett., vol. 97, 2010, 12101.

[186] M. C. Wu, W. Y. Jang, C. H. Lin and T. Y. Tseng, "A study on low-power, nanosecond operation and multilevel bipolar resistance switching in Ti/ZrO_2/Pt

nonvolatile memory with 1T1R architecture", Semicond. Sci. Technol., vol.27, 2012, 065010.

[187] Ameen M. Ali, K.S. Rahman, Lamya M. Ali, M. Akhtaruzzaman, K. Sopian, S. Radiman, N. Amin, "A computational study on the energy bandgap engineering in performance enhancement of CdTe thin film solar cells", Results in Physics, vol. 7, 2017, pp. 1066-1072.

[188] Jesus Rangel-Cardenas and Hugo Sobral, "Optical Absorption Enhancement in CdTe Thin Films by Microstructuration of the Silicon Substrate" Materials, vol. 10, 2017, 607.

[189] Sudipta Banerjee, "High Efficiency CdTe/CdS Thin Film Solar Cell", International Journal of Engineering Research & Technology, vol. 4, 2015.

[190] K.L. Chopra, P.D. Paulson and V. Dutta, Progress in Photovoltaics: Research and Application, vol. 12 (2004) pp. 69–92.

[191] T. Venkatachalam, S. Velumani, S. Ganesan, K.Sakthivel "Band structure and Optical properties CdTe and $CdSn_3Te_4$ thin films", Thermo-physical Properties of Materials and Devices, 2008, pp. 273-277.

[192] A. M. Bakry, "Influence of Film Thickness on Optical Properties of Hydrogenated Amorphous Silicon Thin Films" Egypt. J. Solids, vol. 31, 2008, pp. 11-22.

[193] V. Consonni, S. Renet, J. Garnier, P. Gergaud, L. Artus, J. Michallon, L. Rapenne, E. Appert, A. K. Cachopo "Improvement of the physical properties of ZnO/CdTe core-shell nanowire arrays by $CdCl_2$ heat treatment for solar cells", Nanoscale Res Lett., vol. 9, 2014, 222.

[194] J.Q. Xi, Martin F. Schubert, Jong Kyu Kim, E. Fred Schubert, Minfeng Chen, Shawn-Yu Lin, W. Liu, J. A. Smart, "Optical thin-film materials with low refractive index for broadband elimination of Fresnel reflection" Nature photonics, vol. 1, 2007, pp. 176-179.

List of Publication

1. Praveen K. Jain, Mohammad Salim, Davinder Kaur, "Structural and Optical Properties of Pulsed Laser Deposited ZnO/TiO_2 and TiO_2/ZnO Thin Films", OPTIK (ELSEVIER Publication), vol.126, 2015, pp.3260-3262.

2. Praveen K. Jain, Mohammad Salim, Davinder Kaur "Effect of Phase Transformation on Optical and Dielectric Properties of Pulsed Laser Deposited $ZnTiO_3$ Thin Films", Superlattices and Microstructure (ELSEVIER Publication), vol. 92, 2016, pp. 308-315.

3. Praveen K. Jain, Mohammad Salim, Umesh Chand, C. Periasami, " Switching Characteristics of ZnO/TiO_2 Double Layer Resistive Random Access Memory", Materials Research Express (IOP Science Publication), vol. 4, 2017, pp. 065901

4. Praveen K. Jain, Mohammad Salim, "First Principle Study of (Ga, Al) co-doped ZnO for Optoelectronic Devices Application" Materials Research Express (IOP Science Publication), vol. 4, 2017, pp. 075902

5. Praveen K. Jain, M. Salim, D. Kaur, "Effect of Substrate on Structural and Optical Properties of TiO_2 thin films prepared by Pulsed Laser Deposition", SKIT Research Journal, vol.6 (2), 2016, 45-47.

6. Praveen K. Jain, M. Salim, Neha Sharma, C. Periasamy, "Investigation of Photocurrent Efficiency of ZnO/CdTe based Inorganic Thin Film Solar Cell, International Conference in Thin Films (ICTF-2017), CSIR-NPL, New Delhi.

7. Praveen K. Jain, Mohammad Salim, "Investigation of Photocurrent Efficiency of ITO/ZnO/CdSe/CdTe Solar Cell" International Conference on New and Renewable Energy Resources for Sustainable Future (ICONRER-2017).

Brief CV

Praveen K. Jain has received the M. Tech. degree with specialization in Solid State Electronic Materials from Indian Institute of Technology Roorkee. He has teaching experience of 9 years and research experience of 1 years. He has authored and co-authored more than 10 research publications in peer reviewed International Journals. He is life member of ISTE, IETE, MRSI and Associate member of IE, Kolkata. His current research interest is in Functional Nanostructured Thin Films, RRAM Devices and Solar Cell, Chalcogenide Glasses.

CORRECTIONS TO REVIEWER COMMENTS

Thank you for the useful comments and suggestions on the technical aspects of my thesis. I have modified the thesis accordingly and the detailed corrections are listed below point by point:

Reviewer 1:

Comment 1: Based on the XPS result of Fig.6.6, the oxygen vacancy of TiO_2 layer is higher than that of ZnO layer. But the conducting filament shown in fig. 6.8, the filament in TiO_2 has the same size with that of ZnO. It is contradictory. They should have different filament size between two layers due to different amount of oxygen vacancy containing. Consequently, it needs to make necessary correction in the figure and explanation of conduction mechanism.

Answer: Figure 6.8 has been corrected as per reviewer suggestion and a comprehensive explanation of conduction mechanism has been added.

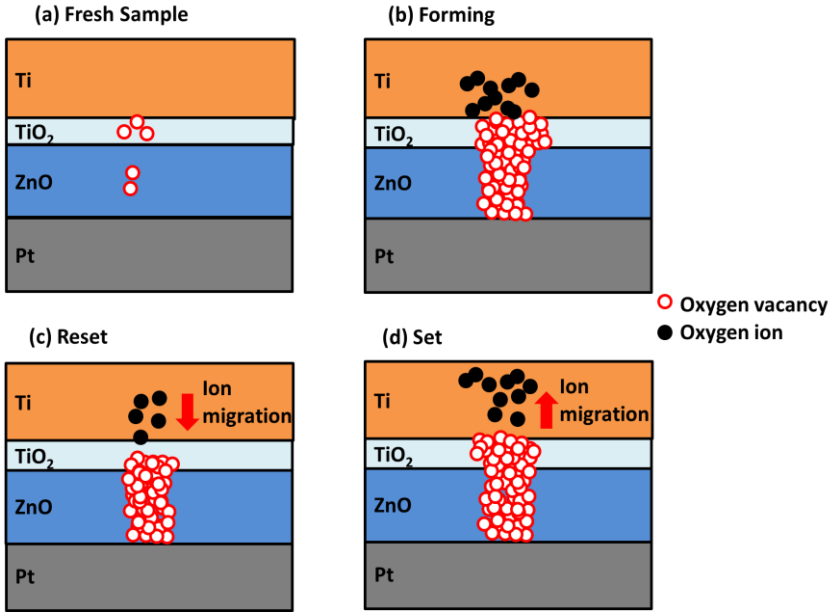

There are various models already proposed to elucidate the resistive switching mechanism, however, the real original of resistive switching phenomenon in RRAM is still under discussion. Recently, there is a general agreement on the conducting filaments formation and rupture as the resistive switching model. It is well-known that the conducting filaments are composed of the oxygen vacancies, hence, as for the conducting filaments model, the forming

process has been known as the defect-induced dielectric soft breakdown and oxygen vacancies are created by external electric field and lined up to form the low resistance conducting filaments in the resistive switching thin film. Moreover, it is believed that the formation and rupture of conducting filament occurs in a specific, confined, and local area of resistive switching layer, rather than in homogeneous one. Hence, the resistance of LRS is dependent of device area. The strength and number of the conducting filaments are proportional to the value of compliance current (set current) during set process, so that set current is comparable to reset current because that the high reset power is required to rupture the more number and stronger conducting filaments.

Comment 2: In chapter 5, Fig. 5.6 (b) and Fig. 5.6 (c) depict dielectric constant and loss tangent changed with frequency, respectively. The description given in p.76 seems different from the results shown in these figures. The author should provide more detailed explanation about the dielectric constant and loss tangent steeply increased in low frequency region. Why?

Answer: As per the reviewer suggestions the text has been modified and a detailed explanation of variation of dielectric constant and loss tangent in the lower frequency region has been provided.

Fig. 5.6 (b-c) shows the measured relative dielectric constant and loss tangent as a function of frequency in the range 500 Hz to 5 MHz of the $ZnTiO_3$ thin films deposited at different substrate temperature. Dielectric constant ε_r is calculated from the measurement of capacitance value which can be obtained using the following equations:

$$\varepsilon_r = \frac{t \times C_p}{A \times \varepsilon_0} = \frac{t \times C_p}{\pi \left(\frac{d}{2}\right)^2 \times \varepsilon_0} \qquad (5.3)$$

where, C_p= equivalent parallel capacitance which is obtained from the measurement data, t = film thickness, d = diameter of the electrode, ε_0 = permittivity of vacuum.

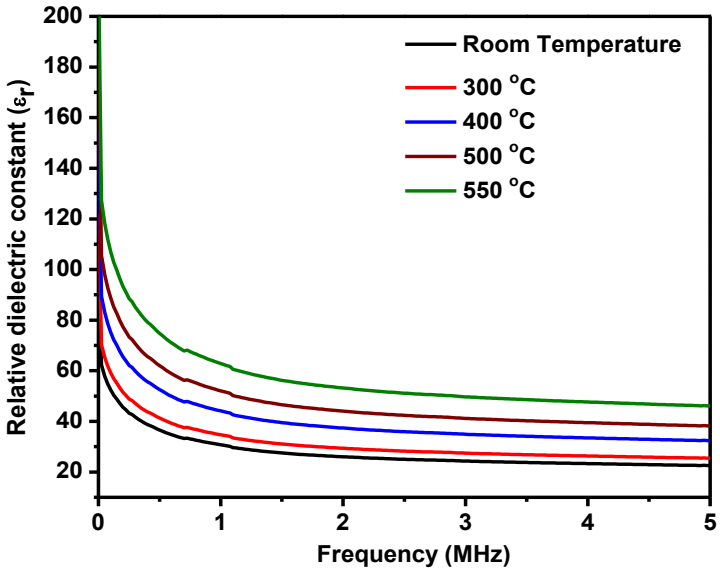

Fig. 5.6(b): The relative dielectric constant as a function of frequency $ZnTiO_3$ thin films deposited at different substrate temperatures

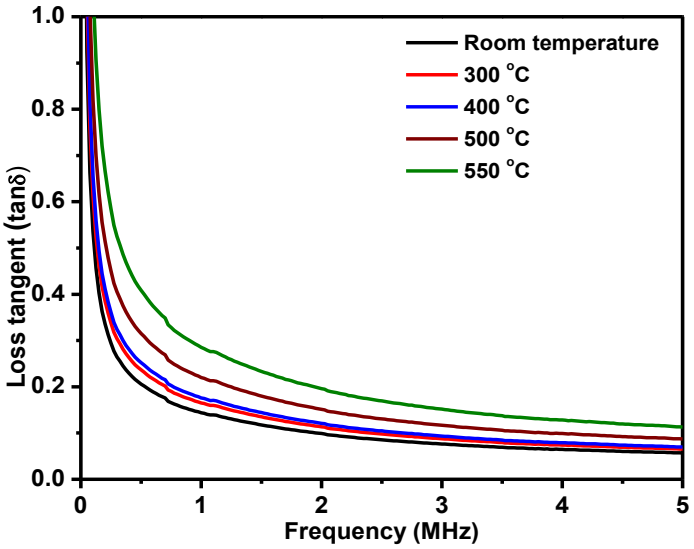

Fig. 5.6(c): The loss tangent as a function of frequency $ZnTiO_3$ thin films deposited at different substrate temperatures

It has been observed that in high frequency region dielectric constant remains constant; while for lower frequencies a steep decrease in the dielectric constant with increase in frequency has been observed.

Dielectric constant values decreased on increasing frequency because when the applied field frequency increased, it was assumed that the dipoles present in the composite cannot re-orient themselves fast enough and therefore dielectric constant decreases.

The high value of dielectric constant at lower frequency is associated with the contributions from ionic, space charge and interface polarization. At higher frequency, dielectric constant becomes independent of frequency. It is due to the inability of electric dipoles to follow the fast variation of the applied electric field. The decrease of dielectric constant with frequency can be explained on the basis of Koop's theory, which assumes the dielectric structure as an inhomogeneous medium of two layers of the Maxwell–Wagner type. This model assumes that the dielectric structure is consisting of well conducting grains, separated by poorly conducting grain boundaries. Moreover, at lower frequencies the grain boundaries are more effective for dielectric constant and conductivity than grain. Consequently, dielectric constant is high at lower frequency and decreases with increase of frequency

Comment 3: The style of References is not consistent in the thesis. Some references are repeat, such as 101, 103, 107 and 108. The page number description, for example, pp.154 is wrong, it should be p.154.

Answer: All corrections suggested by the reviewer have been done. Any repetition in reference number has been omitted and also the page number description as suggested by the reviewer has been modified. The references are written as per standard format.

Comment 4: There are mistakes: such as: (004) plane mentioned in line 7 of p.59 is not shown in the index of XRD pattern of TiO_2/ZnO/Si. The unit of frequency in Fig. 5.6 (b) is not correct.

Answer: TiO_2 thin film exhibit pure anatase phase and crystallinity was improved along (200) plane by inserting the ZnO buffer layer between substrate and TiO_2 thin film.

A correction has been made as per reviewer suggestion. (004) plane in text was written by mistake in place of (200) plane.

The unit of frequency in Fig. 5.6 (b) has been corrected i.e. MHz in place of Hz.

Reviewer 2:

Comment 1: Page No. missing on some pages i.e. 103,104

Answer: The page number has been inserted as per reviewer suggestion.

Comment 2: Page No. 11, in figure 1.6 rewrite the text, as text is not readable.

Answer: Figure 1.6 (page no. 11) has been modified as per reviewer suggestions.

Comment 3: Page No. 15, Figure 1.10, rewrite the text; some of text is very light.

Answer: The corrections have been incorporated.

Comment 4: Page No. 16 in eq. 1.1 to 1.6, define the parameters η, P_m, P_{in}, FF, λ, φ. Also add the reference of these equations.

Answer: In eq. 1.1 to 1.6, all the parameters i.e. η, P_m, P_{in}, FF, λ, φ have been defined.

η = the photocurrent efficiency of a solar cell

P_m= maximum power from the solar cell

P_{in}=the radiation power input

FF= Fill factor

λ= wavelength of the photons

φ= Work function

References of these equations have also been added.

Comment 5: Page No. 40, statement "Schematic of conventional sputtering process is given in Fig 2.2". Write figure 3.6 in place of Figure 2.2.

Answer: The corrections have been made as per reviewer suggestion.

Comment 6: Page No. 55 in figure 3.18 rewrite the text.

Answer: Figure 3.18 (page no. 55), text has been modified as per suggestion.